

University of Montana

## ScholarWorks at University of Montana

---

Graduate Student Theses, Dissertations, &  
Professional Papers

Graduate School

---

2021

# INVESTIGATION OF EMISSIONS AND CHEMISTRY OF FORMIC ACID AND ACETIC ACID IN WILDFIRE SMOKE

Catherine Elizabeth Wielgasz

Follow this and additional works at: <https://scholarworks.umt.edu/etd>



Part of the [Analytical Chemistry Commons](#), and the [Environmental Chemistry Commons](#)

Let us know how access to this document benefits you.

---

### Recommended Citation

Wielgasz, Catherine Elizabeth, "INVESTIGATION OF EMISSIONS AND CHEMISTRY OF FORMIC ACID AND ACETIC ACID IN WILDFIRE SMOKE" (2021). *Graduate Student Theses, Dissertations, & Professional Papers*. 11676.

<https://scholarworks.umt.edu/etd/11676>

This Thesis is brought to you for free and open access by the Graduate School at ScholarWorks at University of Montana. It has been accepted for inclusion in Graduate Student Theses, Dissertations, & Professional Papers by an authorized administrator of ScholarWorks at University of Montana. For more information, please contact [scholarworks@mso.umt.edu](mailto:scholarworks@mso.umt.edu).

INVESTIGATION OF EMISSIONS AND CHEMISTRY OF FORMIC ACID AND ACETIC  
ACID IN WILDFIRE SMOKE

By

CATHERINE ELIZABETH WIELGASZ

Bachelor of Science (Environmental Chemistry), Castleton University, Castleton, VT, 2016

Thesis Paper

presented in partial fulfillment of the requirements  
for the degree of

Master of Science  
in Analytical/Environmental Chemistry

The University of Montana, Department of Chemistry and Biochemistry  
Missoula, MT

December 2020

Approved by:

Scott Whittenburg, Dean of The Graduate School  
Graduate School

Lu Hu, Committee Chair  
Department of Chemistry and Biochemistry

Robert Yokelson  
Department of Chemistry and Biochemistry

Tony Ward  
School of Public and Community Health Sciences

© COPYRIGHT

by

Catherine Elizabeth Wielgasz

2020

All Rights Reserved

## Table of Contents

Abstract.....	vi
Chapter One: Introduction and Background.....	1
Introduction.....	1
Background.....	2
Chapter Two: Experimental Methods.....	6
WE-CAN.....	6
PTR-ToF-MS general description.....	8
PTR-ToF-MS calibrations with standard gas cylinders.....	9
Organic acids' calibrations with permeation tubes.....	11
Organic acid interferences and sensitivities.....	14
Sensitivity dependence on relative humidity.....	17
HRTof-CIMS and quantification.....	19
Chapter Three: Instrument intercomparisons for HCOOH.....	21
Chapter Four: Emissions.....	26
Emission ratio.....	26
Emission factor and modified combustion efficiency.....	30
Chapter Five: Organic acid production.....	36
Normalized excess mixing ratios.....	36
Primary vs secondary source of HCOOH and CH <sub>3</sub> COOH.....	37
Evaporation of organic aerosol as a source of HCOOH and CH <sub>3</sub> COOH.....	39
Heterogeneity in smoke plumes.....	40
Future Directions.....	42
Acknowledgements.....	43
References.....	44
Appendix A: Further WE-CAN details.....	53
Appendix B: HCOOH and CH <sub>3</sub> COOH against altitude for research flights.....	54
Appendix C: Emission factors (and ratios) from previous literature.....	56

## List of Tables and Figures

### Tables

<u>Table 1</u> : Chemical pathways known for HCOOH and CH <sub>3</sub> COOH .....	5
<u>Table 2</u> : 25 calibrated VOCs in gas cylinders.....	10
<u>Table 3</u> : Organic acid interferences .....	15
<u>Table 4</u> : Organic acid calibration details for PTR-ToF-MS .....	18
<u>Table 5</u> : Intercomparisons of instrument specs.....	21
<u>Table 6</u> : HCOOH instrument intercomparisons for all flights.....	22
<u>Table 7</u> : EFs, ERs, and MCE for HCOOH and CH <sub>3</sub> COOH during WE-CAN .....	31
<u>Table 8</u> : Average emission factors and MCE from literature .....	33
<u>Table A1</u> : WE-CAN flight details .....	53
<u>Table C1</u> : HCOOH and CH <sub>3</sub> COOH emission ratios from literature .....	56-60
<u>Table C2</u> : HCOOH and CH <sub>3</sub> COOH emission factors from literature .....	60-72

### Figures

<u>Figure 1</u> : WE-CAN flight paths .....	7
<u>Figure 2</u> : PTR-ToF-MS racked on the NSF/NCAR C-130.....	9
<u>Figure 3</u> : Schematic of in-house permeation system .....	14
<u>Figure 4</u> : Peak fitting of organic acids in PTR-ToF-MS with interferences .....	16
<u>Figure 5</u> : Permeation calibrations: sensitivities dependent on relative humidity.....	18
<u>Figure 6</u> : HRToF-CIMS “fast” zero.....	20
<u>Figure 7</u> : Emission pass and time series of RF09 and RF11 comparing instruments.....	23
<u>Figure 8</u> : Scatter plot of instrument intercomparisons for RF09 and RF11 .....	24
<u>Figure 9</u> : Altitude and RH for RF09 and RF11, with HCOOH instrument ratio.....	25
<u>Figure 10</u> : HCOOH and CH <sub>3</sub> COOH mixing ratios during WE-CAN .....	27
<u>Figure 11</u> : Emission ratios from WE-CAN compared to literature .....	29
<u>Figure 12</u> : Emission factors of WE-CAN compared to literature.....	32
<u>Figure 13</u> : Emission factors compared to fuels and measurement from literature.....	34
<u>Figure 14</u> : Emission factors v. MCE for HCOOH and CH <sub>3</sub> COOH .....	35
<u>Figure 15</u> : Normalized excess mixing ratios of HCOOH and CH <sub>3</sub> COOH .....	37
<u>Figure 16</u> : Normalized excess mixing ratios of organic acids to different precursors.....	38
<u>Figure 17</u> : HCOOH, CH <sub>3</sub> COOH, OA, and altitude dependence.....	40
<u>Figure 18</u> : Heterogeneity in smoke plumes .....	41
<u>Figure B1</u> : Temperature dependence .....	54-55

## List of Abbreviations

CH<sub>3</sub>COOH – acetic acid

CH<sub>3</sub>CO<sub>3</sub> – peroxy acetyl radical

CO – carbon monoxide

CO<sub>2</sub> – carbon dioxide

cps – counts per second

EF – emission factor

ER – emission ratio

FC1 – flow controller #1

FIREX – Fire Influence on Regional and global environments EXperiment

HCOOH – formic acid

HRTof-CIMS – High Resolution Time-of-Flight Chemical Ionization Mass Spectrometer

I<sup>-</sup> – iodide

$I_{H_2O^*H_3O}/I_{H_3O^+}$  – relative humidity proxy measured by the PTR-ToF-MS

NAAQS – National Ambient Air Quality Standards

ncps – normalized counts per second

NEMR – normalized excess mixing ratio

NMOGs – Non-methane organic gases

NMVOCs – Non-methane volatile organic compounds

OA – organic aerosols

OH – hydroxyl radicals

PAA – peroxyacetic acid

PAN – peroxyacetyl nitrate

ppb – parts per billion

ppm – parts per million

PTR-ToF-MS – Proton Transfer Reaction Time-of-Flight Mass Spectrometer

RH – relative humidity

slpm – standard liter per minute

VOCs – volatile organic compounds

WE-CAN – Western wildfire Experiment for Cloud chemistry, Aerosol absorption and Nitrogen

**Abstract**

Chairperson: Lu Hu

Formic acid (HCOOH) and acetic acid (CH<sub>3</sub>COOH) are two of the most ubiquitous organic acids in the atmosphere. Chemical transport models consistently underestimate HCOOH and CH<sub>3</sub>COOH concentrations in environments including fire smoke, implying our incomplete understanding of their global budget. Emissions and secondary production of HCOOH and CH<sub>3</sub>COOH within complex mixtures in fire smoke is uncertain.

I used measurements from the NSF/NCAR C-130 aircraft during the Western Wildfire Experiment for Cloud Chemistry, Aerosol Absorption, and Nitrogen (WE-CAN) campaign to investigate emissions and photochemical production of HCOOH and CH<sub>3</sub>COOH from smoke plumes. First, I compared two instruments to assess the quality of HCOOH measurements in smoke plumes for 15 research flights. HCOOH mixing ratios from the high-resolution time-of-flight chemical ionization mass spectrometer (HRTof-CIMS) on average are approximately 1.48 times higher than the proton-transfer-reaction time-of-flight mass spectrometer (PTR-ToF-MS) for HCOOH, and 1.36 times higher for emission passes. Secondly, I examined emissions of HCOOH and CH<sub>3</sub>COOH through emission ratios (ERs) and emission factors (EFs) of 24 fires sampled during WE-CAN. HCOOH (HRTof-CIMS) ERs average  $6.1 \pm 2.6$  ppb/ppmCO but show an increasing trend at 1.46 ppb/ppmCO/hour, suggesting chemical formation may have occurred prior to plume sampling by the C-130, all of which were less than two hours of physical aging since known fire locations. CH<sub>3</sub>COOH (PTR-ToF-MS) average ER is  $11.5 \pm 2.2$  ppb/ppmCO, with an increase of 0.483 ppb/ppmCO/hour. WE-CAN derived CH<sub>3</sub>COOH EF,  $2.38 \pm 0.57$  g/kg, is consistent with previous studies within  $\pm 25\%$ , despite diversified fuel. HCOOH EFs from WE-CAN,  $1.45 \pm 0.57$  g/kg, were larger than the 75th percentile of previous literature, likely reflecting fast chemistry in the first two hours of physical smoke age in field data.

Third, I explored the production of HCOOH and CH<sub>3</sub>COOH in smoke plumes within 6 hours of aging. HCOOH normalized excess mixing ratios (NEMR) increase moving downwind at the rate 2.23ppb/ppmCO/hour. CH<sub>3</sub>COOH increases 2.05ppb/ppmCO/hour for the first hour, but then on average decreases by -0.76ppb/ppmCO/hour, possibly due to loss processes exceeding formations.

## **Chapter One: Introduction and background**

### ***Introduction***

Formic acid (HCOOH) and acetic acid (CH<sub>3</sub>COOH) are two of the most abundant organic acids within the troposphere. As major sources of natural acidity, they account for 30 – 60 % of free acidity in precipitation for urban and remote environments (Andreae et al. 1988; Keene and Galloway 1984, 1988; Millet, et al. 2015). HCOOH and CH<sub>3</sub>COOH are key to atmospheric aqueous-phase chemistry through effects on pH-dependent reactions, oxidant levels, and solubilities (Millet, et al. 2015). HCOOH and CH<sub>3</sub>COOH also represent a key fate of certain atmospheric hydrocarbons, with potential impacts on secondary aerosol formation (Link et al. 2020).

Recent studies show that models continuously underestimate both HCOOH and CH<sub>3</sub>COOH abundance compared to ground, airborne, and satellite observations, reflecting an incomplete knowledge about their global budget (Alwe et al. 2019; Baasandorj et al. 2015; Le Breton et al. 2012; Cady-Pereira et al. 2014; Millet 2012; Millet et al. 2015; Paulot et al. 2011; Stavrou et al. 2012; Yuan et al. 2015). The model underestimation implies an existence of one or more large missing primary or secondary source such as biomass burning or anthropogenic sources, or individual chemistry including acetaldehyde tautomerization, photooxidation of carbonyls, or photooxidation of acetone (Chattopadhyay, Chatterjee, and Chakraborty 2015; Millet 2012; Millet et al. 2015).

Direct emissions of HCOOH and CH<sub>3</sub>COOH from biomass burning smoke some of the top emitted VOCs. 16% of average emissions by mass measured from all fires are HCOOH and CH<sub>3</sub>COOH, with the latter being a top emitted VOC, and further proving the significance of these organic acids in wildfires (Permar et al. In review). Several studies have also shown that substantial secondary production occurs within smoke plumes when organic gases are oxidized by hydroxyl radical (OH) or react with ozone (Akagi et al. 2012; Goode et al. 2000; Grutter et al. 2010; Yokelson et al. 1999, 2009). Efforts to

understand secondary sources for HCOOH and CH<sub>3</sub>COOH from fires have been challenging due to the limited identification and quantification of volatile organic compounds (VOCs) and the incomplete understanding of chemical processes within fires (Akagi et al. 2013). Thus, initial and downwind smoke chemistry within biomass burning plumes are both poorly characterized and cause major limiting factors within atmospheric chemistry models (Chaliyakunnel et al. 2016). Studies of prescribed burns, ground measurements, aircraft field campaigns, and laboratory burn experiments are slowly increasing our understanding of the chemistry within different fire plumes. The Western wildfire Experiment for Cloud chemistry, Aerosol absorption and Nitrogen (WE-CAN) airborne campaign occurred during the summer of 2018. WE-CAN focused on sampling wildfire smoke in the western United States and characterizing their chemical evolution within the first few hours since emissions. HCOOH and CH<sub>3</sub>COOH measurements were obtained to study the primary emissions of wildfires, and observations were also measured downwind of the fire plume to learn the importance of their primary versus secondary sources. Emissions and downwind mixing ratios of HCOOH and CH<sub>3</sub>COOH were compared to previous literature that studied field or laboratory burns. HCOOH mixing ratios were also compared between two state-of-the-art instruments aboard the research aircraft to further understand how accurately it could be measured in smoke plumes.

### ***Background***

HCOOH and CH<sub>3</sub>COOH are the simplest and most abundant carboxylic acids present in the atmosphere yet models continuously underestimate these species in a multitude of different environments, including wildfire smoke. In general, the sinks of HCOOH and CH<sub>3</sub>COOH include wet and dry deposition, photochemical oxidations by OH radicals, and the irreversible uptake on dust. They are considered relatively well known and quantified with total global estimates of ~58 to ~86 Tg yr<sup>-1</sup>. The lifetime of HCOOH in the atmosphere is 2 to 4 days, while CH<sub>3</sub>COOH is approximately 2.3 days (Chebbi and Carlier 1996; Millet et al. 2015; Paulot et al. 2011; Stavrakou et al. 2012). The sources, precursors, and their contribution to the formation of HCOOH and CH<sub>3</sub>COOH are highly uncertain (Glasius et al. 2000;

Link et al. 2020; Millet et al. 2015; Paulot et al. 2011; Stavrou et al. 2012). Most field measurements show that HCOOH and CH<sub>3</sub>COOH have a high correlation, suggesting similar sources. Radiocarbon studies in Europe have shown that HCOOH and CH<sub>3</sub>COOH are primarily composed of modern carbon, which is consistent with biomass burning and biogenic sources and also suggests that the fossil fuel contribution is small (Glasius et al. 2000, 2001). Both HCOOH and CH<sub>3</sub>COOH can be emitted directly (primary) or formed via photochemical production (secondary). Primary emissions include anthropogenic waste, soil, cattle, biofuel and biomass burning, and terrestrial vegetation. However, simulations have shown that primary emissions only make up approximately 15 – 26 % of the total global sources for HCOOH and approximately 26 – 32 % for CH<sub>3</sub>COOH (Millet et al. 2015; Paulot et al. 2011; Stavrou et al. 2012).

The current global estimates reported for HCOOH sources are (with the contribution from photochemical production reported in parenthesis) 61.5 Tg yr<sup>-1</sup> (51.0), 32.0 Tg yr<sup>-1</sup> (21.5), 56.7 Tg yr<sup>-1</sup> (48.6), and 100 – 120 Tg yr<sup>-1</sup> (90%) ( Millet et al. 2015; J. Müller, Stavrou, and Peeters 2018; Paulot et al. 2011; Stavrou et al. 2012). CH<sub>3</sub>COOH current global sources have been estimated to be 31.4 Tg yr<sup>-1</sup> (with 13.8 from photochemical production), to 85.5 Tg yr<sup>-1</sup> (58.6 from photochemical production) (Müller et al. 2018; Paulot et al. 2011). These values imply photochemical production from biomass burning or biogenic precursors of volatile organic compounds (VOCs) are responsible for the formation (~75%) of HCOOH and CH<sub>3</sub>COOH (J. Müller, Stavrou, and Peeters 2018; Paulot et al. 2011).

HCOOH and CH<sub>3</sub>COOH are photochemically produced (Table 1) via isoprene oxidation by OH radicals and ozonolysis of terminal alkenes that form stabilized Criegee reactions (which can also be formed from methane reacting with OH radicals). The stabilized Criegee intermediates react with water vapor to form hydroxymethyl hydroperoxide, which decomposes into HCOOH at a relatively high rate, though Criegee intermediates can instead choose to react with CO, SO<sub>2</sub>, NO and NO<sub>2</sub>, depending on availability of species and environmental conditions (Bossolasco et al. 2014; Millet, et al. 2015; Yuan et al. 2015). Both isoprene epoxydiol and isoprene hydroxyl hydroperoxide oxidation by OH can also form organic acids,

but their yields increase as the NO concentration decreases (Link et al. 2020). Isoprene can also undergo ozonolysis to form organic acids. Other ways organic acids are photochemically produced include OH oxidation of any terminal alkene, monoterpene, and glycolaldehyde. Monoterpene ozonolysis, and keto-enol tautomerization (which forms vinyl alcohol and in turn can be photooxidized by OH to form HCOOH) are also thought to play a role (Millet, et al. 2015; J. Müller, Stavrakou, and Peeters 2018; Paulot et al. 2011). Reactions of HOCH<sub>2</sub>OO, a product from formaldehyde reacting with HO<sub>2</sub> radicals, also contribute the formation of HCOOH, but this pathway is more prevalent at low ambient temperatures (Atkinson et al. 2006; Yuan et al. 2015). Many studies have also shown that HCOOH is formed through OH oxidation of aromatics, but the yields among both different species and one single species are highly variable (Baltensperger et al. 2005; Wyche et al. 2008). Many of the photochemical source quantities are poorly understood. Millet et al. (2015) and Paulot et al. (2011) stated that their simulated photochemical sources of HCOOH are approximately 51.0 Tg yr<sup>-1</sup> and mostly was formed from isoprene and its oxidation products (~45%) (Millet, et al. 2015; Paulot et al. 2011). A recent study exclaims that the isoprene chemistry sink (87% from oxidation by OH and 10% from ozonolysis) created a global production rate of 74.0 Tg yr<sup>-1</sup> for HCOOH, which is approximately three times larger than the studies stated above (Link et al. 2020).

For CH<sub>3</sub>COOH, both Müller et al. (2018) and Paulot et al. (2011) have simulated that the largest known photochemical source is the peroxy acetyl radical (CH<sub>3</sub>CO<sub>3</sub>), formed from acetaldehyde oxidation and photolysis of acetone and methylglyoxal (Fischer et al. 2014), reacting with peroxy radicals, which accounts for almost 40.0 Tg yr<sup>-1</sup> (Müller et al. 2018; Paulot et al. 2011). Link et al. (2020), which focused on isoprene formation of these organic acids, stated that the isoprene chemical sink creates a global annual production rate of 15.0 Tg yr<sup>-1</sup> (Link et al. 2020). Constraints on the global budget of HCOOH and CH<sub>3</sub>COOH will help us better understand their interaction between the biosphere and atmosphere (Akagi et al. 2012; Bossolasco et al. 2014; Chaliyakunnel et al. 2016; Goode et al. 2000; Paulot et al. 2011; Shaw et al. 2018).

**Table 1:** Known chemistry that produces HCOOH and CH<sub>3</sub>COOH, with where the precursors are important, and estimated yields in relation to the total formation from photochemical production. References for each yield are in footnotes below. Blank spaces indicate no reported yields.

Chemical pathways	Potentially influenced environments	HCOOH yield of photochemical production (%)	CH <sub>3</sub> COOH yield of photochemical production (%)
Isoprene oxidation by OH	Biogenic emissions; wildfires	<sup>a</sup> 75 <sup>b</sup> 45 <sup>d</sup> 20	
Isoprene ozonolysis	Biogenic emissions; wildfires	<sup>a, b</sup> 14 <sup>d</sup> 18 <sup>e</sup> 39*	
Monoterpene oxidation by OH	Biogenic emissions; wildfires	<sup>a</sup> 6 <sup>b</sup> 15.5* <sup>f</sup> 5* <sup>d</sup> 7.4	<sup>a</sup> 15.5*
Monoterpene ozonolysis	Biogenic emissions; wildfires	<sup>b</sup> 7.5* <sup>f</sup> 5*	<sup>a</sup> 8*
Peroxy acetyl radical with peroxy radicals (HO <sub>2</sub> & RO <sub>2</sub> ) from acetaldehyde oxidation and photolysis of acetone and methylglyoxal	NM VOC <sup>g, h</sup> source regions; high NO <sub>x</sub> conditions		<sup>a</sup> 77 <sup>d</sup> 70 <sup>e</sup> 52*
Keto-enol tautomerization forming vinyl alcohol which oxidizes by OH	Intermediates in combustion	<sup>b</sup> 21* <sup>d</sup> 33.5 <sup>e</sup> 14*	
Ozonolysis of terminal alkenes forming stabilized Criegee intermediates which react with water vapor to form hydroxymethyl hydroperoxide and decomposes	Wet conditions that allow high water vapor content	<sup>a, b</sup> 12* <sup>d</sup> 9.3	<sup>d</sup> 0.35
Formaldehyde degradation	Urban areas; low ambient temperatures		
Aromatics oxidation by OH	Urban areas; wildfires	<sup>c</sup> 10*	
Alkyne oxidation by OH (mainly acetylene)	Biomass burning processes; residential combustion; automobile tailpipe emissions	<sup>a</sup> 6.5 <sup>b</sup> 36.4* <sup>d</sup> 12	
Isoprene oxidation forming glycolaldehyde that oxidizes by OH	Biomass burning	<sup>c</sup> 8* <sup>e</sup> <5*	

<sup>a</sup> (Paulot et al. 2011); <sup>b</sup> (Millet et al. 2015); <sup>c</sup> (Yuan et al. 2015); <sup>d</sup> (Müller et al. 2018); <sup>e</sup> (Link et al. 2020); <sup>f</sup> (Stavrakou et al. 2012); <sup>g</sup> (Fischer et al. 2014)

<sup>h</sup> NMVOC is non-methane volatile organic compounds

“\*” represents HCOOH or CH<sub>3</sub>COOH molar yields formed from specified chemical pathway

Wildfires are an important source of VOCs that impact downwind air quality and the formation of secondary air pollutants including ozone. However, wildfire emission estimates are extremely uncertain and difficult to predict. Aircraft campaigns that focus on constraining VOC emissions and downwind chemistry in smoke plumes have occurred throughout the southeastern and southwestern US, Alaska, along with Brazil, Mexico, and Africa (Akagi et al. 2013; Burling et al. 2011; Goode et al. 2000; Müller et al. 2016; Yokelson et al. 1999, 2003, 2007, 2011). Each airborne campaign varied in fuel type, climate, instrumentation, and fire conditions including combustion phases.

To further constrain HCOOH and CH<sub>3</sub>COOH emissions and downwind chemistry within smoke plumes, there have also been several large laboratory burn experiments which sampled a multitude of different fuels from various locations and many instruments (Bertschi et al. 2003; Burling et al. 2010; Christian et al. 2003; Goode et al. 1999; Koss et al. 2018; Mckenzie et al. 1995; Selimovic et al. 2018). Laboratory experiments attempt to simulate burning conditions present in the real-world by using fuels selected to reflect their natural composition. However, laboratory burning experiments are imperfect as they cannot replicate the dynamic burning processes or meteorological conditions, and most fuels are very dry. To most accurately characterize wildfire emissions, combining both laboratory and field measurements are ideal (Selimovic et al. 2018).

## **Chapter Two: Experimental Methods**

### ***WE-CAN***

The Western wildfire Experiment for Cloud chemistry, Aerosol absorption and Nitrogen, or WE-CAN, field project occurred during the summer of 2018 in Boise, Idaho. Over 100 hours of sampling occurred in the western United States (ID, CA, MT, OR, WA, UT, NV) on the NCAR/NSF C-130 research aircraft with a suite of instruments aboard for comprehensive gas and aerosol measurements. Most flights took off at approximately 14:00 (local time) and flew for six hours. For further details on each research flight can be found at <http://catalog.eol.ucar.edu/we-can/tools/missions>. Figure 1 depicts the C-130 flight tracks during WE-CAN, colored by observed HCOOH and CH<sub>3</sub>COOOH concentrations. During WE-CAN, the C-130 attempted to sample twelve fires with pseudo-Lagrangian approaches, that have a stepwise pattern where the plane enters the plume, transects it, exits the other side, and then circles back into the plume. The goal of such flight pattern is to measure the same air mass as the airplane moves downwind of the plume to learn of chemical evolutions. Measurements during the emission transects and pseudo-Lagrangian (stepwise) sampling were used for analysis in the thesis.

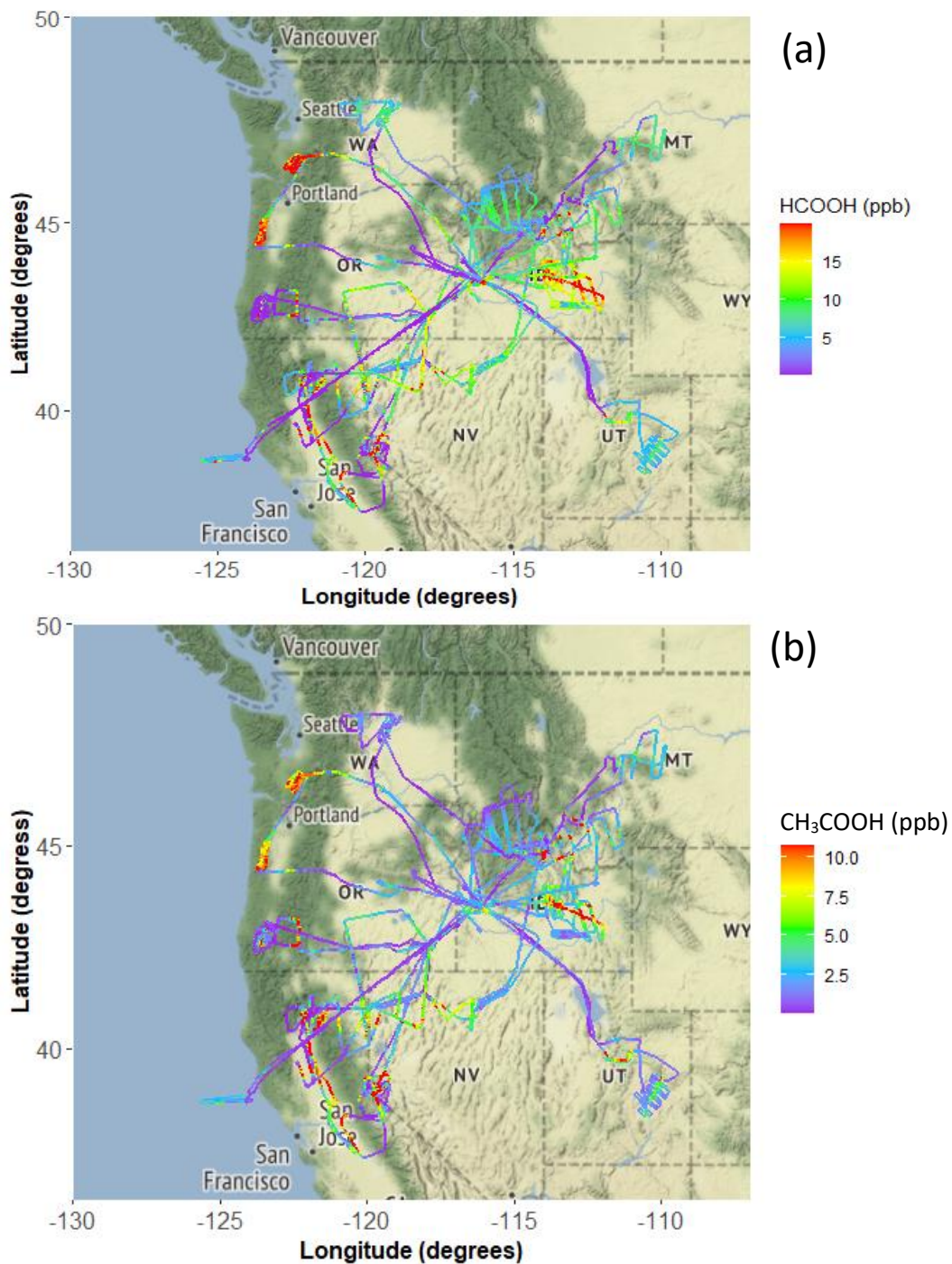


**Figure 1:** Flight paths for all flights during the WE-CAN campaign, with each differing flight path being a different research flight colored by mixing ratio of (a) HCOOH (ppb) measured by the high-resolution time-of-flight chemical ionization mass spectrometer (HRTof-CIMS) and of (b) CH<sub>3</sub>COOH (ppb) measured by proton transfer reaction time-of-flight mass spectrometer (PTR-ToF-MS), overlaying a terrain satellite map from Google Maps of the western United States (Kahle and Wickham 2013; Wickham 2016; Wickham et al. 2016, 2019). All concentrations shown are within the 95<sup>th</sup> percentile of the entire campaign and those larger than the 95<sup>th</sup> percentile were capped at this maximum value. The 95<sup>th</sup> percentile for HCOOH concentrations measured by HRTof-CIMS is 19.84 ppb, while CH<sub>3</sub>COOH concentrations measured by the PTR-ToF-MS are 10.80 ppb.

### ***PTR-ToF-MS general description***

The proton-transfer-reaction time-of-flight mass spectrometer (PTR-ToF-MS 4000, IONICON Analytik, Innsbruck, Austria) from the University of Montana was rack-mounted aboard the C-130 during WE-CAN (Figure 2). The PTR-ToF-MS uses soft chemical ionization, and protonated VOCs are measured at their mass plus 1.008  $m/z$ . Thus, HCOOH is identified as 47.013  $m/z$  and CH<sub>3</sub>COOH at 61.028  $m/z$ . The PTR-ToF-MS reports real-time measurements of VOCs with high response times, sensitivities and mass resolution. The PTR-ToF-MS is composed of a sample inlet, an ion source consisting of a hollow cathode discharge, drift-tube, transfer lens system, and a time-of-flight mass spectrometer (de Gouw and Warneke 2007). Briefly, using ultra-pure water, H<sub>3</sub>O<sup>+</sup> ions are generated within the hollow cathode discharge tube. H<sub>3</sub>O<sup>+</sup> ions are then moved directly from the ion source into a drift tube where ambient air is introduced and mixed directly. VOCs with higher proton affinity than water (691 kJ mol<sup>-1</sup>) will undergo a proton transfer and become ionized. An advantage of this technique is that most VOCs can be ionized while other inorganic and main components of air like N<sub>2</sub> and O<sub>2</sub> are not. Ions are then moved through a series of transfer lenses to focus the ion beam into the TOF mass analyzer. The PTR-TOF-MS uses a reflectron as a grid of charged plates, which bends the flight path and ultimately reaches the detector.

During WE-CAN, the PTR-ToF-MS mass resolution is 2675  $m/\Delta m$  at  $m/z$  47.013 and 3150  $m/\Delta m$  at  $m/z$  61.028, where  $\Delta m$  is the full width at half mass for an ion peak of mass  $m$ . A full mass spectra with a mass-to-charge ratio of 20 – 350  $m/z$  was obtained at 5 Hz for the first 9 research flights, and then 2 Hz for the following 10 flights.

During WE-CAN, the PTR-ToF-MS inlet was sampling air underneath the aircraft at mid-cabin. Ambient air was sampled at 15 – 20 slpm (standard liters per minute) through a heated (60 °C) inlet that was ~3 m of 6.35 mm O.D. PFA tubing to the instrument rack. Once reaching the instrument rack, the main line was sub-sampled directly into the PTR-ToF-MS drift tube through ~100 cm of 1.588 mm O.D. PEEK tubing. Drift tube conditions during the campaign were 810 V, 60 °C, and 3.00 mbar, resulting in a collisional energy (E/N) of 130.5 Td. The residence time from the outside of the plane into the drift tube is less than

2 seconds. However, some VOCs (including HCOOH and CH<sub>3</sub>COOH) may adsorb to the surface of the PFA sampling tubing, creating a delayed response (memory effect) (Müller et al. 2016). Memory lag will cause ambiguous plume mixing ratio measurements, resulting in an underestimation of organic acid mixing ratios inside the smoke plume as well as an overestimation (and tail) of the background. During WE-CAN, ambient background air (outside of the smoke plume) was measured for at least two minutes to allow time for VOCs interacting with the inlet to be flushed out of the system. The PTR-ToF-MS memory lag was improved upon by both heating the inlet and removing the first 60 – 90 seconds of instrument zeroing. More details in PTR-ToF-MS operations and data processes are available at Permar et al. (In review).



**Figure 2:** The PTR-ToF-MS (left) installed on the left side of the (right) NSF/NCAR C-130.

### ***PTR-ToF-MS calibrations with standard gas cylinders***

During WE-CAN, the PTR-ToF-MS was calibrated through an addition of 25 distinct VOCs from two standard gas cylinders (Apel-Reimer Environmental Inc., Miami, Florida, USA with an accuracy stated as 5 % at ~1 ppm) in the range of 1 – 10 ppb. Sensitivities and limits of detection (LOD) for the VOCs calibrated from the gas cylinders are shown in Table 2. The LOD is when our signal/noise (S/N) is 3 and includes a scaling factor that weights sampling time. The detection limits are obtained by finding the root for  $[X]$  in equation 1:

$$\frac{S}{N} = \frac{C_f[X]t}{\alpha \sqrt{C_f[X]t + 2Bt}} = 3 \quad (1)$$

Where  $C_f$  is the sensitivity (cps/ppb) of species  $X$ ,  $B$  is the background signal (cps),  $[X]$  is the concentration of species  $X$  (ppb),  $t$  is the measurement period (s), and  $\alpha$  is a scaling factor estimated from scatter plots of the standard deviation of the background signals versus the background signals (Yuan et al. 2017). A 4-point calibration curve of all species reported an  $R^2$  of 0.99 or larger, with average residual standard errors of less than 10 %. In almost all cases, this residual standard error was less than 3 %. Using a 95 % confidence interval, the standard error of the sensitivities for these calibrated VOCs was typically less than 9 % during the WE-CAN campaign. Thus, campaign sensitivities were averaged and applied to all research flights. Based on the quadrature addition of individual errors, the overall uncertainty for most gas standard VOCs is less than 15 %.

**Table 2:** Average sensitivities and limits of detection at 1 Hz for the 25 species calibrated in the gas cylinders using the PTR-ToF-MS during the WE-CAN campaign obtained by Wade Permar. Both formula masses and protonated masses ( $m/z + 1.008$ ) are given. Also shown are the mixing ratios VOCs present in two compressed cylinders that were purchased and certified in June 2017.

Calibrated Species	Formula Mass (m/z)	Protonated Mass (m/z)	Standard Concentration (ppb)	Sensitivity (ncps ppb <sup>-1</sup> )	Limit of Detection (ppt)
Methanol	32.026	33.034	1022	14.9	234
Propyne	40.031	41.039	1007	9.2	164
Acetonitrile	41.027	42.035	1016	21.0	71
Acetaldehyde	44.026	45.034	1022	18.2	198
Ethanol	46.042	47.050	1019	1.0	1029
1-Butene	56.063	57.071	1003	6.6	149
Acetone	58.042	59.050	972	18.9	131
Dimethyl sulfide (DMS)	62.019	63.027	1000	10.6	83
Furan	68.026	69.034	1022	10.4	65
Isoprene	68.063	69.071	989	6.8	162
Methyl vinyl ketone (MVK)	70.042	71.050	971	14.6	62
Methacrolein (MACR)	70.042	71.050	1007	11.2	116
Methyl ethyl ketone (MEK)	72.058	73.066	1011	16.3	61
Benzene	78.047	79.055	999	9.2	89
2-Methylfuran	82.042	83.050	978	9.6	63
Toluene	92.063	93.071	994	10.2	70
2-Furaldehyde	96.021	97.029	1000	11.3	70
3-Hexanone	100.089	101.097	943	11.8	43
Ethylbenzene	106.078	107.086	1003	4.6	89
<i>m</i> -Xylene	106.078	107.086	990	9.2	53
5-Methylfurfural	110.037	111.045	977	7.4	62
1,2,4-Trimethylbenzene	120.094	121.102	999	8.3	44
1,3,5-Trimethylbenzene	120.094	121.102	989	9.8	49
1,2,3,5-Trimethylbenzene	134.110	135.118	997	10.5	48
$\alpha$ -Pinene	136.125	137.133	967	5.1	108

### *Organic acids' calibrations with permeation tubes*

HCOOH and CH<sub>3</sub>COOH calibrations were completed pre- and post- campaign via an in-house permeation system (Figure 3) (Baasandorj et al. 2015; Veres et al. 2010). This system contains an aluminum block, heater, thermocouple, and two permeation chambers made of PTFE tubes (O.D. of 1.27 cm and I.D. of 0.9525 cm) which can be maintained at constant and uniform temperature. During calibrations, 20 sccm (standard cubic centimeters) of ultra-pure zero grade air were consistently passed through the permeation chamber heated at 45 °C. Home-made permeation tubes (0.635 cm O.D. PFA tube) containing analytical grade of either HCOOH (98% formic acid, ACS grade, EMD Millipore Corporation, Darmstadt, Germany) or CH<sub>3</sub>COOH (acetic acid, glacial, ACS grade, VWR International, LLC) were made and one was placed in the chamber for at least two days prior to calibrations to ensure stable and consistent permeation rates of analytes. Permeation tubes are made by cutting 0.635 cm O.D. PFA tubing approximately 5.08 – 6.35 cm long. A heat gun is directed towards one end of the permeation tube to make malleable. Once translucent, the end of the tube can be clenched shut with needle nose pliers. The end of the tube, after closed, can be reheated to further narrow the end; this allows the permeation tube to fit into the chamber. Once the first end is cooled, the open end can be rinsed and then filled (approximately 1 cm of space at the top) with either HCOOH or CH<sub>3</sub>COOH using a pipet. The heat gun is carefully directed to the top portion of the permeation tube to close. If heat is accidentally directed toward the chemical, the permeation tube may burst and will need to be remade. A second way to create permeation tubes is to heat up the PTFE tubing to fit a solid PTFE cylinder into the end to act as a cap. For WE-CAN permeation calibrations, the first method was used.

The mixing ratio of the desired organic acid from the permeation source is calculated stoichiometrically via a heated catalyst (450 °C, platinum bead, 3.2 mm O.D. 1 % wt. Pt, Sigma Aldrich) converting VOCs to CO<sub>2</sub> and then is measured by a non-dispersive infrared CO<sub>2</sub> detector (LI-840A, LI-COR Biosciences, Lincoln, Nebraska, USA). Ideally, as long as the flow rate of ultra-pure zero grade air and the temperature remain constant, the permeation rate of the tube will also stay consistent. The gas mixture is

then redirected to the PTR-ToF-MS via a dynamic dilution calibration via changing the amount of zero air that VOCs are being diluted into. The uncertainty throughout this in-house permeation system is less than 30 %, with most of the error coming from the CO<sub>2</sub> detector.

Using the schematic of Figure 3, ultra-pure zero grade air (20 sccm) is able to pass through each mass flow controller (FC1, FC2, FC3) based on the calibration step. 3-way valves control the air travel; for example, turning on Valve 13 (V13) will direct air to the PTR-ToF-MS, while turning on V10 or V11 will allow the air to flow from the permeation source to the rest of the system. Prior to sampling, the permeation system should be on for at least 2 days with a constant temperature and zero air flow. To run the permeation system:

1. The background is quantified by running UHP (ultra-high pressure) air as carrier gas through a flow controller (FC3 in Figure 3) and into the CO<sub>2</sub> analyzer. All 3-way valves (VICI Valco Instruments, Huston, TX, USA) are off during this step, and should take 20 minutes minimum (usually 1 hour is safe) to level out. This amount of time is needed to confirm we are actually getting backgrounds and stabilization in the amount of VOC for each step.
2. The VOC concentration from the carrier gas is then found by allowing the gas to flow through the catalyst converter (which converts VOC to CO<sub>2</sub>) followed by the LI-COR. In this step, which takes approximately an hour to stabilize, all of the flow controllers (FC1, FC2, and FC3) are still on, and 3-way valves (V#) labeled as V12, V14, V15, and V16 are also turned on.
3. The concentration of CO<sub>2</sub> from the permeation source and background is found by flowing air through the heated chamber containing either HCOOH or CH<sub>3</sub>COOH and moving directly to the CO<sub>2</sub> analyzer. Again, approximately 1 hour should be spent on this step (20 minutes minimum) to allow for stabilization. Depending on which species is being analyzed, either FC1 and V10 or FC2 and V11 will be on, with FC3 off.
4. The concentration of CO<sub>2</sub> in the permeation source is found by flowing the air through the heated chamber into the catalyst converter followed by the CO<sub>2</sub> analyzer, and V10 (or V11), V12, V14, V15 and V16 are on, while FC3 is off. This step should take around 1-2 hours for the signal to

stabilize. Once stable for at least 30 minutes, the next step can be completed. The amount of organic acid measured for each step is found by the average CO<sub>2</sub> (ppm) recorded from the CO<sub>2</sub> analyzer for each step via the stoichiometry of carbon for species.

5. The amount of organic acid in each permeation tube is found by subtracting the backgrounds from the concentration of VOCs in the permeation source. All steps can be repeated to measure the organic acid from the other permeation tube. HCOOH and CO<sub>2</sub> have a 1:1 ratio of carbon, while CH<sub>3</sub>COOH has the 2:1 ratio of CO<sub>2</sub> which must be accounted for.

After the concentration of HCOOH and CH<sub>3</sub>COOH emitted from the permeation system are found, the PTR-ToF-MS is used to test the VOCs from the permeation source. FC3, V1, and V13 are turned on to get the PTR-ToF-MS zeroing, which should occur for at least 5-10 minutes and then be subtracted from the final signal. FC3 is then turned off, while either V10 or V11 is turned on; this is the second calibration step (the first was a zero). The dilution rate is changed by decreasing the flow through the calibration box catalyst, which is done by the flow controller. Each step only needs to be a few minutes, but long enough for the PTR-ToF-MS trace to stabilize. This step can be repeated two or three times to get a 3 to 4-point calibration.

The CO<sub>2</sub> analyzer and measurements from the PTR-ToF-MS are used to calculate the sensitivity of the VOC during the calibration. Using the dilution equation:

$$M_1V_1 = M_2V_2 \quad (2)$$

Where M<sub>1</sub> is the [VOC] measured from the CO<sub>2</sub> analyzer, V<sub>1</sub> is the 20 sccm of zero air, V<sub>2</sub> is the total dilution (the average instantaneous flow plus the zero-air dilution), and M<sub>2</sub> is the diluted organic acid mixing ratio. The normalized counts per second of the calibrated VOC is calculated by obtaining the peak fitted counts per second, multiplying by 10<sup>6</sup>, and dividing by the H<sub>3</sub>O<sup>18</sup> + H<sub>3</sub>O\*H<sub>2</sub>O<sup>18</sup> signals. The diluted concentration (M<sub>2</sub>) is plotted against the ncps of that VOC to obtain a sensitivity value.

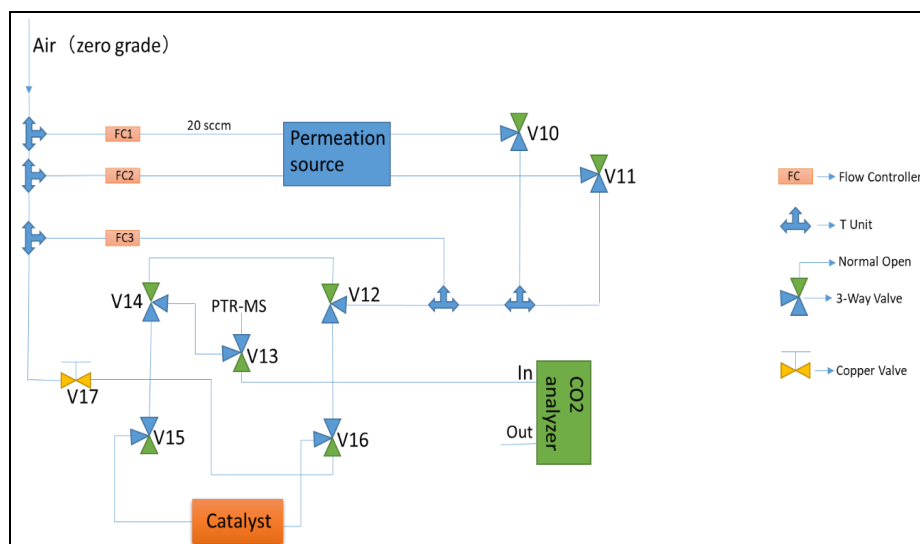


**Figure 3:** The schematic of the in-house permeation system is shown, created by Qian Wang and Wade Permar, with the direction of air flow present. Air is able to pass through each flow controller (FC1, FC2, FC3) depending on the step in the calibration. 3-way valves also control the air travel, with the blue and green arrows on the valve representing the normal open. Turning on valve 13 will allow the air to get directed to the PTR-ToF-MS while turning on valve 10 or 11 will allow the air to flow through the permeation source to the rest of the system. Through these valves, an automation is made to control each step of the permeation calibrations.

### *Organic acid interferences and sensitivities*

Due to the limited mass resolving power in the PTR-TOF-MS, HCOOH measurements could be interfered by dimethyl ether (DME, with protonated  $m/z$  47.069), ethanol ( $m/z$  47.050), and  $N_2H_3O^+$  ( $m/z$  47.024) (Baasandorj et al. 2015; Koss et al. 2017). We did not attempt to identify DME during WE-CAN as no corresponding signals were enhanced due to either no-to-low fire emission or instrument sensitivity. The mass resolution of 2675  $m/\Delta m$  at  $m/z$  47 would also be able to distinguish between DME and HCOOH. Because the instrument sensitivity for ethanol is approximately ten times lower than that of HCOOH ( $\sim 0.5$  ncps ppb $^{-1}$  versus 5.9 ncps ppb $^{-1}$ ) and their counts are so low in wildfires, we can assume that the  $m/z$  47 signal is primarily HCOOH (Baasandorj et al. 2015; de Gouw and Warneke 2007; Yuan et al. 2017).  $N_2H_3O^+$  is thought to be present in all samples but would require a mass resolution of  $\sim 8373$   $m/\Delta m$  to be separated from HCOOH (Figure 4). Since it is constantly present in all measurements and is not likely affected by emission source strengths,  $N_2H_3O^+$  is classified here as an instrumental background. Interferences of  $CH_3COOH$  in PTR-TOF-MS measurements include glycolaldehyde (protonated  $m/z$  61.028), 2-propanol and n-propanol ( $m/z$  61.065), methyl formate ( $m/z$  61.028), peroxyacetic acid

fragment (at  $m/z$  61.028, fragments at 70% when PAA reacts with  $O_2^+$ ), and ethyl acetate fragment (30% fragment at  $m/z$  61.028) (Baasandorj et al. 2015; Fortner et al. 2009; Gilman et al. 2015; Koss et al. 2017; Španěl et al. 2003; Yuan et al. 2017). The PTR-ToF-MS can resolve the propanol molecules from  $CH_3COOH$ . Glycolaldehyde, methyl formate, the PAA fragment, the ethyl acetate fragment, and  $CH_3COOH$  are isomers thus cannot be separated by PTR-ToF-MS. For methyl formate, a small peak can be seen in the GC-MS, but FTIR comparison suggests there is a negligible contribution (Sekimoto et al. 2017). Ethyl acetate is used in coatings, many adhesives and cosmetics, and as a process solvent and is mainly found in anthropogenically polluted areas. PAA is found by the reaction of  $CH_3C(O)O_2$  radicals with  $O_2$ , which may be important when  $NO_x$  concentrations are low (Baasandorj et al. 2015). However, no previous study reports PAA nor ethyl acetate fragments found at  $m/z$  61 while measuring smoke plumes. WE-CAN contribution thus do not include these as interferences (Permar et al, in review).

**Table 3:** Details on organic acids and their potential interferences in PTR-ToF-MS measurements.

Species	Molecular Formula	Interference to HCOOH or $CH_3COOH$ ?	Exact Mass ( $m/z$ )	Protonated Mass ( $m/z$ )	Mass Resolving Power for Separation ( $m/\Delta m$ )
Formic acid	HCOOH	-	46.005	47.013	NA
Acetic acid	$CH_3COOH$	-	60.020	61.028	NA
Dimethyl ether (DME)	$CH_3OCH_3$	HCOOH	46.069	47.077	1471
Ethanol	$CH_3CH_2OH$	HCOOH	46.042	47.050	2543
$N_2H_3O^+$	$N_2H_3O^+$	HCOOH	47.024	NA	8373
Glycolaldehyde	$HOCH_2-CHO$	$CH_3COOH$	60.020	61.028	NA
2-propanol	$CH_3CHOHCH_3$	$CH_3COOH$	60.057	61.065	3301
n-propanol	$CH_3CHOHCH_3$	$CH_3COOH$	60.057	61.065	3301
Peroxyacetic acid fragment	$C_2H_4O_2^+$	$CH_3COOH$	61.028	NA	NA
Ethyl acetate fragment	Unknown	$CH_3COOH$	61.028	NA	NA
Methyl formate	$C_2H_4O_2$	$CH_3COOH$	60.020	61.028	NA

Mass resolving power was calculated by finding the full width half maximum (FWHM) via the mass difference between the interfering species and HCOOH or  $CH_3COOH$  and then dividing by 2. The protonated mass of each interference is divided by the FWHM to obtain a mass resolving power needed for separation.

In biomass-burning plumes,  $CH_3COOH$  concentrations are usually four times higher than glycolaldehyde (Baasandorj et al. 2015; Stockwell et al. 2015), while in an urban environment, glycolaldehyde takes about 20 – 40 % of the  $m/z$  61 peak (Baasandorj et al. 2015). Therefore, we here infer the measured  $m/z$

61 signal has 33 % from glycolaldehyde with the remainder from CH<sub>3</sub>COOH for WE-CAN; data presented here is a combination of CH<sub>3</sub>COOH and glycolaldehyde.

Figure 4 shows an example peak fitting used in WE-CAN along with the interferences present for both organic acids. Interferences are not quantified or further explored in this thesis but may be impacted by reduced electric field (E/N) of the instrument and the relative humidity (RH) during observations (Baasandorj et al. 2015).

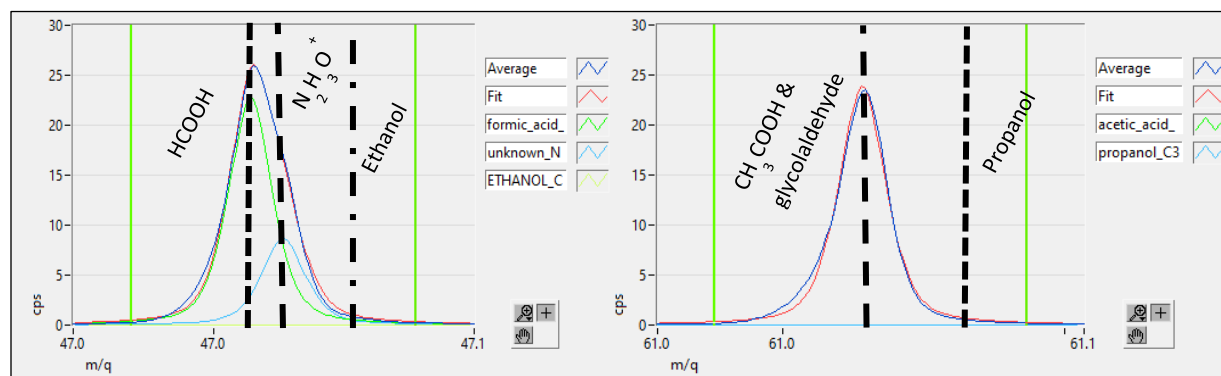


**Figure 4:** Example peak fitting used during WE-CAN for HCOOH and CH<sub>3</sub>COOH. The interferences present for HCOOH with this peak fitting are N<sub>2</sub>H<sub>3</sub>O<sup>+</sup> and ethanol. The ethanol peak is not present in WE-CAN due to a sensitivity 10 times lower than HCOOH. N<sub>2</sub>H<sub>3</sub>O<sup>+</sup> is a shoulder off of the HCOOH peak that is approximately 3 times lower in counts per second (cps) than HCOOH. CH<sub>3</sub>COOH interferences present are glycolaldehyde and propanol, while fragments of peroxyacetic acid or ethyl acetate could also potentially contribute to m/z 61 signals, but no literature has discussed these species present in biomass burning. CH<sub>3</sub>COOH has a sensitivity approximately 200 times larger than that of propanol (hence why it is not present in the peak fitting). During WE-CAN, glycolaldehyde is thought to contribute 33 % while CH<sub>3</sub>COOH is the other 67 % in our m/z 61 signal. Our study calculates a sensitivity of 7.6 ncps ppb<sup>-1</sup> for CH<sub>3</sub>COOH.

For data processing, the PTR-ToF-MS instrument sensitivities for each ion mass were determined using the weighted sensitivity of known isomers for that specific mass. For species with available standard gases (Table 2), their sensitivities were from calibrations conducted during WE-CAN. For those ions/species that were not directly calibrated, their sensitivities were estimated according to their molecular properties (Sekimoto et al. 2017). If ions were contributed by multiples isomers or fragments, the sensitivities for each contributor were then weighted using the fractional information determined from the FIREX lab burning experiment when available (Koss et al. 2018):

$$sensitivity_{average} = \left( \sum \frac{contribution_i}{sensitivity_i} \right)^{-1} \quad (3)$$

As stated above, for PTR-ToF-MS measured  $m/z$  61.028, we attributed 33 % of signals from glycolaldehyde and 67 % from  $\text{CH}_3\text{COOH}$ . The average sensitivity for this mass is thus weighted by the calibrated sensitivity for  $\text{CH}_3\text{COOH}$  and the estimated sensitivity for glycolaldehyde.

### *Sensitivity dependence on relative humidity*

In PTR-MS measurements, it is known that  $\text{HCOOH}$  sensitivity is relative humidity (RH) dependent, and that the sensitivity decreases with humidity throughout the whole range of  $E/N$  (Baasandorj et al. 2015). In contrast,  $\text{CH}_3\text{COOH}$  sensitivity decreases with humidity when there is high collisional energy within the drift tube ( $E/N > 125$  Td) due to fragmentation of a protonated  $\text{CH}_3\text{COOH}$  by water. At a low  $E/N$  ( $< 110$  Td), sensitivity increases with humidity due to the reaction of proton transferring between  $(\text{H}_2\text{O})\text{-H}_3\text{O}^+$  and  $\text{CH}_3\text{COOH}$  (Baasandorj et al. 2015). With an intermediate  $E/N$ , the fragmentation of the protonated  $\text{CH}_3\text{COOH}$  and the proton transfer reaction offset each other, so the sensitivity becomes independent of humidity. Sensitivity towards propanol is extremely low ( $< 1$  % compared to  $\text{CH}_3\text{COOH}$  under instrument operating conditions), so it will not represent significant interference under most circumstances. At  $E/N = 125$  Td, PTR-ToF-MS sensitivity of  $\text{CH}_3\text{COOH}$  decrease with humidity, while glycolaldehyde's sensitivity will increase with humidity. For further detail on sensitivity locations of both organic acids and their interferences, refer to Table 1 of Baasandorj et al. (2015).

During WE-CAN, the relative humidity during sampling for all research flights ranged from 8 – 80 %, with the larger RH occurring during in-cloud sampling or flying over the ocean. PTR-ToF-MS's  $E/N$  was maintained at 130.5 Td during the campaign. Calibrations prior and post- WE-CAN campaign using the in-house permeation system had an  $I_{\text{H}_2\text{O}^*\text{H}_3\text{O}}/I_{\text{H}_3\text{O}^+}$  measured by the PTR-ToF-MS (a proxy to relative humidity (de Gouw and Warneke 2007)) had a range of 0.77 – 0.98 %. Other permeation calibrations of the organic acids were analyzed to allow a larger range of  $I_{\text{H}_2\text{O}^*\text{H}_3\text{O}}/I_{\text{H}_3\text{O}^+}$  (0.77 – 1.84 %) (Figure 5). In comparison, the  $I_{\text{H}_2\text{O}^*\text{H}_3\text{O}}/I_{\text{H}_3\text{O}^+}$  during the WE-CAN campaign ranged from 0.02 – 2.54 %, with an average of  $0.52 \pm 0.33$  %. For the campaign, 93.6 % of the  $I_{\text{H}_2\text{O}^*\text{H}_3\text{O}}/I_{\text{H}_3\text{O}^+}$  signals were  $< 1$  %.

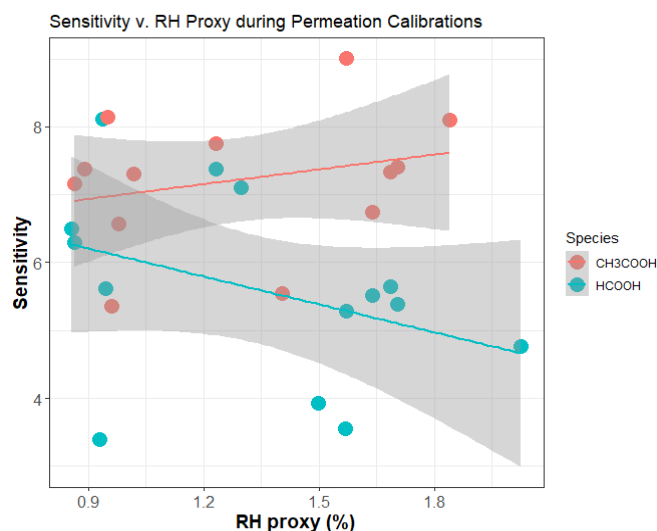


**Figure 5:** Permeation calibrations of HCOOH and CH<sub>3</sub>COOH post and prior the WE-CAN campaign, along with additional calibrations completed during two different field campaigns to obtain a larger range of RH (using PTR-MS's  $I_{H_2O^*H_3O}/I_{H_3O^+}$  and a RH proxy). The shaded area is the 95% confidence interval for predictions from the linear model. The sensitivity for HCOOH is decreasing as  $I_{H_2O^*H_3O}/I_{H_3O^+}$  increases, while the opposite is seen for CH<sub>3</sub>COOH.

The sensitivity for HCOOH is 5.9 ncps ppb<sup>-1</sup> and CH<sub>3</sub>COOH sensitivity is 7.6 ncps ppb<sup>-1</sup> and are applied throughout the entire campaign. However, the HCOOH sensitivity is known to show large decreases in when the  $I_{H_2O^*H_3O}/I_{H_3O^+}$  signals are <1 % (Baasandorj et al. 2015). The lack of humidity-dependent-sensitivity can limit the quality of PTR-MS measured organic acid data. To improve accuracy in concentrations and reduce variability in instrument intercomparisons (Chapter 3) during WE-CAN, future work can include the humidity dependency for organic acid sensitivities.

**Table 4:** Organic acid species were calibrated for the WE-CAN campaign only with our in-house permeation system, depicting the mass identified for each species in the PTR-ToF-MS (protonated mass in m/z), sensitivities, limit of detections, and humidity conditions. The limit of detection was calculated using equation 1 (Yuan et al. 2017).

Calibrated Species	Protonated Mass in PTR-ToF-MS	Sensitivity (ncps ppb <sup>-1</sup> )	LOD (ppt)	Average $I_{H_2O^*H_3O}/I_{H_3O^+}$ (%)
HCOOH	47.013	5.88	450	0.86
CH <sub>3</sub> COOH	61.028	7.58	350	0.89

### ***HRTof-CIMS and quantification***

In addition to the PTR-ToF-MS, the High-Resolution Time-of-Flight Chemical Ionization Mass Spectrometer (HRTof-CIMS) measured HCOOH and CH<sub>3</sub>COOH in real-time during the WE-CAN. The HRTof-CIMS, using an iodide (I<sup>-</sup>) adduct ionization described in detail elsewhere (Lee et al. 2014), was running for all research flights during WE-CAN excluding RF17, RF18, and RF19. Briefly, the HRTof-CIMS has I<sup>-</sup> anions that are produced and collide with neutral analytes inside of an ion-molecule-reaction (IMR) chamber. These clusters are then sampled by the (Tofwerk, AG, Aerodyne Research Inc., Switzerland) high resolution time-of-flight mass spectrometer, which has a high mass resolving power and mass accuracy (ranging between 4500 and 5000  $m/\Delta m$ ).

During WE-CAN, ambient air was sampled at 20 slpm through 18 mm O.D. Teflon tubing that was 40 cm in length. This air was then subsampled into the IMR region. Between the inlet and IMR region, the residence time was < 0.7 seconds. Also, a full inlet zeroing occurred by flowing ultra-high purity N<sub>2</sub> from the entrance of the inlet for 10 seconds approximately every 20 minutes. The IMR was also zeroed by flowing the N<sub>2</sub> at the pinhole through which ambient air enters the IMR region.

Besides full inlet zeroing, the HRTof-CIMS was background corrected within the IMR. Some molecules can adsorb onto the inlet surface while being transported to the instrument. The molecules that adsorb will then desorb and be measured seconds later, creating a tail within the measurements. A 6 second background concentration within the IMR was found every minute (Figure 6). This occurred both in and out of smoke plumes as the background signal changes depending on sampling history. The backgrounds increase with the higher concentrations in smoke plumes and is accounted for to allow the best time response.

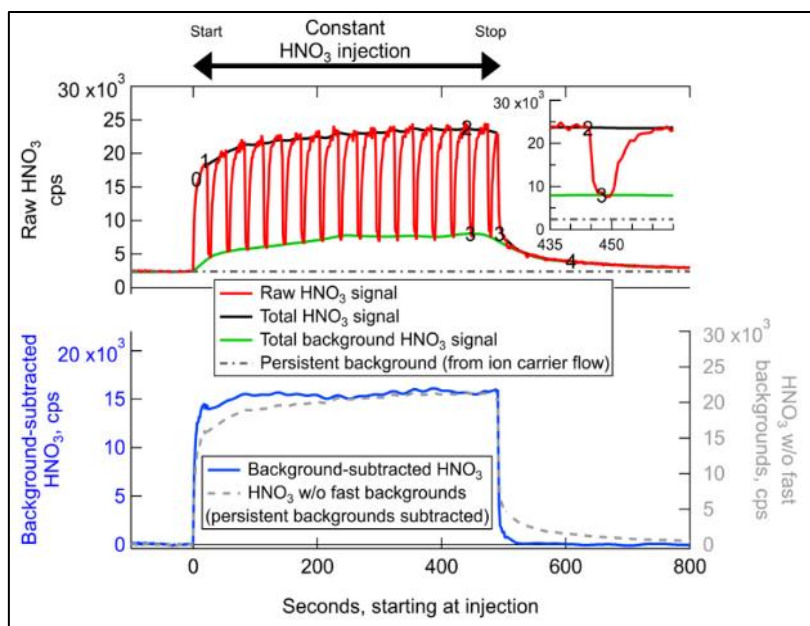


**Figure 6:** During WE-CAN, the HRTof-CIMS background corrected via a fast zeroing (6 second) method for the measurement of a constant 2ppb HNO<sub>3</sub> from a permeation tube. The panel depicts the benefit of a fast background signal subtractions (blue) as opposed to subtracting only a persistent background signal from the ion carrier flow (black). Figure 2b. (Palm et al. 2019).

HCOOH was calibrated in the lab prior to the WE-CAN campaign and completed in a similar manner to the calibrations of HCOOH and CH<sub>3</sub>COOH for the PTR-ToF-MS. Air was flown over a permeation tube with HCOOH present, and the permeation rate was verified through other methods so that the exact concentration flowing into the HRTof-CIMS was known. The relative sensitivity of the HRTof-CIMS during the campaign was calculated by injecting Cl<sub>2</sub> as a calibrant. For more details on HRTof-CIMS during WE-CAN, refer to (Palm et al. 2019) and (Peng et al. 2020).

The PTR-ToF-MS and the HRTof-CIMS organic acid measurements were compared to see if they were within instrument uncertainty of each other (Table 5). The HRTof-CIMS instrument was not calibrated to CH<sub>3</sub>COOH and it is twenty times less sensitive to it than HCOOH. Thus, only the PTR-ToF-MS measurements of CH<sub>3</sub>COOH are used for further analysis.

**Table 5:** Instrument spec details for both the PTR-ToF-MS and HRTToF-CIMS during the WE-CAN campaign. Limit of detection from PTR-ToF-MS was found via equation 1 (Yuan et al. 2017).

Instrument Specs	PTR-ToF-MS	HRTToF-CIMS
Zero frequency	2 minutes every 30 minutes	10 seconds every 20 minutes for full inlet zeroing
Measurement frequency	5 Hz, then 2 Hz <sup>a</sup>	1 Hz
Mass range	0-400 m/z	0-350 m/z
Mass resolution of instrument	> 4000 m/ $\Delta$ m	4500-5000 m/ $\Delta$ m
Ambient air sampling	15-20 slpm; 6.33mm O.D. Teflon at 3m length	20 slpm; 18mm O.D. Teflon at 40cm length
Residence time	< 2 seconds to drift tube	0.01 seconds in inlet
Memory effects corrected by	Heating inlet	6 second backgrounds
Instrument uncertainty	$\pm$ 30%	$\pm$ 30% <sup>b</sup>
Limit of detection for organic acids (ppt)	450 ppt for HCOOH and 350 ppt for CH <sub>3</sub> COOH	20 ppt
Sensitivity	HCOOH and CH <sub>3</sub> COOH decrease with humidity	Sensitive to hydroxyl groups; not very sensitive to CH <sub>3</sub> COOH
Calibrations for organic acids	In-house permeation system; both HCOOH and CH <sub>3</sub> COOH prior and post campaign	In-house permeation system, HCOOH only prior and post campaign

Uncertainty of 30 % in the HRTToF-CIMS is from the permeation system while calibrating HCOOH. HRTToF-CIMS had the ion molecule reaction region (IMR) water vapor corrections for HCOOH via relative sensitivity =  $a \cdot x^2 + b \cdot x + c$ , where  $x$  is the relative ratio of  $I_{H_2O}/I^-$  signal.  $I_{H_2O}/I^-$  is a way to measure the water vapor concentration in IMR, but that concentration is dependent the MS voltages due to clustering/declustering. Refer to Palm et al. 2019 and Peng et al. 2020 for more details. The mass resolution of the instruments is the total mass resolution, not at a specific mass.

<sup>a</sup>. The PTR-ToF-MS had a measurement frequency of 5 Hz for RF01-RF09, and then 2 Hz for RF10 – RF19.

<sup>b</sup>. HRTToF-CIMS specs and uncertainty from (Peng et al. 2020).

### Chapter Three: Instrument intercomparisons for HCOOH

HCOOH measurements were available for both HRTToF-CIMS and the PTR-ToF-MS for all research flights (excluding RF15, RF17, RF18, and RF19). To see if observed HCOOH mixing ratios were consistently larger in the HRTToF-CIMS, emission passes, and time series (the complete flight) were analyzed for each research flight that had both instruments running (Table 6). On average, the HRTToF-CIMS HCOOH concentrations were larger on average by approximately 1.41 times than the PTR-ToF-MS. The ratio of HCOOH measurements from HRTToF-CIMS to PTR-ToF-MS for all research flights range from 0.65 – 2.14, while the  $R^2$  values range between 0.37 and 0.92. However, the research flights with a large ratio and low  $R^2$  are those that included cloud sampling (RF04 and RF06) or during the initial

flight when many instruments were still being tested (RF01). RF16 was the only HRTof-CIMS to PTR-ToF-MS HCOOH ratio that was below 1. If we exclude these flights, we obtain ratios of 1.06 – 1.8 and  $R^2$  of 0.65 – 0.90. The emission pass ratios for all research flights range between 1.03 – 2.07, with  $R^2$  between 0.01 – 0.92. If we exclude RF04 and RF06, the ratios range between 1.03 – 1.58 with  $R^2$  of 0.18 – 0.92. If the emission pass of RF03 is excluded, the  $R^2$  becomes 0.58 – 0.92. These results imply that while the instruments will have some deviation within measurements of HCOOH, the difference between them is quite consistent regardless of the fire.

**Table 6:** The ratios of HRTof-CIMS/PTR-ToF-MS for all research flights using the whole flight path along with emission passes. Research flights 1, 2, 5, 6, 8, 12, 14, 15, and 16 will be removed from further analysis due to (1) no emission pass visible, (2) no smoke sampling occurred, (3) cloud sampling occurred, (4) the distance from the source was unknown, or (5) no pseudo-Lagrangian flight path at a single altitude occurred. During RF15, the PTR-ToF-MS was not running, while the HRTof-CIMS was not running for RF17, RF18, and RF19. The ratio of HRTof-CIMS/PTR-ToF-MS is found by integrating the time series (or emission pass) and taking the ratio between the two integrated instruments. In contrast, the slope is found by calculating the line of best fit when plotting HRTof-CIMS against the PTR-ToF-MS HCOOH measurements.

Research Flight	Whole Flight (CIMS/PTR)	Whole Flight R <sup>2</sup>	Whole Flight Slope	Emission Pass (CIMS/PTR)	Emission Pass R <sup>2</sup>	Emission Pass Slope
1	2.058	0.5525	1.0225	-	-	-
2	1.758	0.7433	1.4302	1.615	0.629	1.6374
3	1.194	0.7485	1.4974	1.354	0.1776	0.6665
4	2.094	0.6975	1.5523	1.577	0.7084	0.9713
5	1.683	0.7693	1.6461	1.486	0.7221	1.4147
6	2.138	0.3702	1.1779	2.069	0.0069	0.1435
7	1.425	0.8901	1.4971	1.451	0.7616	1.5404
8	1.235	0.9041	1.1451	-	-	-
9	1.470	0.7333	1.1936	1.384	0.5768	1.3014
10	1.655	0.6533	1.2408	1.533	0.7977	1.2987
11	1.310	0.8913	1.3378	1.025	0.8522	1.4009
12	1.560	0.919	1.6163	-	-	-
13	1.231	0.8847	1.3035	1.197	0.9177	1.4274
14	1.058	0.8659	1.3623	-	-	-
16	0.6485	0.7469	1.0622	-	-	-

Figure 7 shows the intercomparisons of HCOOH from the two instruments for RF09 and RF11.

Integrating the emission pass shows the HRTof-CIMS to PTR-ToF-MS ratio to be  $1.38 \pm 0.20$  while integrating the entire research flight shows a ratio of  $1.47 \pm 0.30$  for RF09. Integrating the emission pass of RF11 shows the ratio to be  $1.03 \pm 0.20$  while the entire research flight ratio is  $1.31 \pm 0.30$ . However, the uncertainty of the HCOOH measurements is larger in the PTR-ToF-MS, reflected by the larger concentration variation with the plume and background passes. HRTof-CIMS has a lower signal-to-noise present in the HCOOH measurements during WE-CAN (variability of 1 ppb) compared to PTR-ToF-MS (variability of approximately 2 ppb). The background of HRTof-CIMS for HCOOH before entering the smoke plume is approximately 2x larger than when leaving the smoke in RF09, but not apparent in RF11.

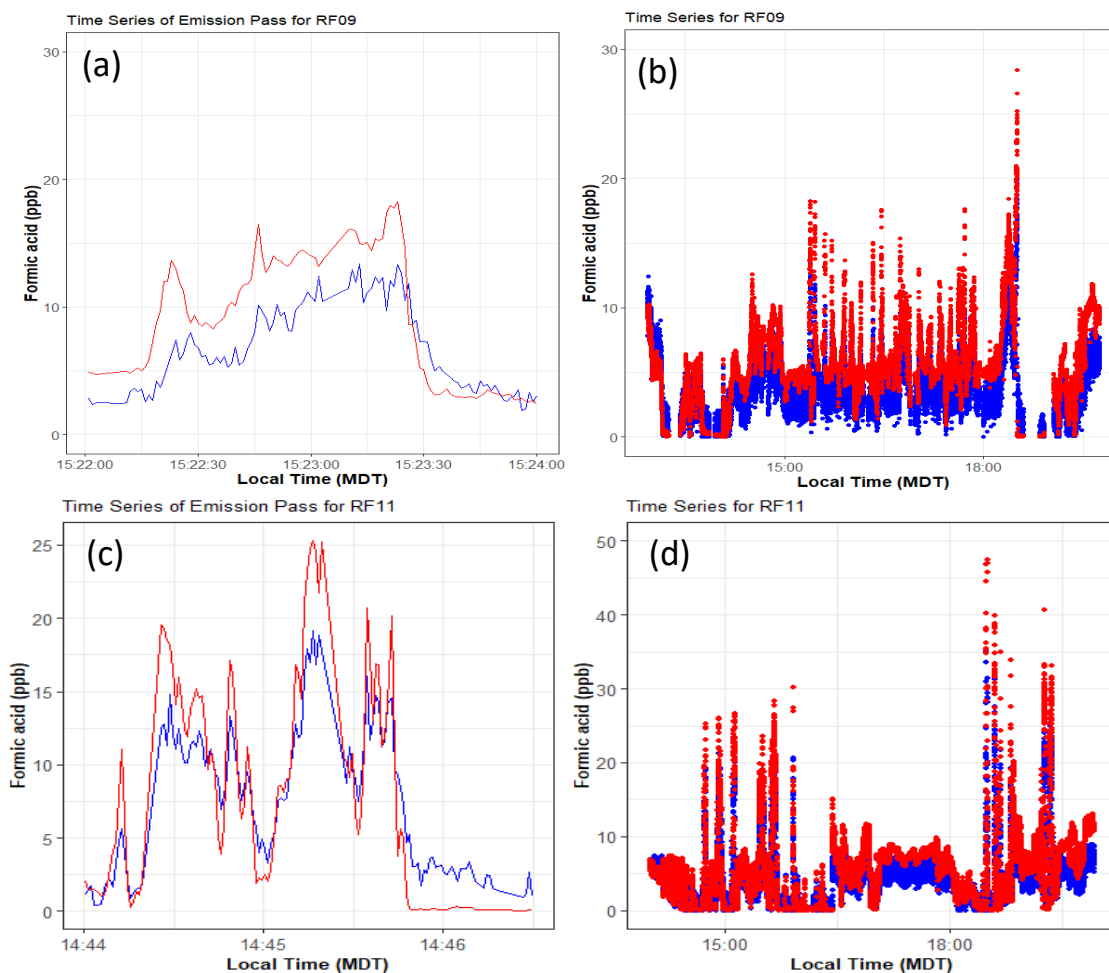


**Figure 7:** Emission pass and time series of research flights 09 (RF09) and 11 (RF11) from HRTof-CIMS (red) and PTR-ToF-MS (blue) HCOOH measurements. For RF09, the emission pass (a) ratio of HRTof-CIMS to the PTR-ToF-MS is 1.38, while the ratio for the entire research flight (b) is 1.47. For RF11, the emission pass (c) ratio of HRTof-CIMS to the PTR-ToF-MS is 1.04, while the ratio for the entire research flight (d) is 1.31.

Aside from the HRTof-CIMS and PTR-ToF-MS HCOOH measurements being compared via integration, they were also compared by finding the line of best fit with each other (Figure 8). Each research flight has the slope of these instruments (HRTof-CIMS:PTR-ToF-MS) to be larger than 1.0, with a range between 1.02 – 1.65 ( $R^2$ 's range 0.37-0.92), indicating HRTof-CIMS HCOOH measurements are larger than PTR-ToF-MS for all flights. HRTof-CIMS to PTR-ToF-MS HCOOH concentrations for the entire flight are 1.19 for RF09 and 1.34 for RF11. Emission pass slopes vary, with RF03, RF04, and RF06 being less than 1 (0.14 – 0.17). RF03 and RF06, with the lowest slopes, also have the smallest  $R^2$  (0.18 and 0.01). For those above 1, slopes range between 1.30 – 1.64 (RF09 is 1.30 and RF11 is 1.40).

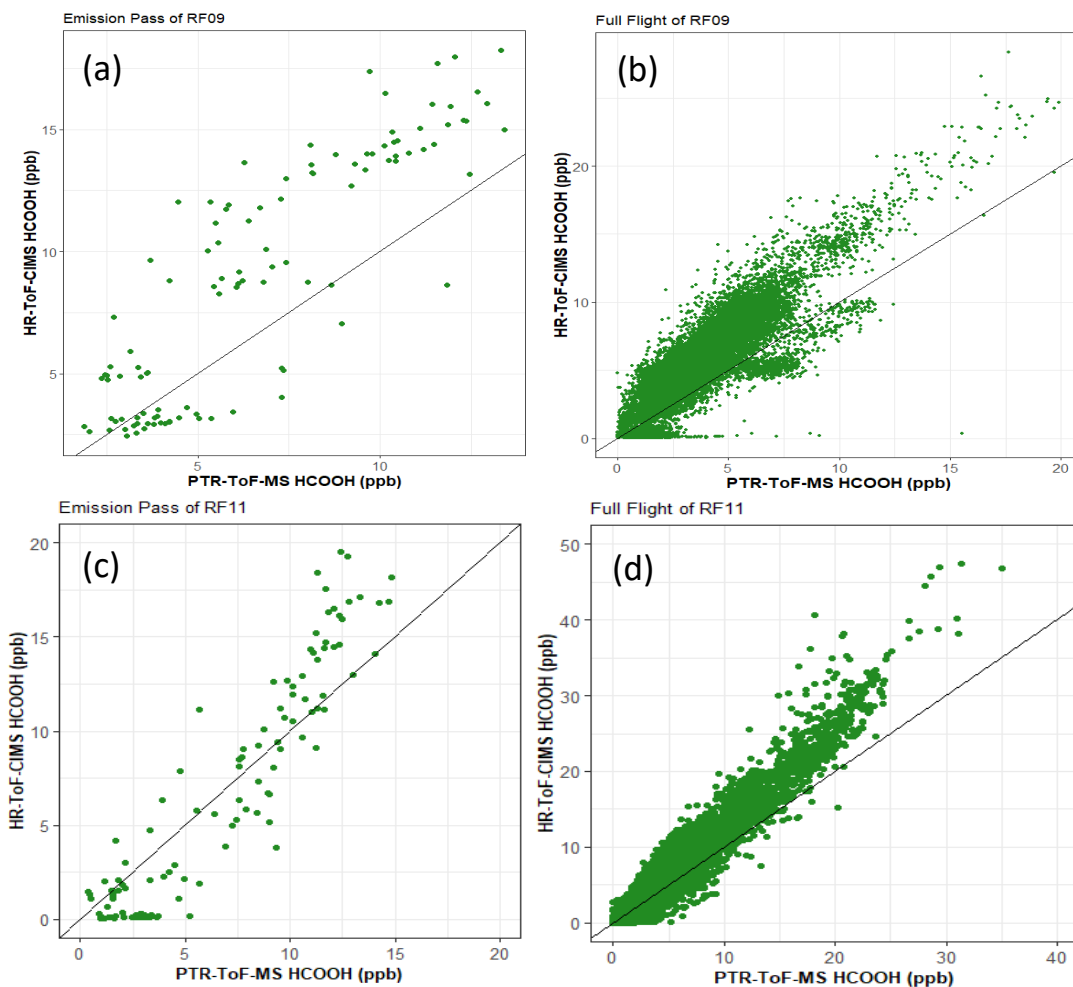


**Figure 8:** Scatter plots of the HRTof-CIMS v. PTR-ToF-MS for the emission passes and time series with a 1:1 line present (black). For RF09, the slope of the emission pass (a) is 1.30 ( $R^2 = 0.58$ ); the time series (b) has a slope of 1.19 ( $R^2 = 0.73$ ). For RF11, the emission pass (c) has a slope of 1.40 ( $R^2 = 0.85$ ), and the total flight (d) has a slope of 1.34 ( $R^2 = 0.89$ ). Both flights and emission passes show that HRTof-CIMS HCOOH measurements are larger than the PTR-ToF-MS.

It is known that HCOOH sensitivity is dependent to relative humidity. Thus, RF09 and RF11 HCOOH measurements (HRTof-CIMS:PTR-ToF-MS) were measured against altitude and the PTR-ToF-MS RH proxy of  $I_{H_2O+H_3O}/I_{H_3O+}$  (Figure 9). RF09 measured the RH proxy between 0 – 1.25 %, while RF11 ranged between 0 – 1.17 %. The ratio of HCOOH measurements between instruments were smallest at high altitude/low RH. The PTR-ToF-MS only calibrated for HCOOH at 0.77 – 0.98 %, and this lack of humidity-dependent-sensitivity can limit the quality of PTR-MS measured organic acid data. With the PTR-ToF-MS and HRTof-CIMS both having an uncertainty of approximately 30 % during the campaign, we can conclude that both the instruments can measure large and fast gradient changes with accuracy. The difference between instruments may be caused by different standards or corrections of humidity dependence for sensitivities. It is inconclusive if these differences between instrument measurements are only systematic, but if so, both the HRTof-CIMS and PTR-ToF-MS are accurate for HCOOH measurements.

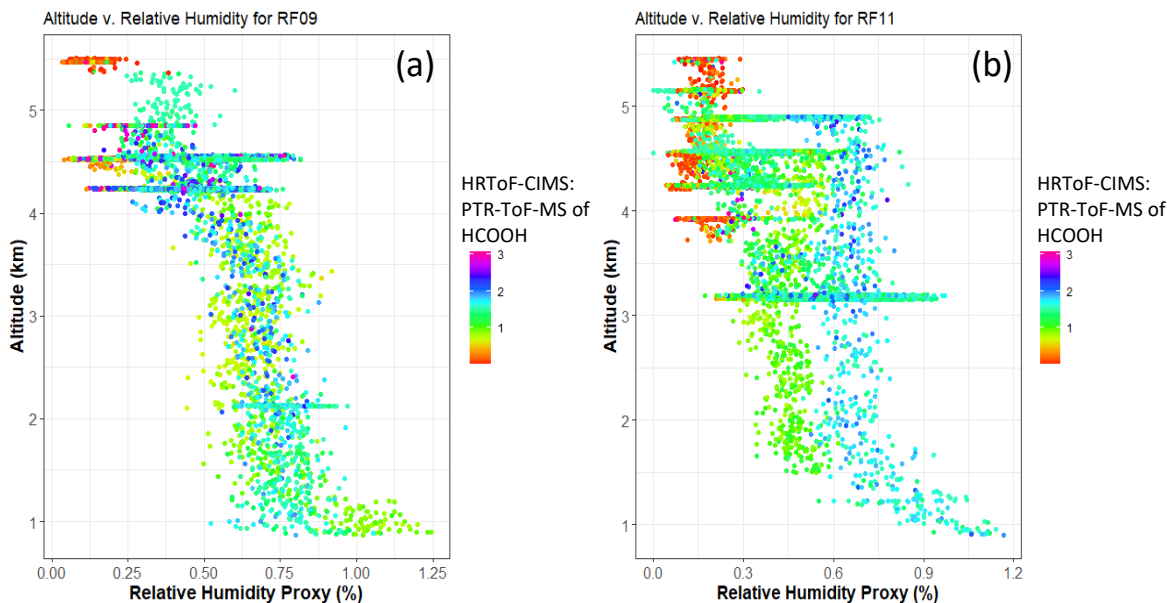


**Figure 9:** (a) Relative humidity proxy, or  $I_{H_2O+H_3O}/I_{H_3O+}$ , was compared to altitude and the ratio of HCOOH from HRTof-CIMS and PTR-ToF-MS. With an altitude increase, the RH proxy decreases. The colors represent the ratio of HRTof-CIMS and PTR-ToF-MS. For RF09, the  $I_{H_2O+H_3O}/I_{H_3O+}$  ranges from 0 – 1.25 %. For RF11 (b), the  $I_{H_2O+H_3O}/I_{H_3O+}$  is 0 – 1.17 %. In contrast, the permeation calibrations of HCOOH (and  $CH_3COOH$ ) have a range of 0.77 – 0.98 %.

In this work, the PTR-ToF-MS had an average sensitivity applied throughout the entire campaign (5.9 and 7.6 ncps ppb<sup>-1</sup> for HCOOH and CH<sub>3</sub>COOH, with  $I_{\text{H}_2\text{O}^*\text{H}_3\text{O}}/I_{\text{H}_3\text{O}^+}$  at 0.77 – 0.98 % during calibrations). The flights with higher RH will not be as accurate. If, in the future, HCOOH sensitivity is tested among many RH's, and a line of best fit is applied, the sensitivity can be calculated from the RH. At higher RH, the sensitivity of HCOOH is lower. This in turn will increase our concentration reported and will reduce the difference between HRTof-CIMS and PTR-ToF-MS HCOOH measurements. Thus, for the analysis thereafter, the HRTof-CIMS HCOOH concentrations were used due to the lower LOD and signal-to-noise. CH<sub>3</sub>COOH concentrations from the PTR-ToF-MS were used instead of from HRTof-CIMS since it is more sensitive to CH<sub>3</sub>COOH and was calibrated both pre- and post-campaign.

This campaign was unique in which there were multiple instruments measuring similar VOCs or aerosols to allow for instrument intercomparisons such as this. In most experiments, only one instrument present measures a set of VOCs (such as organic acids). In future campaigns, if the PTR-ToF-MS is the instrument present measuring organic acids, recommendations include setting the E/N at an intermediate Td, such as 125, calibrating prior and post campaign at a range of RH's to allow for a relative humidity correction, and frequent calibrating (every 1-2 days) in the field to capture the natural RH variability and how it affects the instrument sensitivities.

## **Chapter Four: Emissions**

### ***Emission ratio***

WE-CAN emission ratios (ERs) and emission factors (EFs) were found for 31 emission passes of 14 fires, including 1 prescribed burn. Criteria to be used for these calculations included that plume transects had to be from a well-defined smoke plume that could be traced to a single emission source, the transect was closest to the source of the fire, and there was a physical age of less than 130 minutes (Permar et al. In review). Physical age was obtained through wind speeds measured on the C-130 and the location of fire source as reported in the U.S. Forest Service (<http://catalog.eol.ucar.edu/we-can/tools/fuels>).

During WE-CAN, all HCOOH and CH<sub>3</sub>COOH mixing ratios were averaged to 1 Hz. For this campaign (excluding RF17, RF18, and RF19 for HCOOH measurements, and RF15 for both HCOOH and CH<sub>3</sub>COOH), a majority of the HCOOH concentrations are below 1.0 ppb, and below 4.0 ppb for CH<sub>3</sub>COOH (Figure 10). During WE-CAN, HCOOH and CH<sub>3</sub>COOH have a correlation ( $R^2$ ) of 0.56, which suggests similar sources. HCOOH concentrations ranged between  $3.34 \times 10^{-3}$  – 98.10 ppb for HRTof-CIMS and  $6.77 \times 10^{-4}$  – 54.09 ppb for PTR-ToF-MS. CH<sub>3</sub>COOH concentrations ranged between  $1.68 \times 10^{-5}$  – 94.16 ppb (measured by the PTR-ToF-MS), and CO had a range of 53.5 – 7969 ppb. However, fires that sampled cleaner air had lower maximum concentrations of 21.7 ppb for HCOOH (HRTof-CIMS), 14.99 ppb HCOOH (PTR-ToF-MS), and 15 ppb CH<sub>3</sub>COOH.

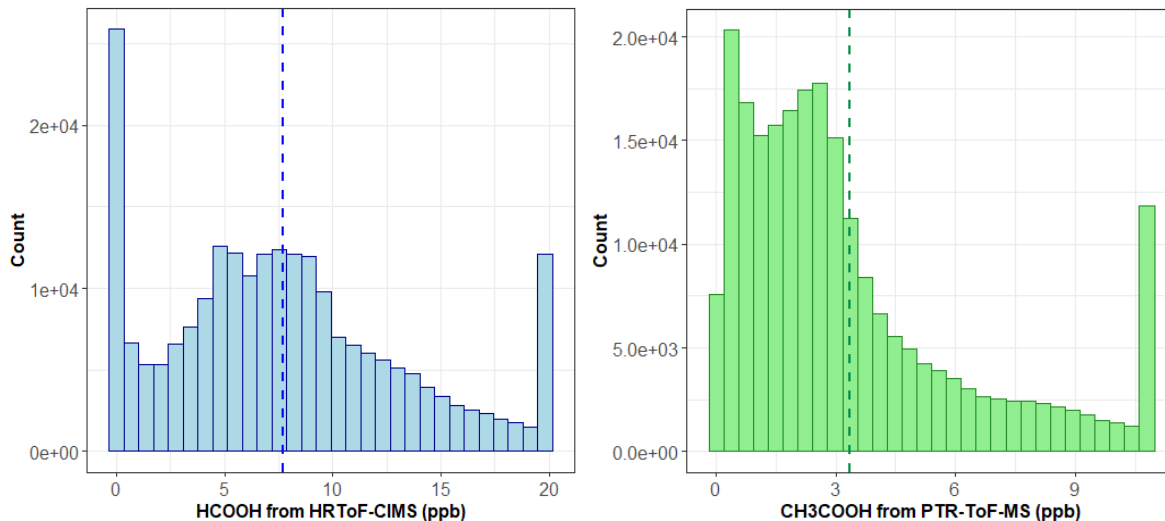


**Figure 10:** Histograms of HCOOH (left) and CH<sub>3</sub>COOH (right) concentrations averaged to 1 Hz during the WE-CAN campaign. All concentrations shown are within the 95<sup>th</sup> percentile of the entire campaign and those concentrations larger than the 95<sup>th</sup> percentile were capped at this maximum value. The 95<sup>th</sup> percentile for HCOOH concentrations measured by HRTof-CIMS is 19.84 ppb, while CH<sub>3</sub>COOH concentrations measured by the PTR-ToF-MS are 10.80 ppb. The dashed vertical line depicts the mean of both organic acids mixing ratios (3.16 ppb for CH<sub>3</sub>COOH and 7.05 ppb for HCOOH).

When the C-130 flight path repeated the sampling of emissions, those sampled within 30 minutes of each other were averaged, while those larger than 30 minutes apart were classified as individual fires. Using these criteria, 24 fires and their emissions were found. Further details on each emission pass during WE-CAN are discussed in Permar et al. (in review) and also shown in Table 1A. Emission ratios (ERs) are calculated by the integration of background corrected in-plume measurements of desired VOCs (HCOOH

and CH<sub>3</sub>COOH as X) divided by the integrated CO concentration, as Y (Equation 4). CO is chosen as the reference species as it is a wildfire tracer, long-lived species, and can account for the dilution effects within a smoke plume. It is noted that ERs are calculated via integration PTR-ToF-MS and CO real-time measurements instead of finding the slope of the least-squares regression. For the case of all emission passes, the difference between the two approaches for ER are small when there are large enhancements.

$$ER = \frac{\sum \Delta X}{\sum \Delta Y} = \frac{\sum (X_{plume} - X_{background})}{\sum (Y_{plume} - Y_{background})} \quad (4)$$

During WE-CAN, the ERs range between 2.1 – 13.4 ppb(HCOOH) ppm(CO)<sup>-1</sup> and 6.4 –16.7 ppb(CH<sub>3</sub>COOH) ppm(CO)<sup>-1</sup> for each fire, with HCOOH ERs lower than CH<sub>3</sub>COOH. On average for this campaign, ERs were 6.1 ± 2.6 ppb(HCOOH) ppm(CO)<sup>-1</sup> and 11.5 ± 2.2 ppb(CH<sub>3</sub>COOH) ppm(CO)<sup>-1</sup>. During the first 60 minutes of physical aging, ERs increase (5.2 ppb(HCOOH) ppm(CO)<sup>-1</sup> and 5.5 ppb(CH<sub>3</sub>COOH) ppm(CO)<sup>-1</sup>). Both ERs tend to stabilize after the first hour, likely reflecting a compensation of chemical productions and losses (Figure 11). If applying a linear fit for all ERs, HCOOH shows an increasing trend of 1.5 ppb/ppmCO/hour, and 0.5 ppb/ppmCO/hour for CH<sub>3</sub>COOH. We did not observe correlations between ERs and combustion phases (as indicated by modified combustion efficiency; see discussion below). Thus, the large variations in ERs (and the increasing tendency within 1-2 hours of aging) from WE-CAN emission passes could imply secondary formation of organic acids within smoke plumes, even prior to the C-130 sampling, and that HCOOH has much faster chemistry than CH<sub>3</sub>COOH within fire smoke.

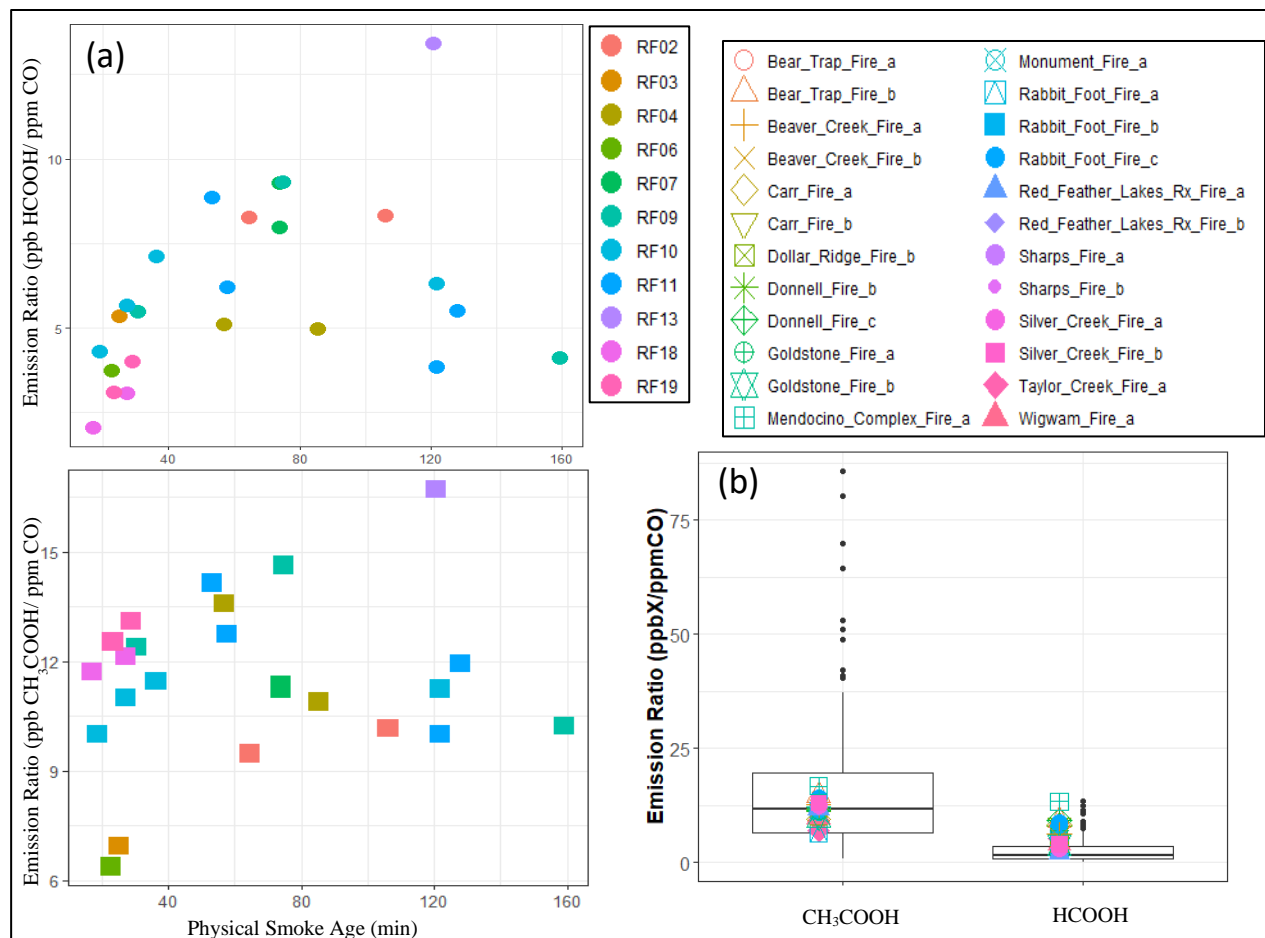


**Figure 11:** (a) Emission ratios of HCOOH (top) and CH<sub>3</sub>COOH (bottom) observed in WE-CAN research flights (excluding those that did not have a distinct emission pass, no data was available, or only cloud sampling occurred). On average, we see an increase of 1.5 ppb/ppmCO/hour for HCOOH, and 0.5 ppb/ppmCO/hour for CH<sub>3</sub>COOH. These reported ERs were also compared to previous literature (b) with the boxplot being all 156 CH<sub>3</sub>COOH and 168 HCOOH ERs from 10 previous studies. Data points represent each WE-CAN fire.

Emission ratios in previous literature (10 studies) that have been reported range between 0.2 – 13.4 ppb(HCOOH) ppm(CO)<sup>-1</sup> and 0.9 – 85.6 ppb(CH<sub>3</sub>COOH) ppm(CO)<sup>-1</sup>. HCOOH literature ERs have 168 data points and average to  $2.7 \pm 2.6$  ppb(X) ppm(CO)<sup>-1</sup>, while CH<sub>3</sub>COOH have 156 data points with an average of  $15.5 \pm 14.1$  ppb(X) ppm(CO)<sup>-1</sup> (Akagi et al. 2012; Bertschi et al. 2003; Christian et al. 2003; Goode et al. 2000; Koss et al. 2018; Mckenzie et al. 1995; Müller et al. 2016; Stockwell et al. 2015; Yokelson et al. 1999, 2003). HCOOH ERs during WE-CAN span the 25<sup>th</sup> percentile to maximum outliers of previous literature ER values, which validates the hypotheses of fast formation of HCOOH during WE-CAN prior to sampling. In contrast, our CH<sub>3</sub>COOH ERs align well with previous literature, as it fits

within the 25<sup>th</sup> – 75<sup>th</sup> percentile (Figure 10b). More details of emission ratios from previous studies are in Appendix C, Table C1.

Physical ages are not reported in most previous studies though they were likely to be less than a few hours, and I do not attempt to further compare to the WE-CAN results. Future investigations on the relationship between emission ratios and smoke age from all available studies can help examine the chemistry of organic acids in early/young smoke. The relationship of normalized excess mixing ratios (NEMR) and smoke age (Chapter 5) is an initial attempt to examine this chemistry within WE-CAN observations.

### ***Emission factor and modified combustion efficiency***

Emission factors (EFs), expressed as the amount of VOC emitted per amount of fuel burned in grams per kilogram, were calculated using the carbon balance method where it is assumed that all burnt carbon is volatilized and detected (Yokelson et al. 1999; Yokelson, Griffith, and Ward 1996):

$$EF_{VOC_i}(VOC_i) = F_c \times 1000 \left( \frac{g}{kg} \right) \times \frac{MW_{VOC_i}}{12} \times \frac{\frac{\Delta VOC_i}{\Delta CO}}{\sum_{j=1}^n (NC_j \times \frac{\Delta VOC_i}{\Delta CO})} \quad (5)$$

With  $F_c$  corresponding to the mass fraction of carbon within the fuel (45.7 % for western US fuels (Liu et al. 2017; Santín et al. 2015)),  $MW_{VOC_i}$  is the molecular weight of the desired VOC ( $VOC_i$ ), 12 is the atomic mass of carbon,  $\frac{\Delta VOC_i}{\Delta CO}$  is the background corrected mixing ratio of  $VOC_i$  to CO, and  $NC_j$  is the number of carbon atoms in species  $j$  summed over all species. During the WE-CAN campaign, the average EFs are  $1.45 \pm 0.57 \text{ g kg}^{-1}$  (range 0.53-2.39) for HCOOH and  $2.38 \pm 0.57 \text{ g kg}^{-1}$  (range 1.15-3.16) for CH<sub>3</sub>COOH (Permar et al. In review). EFs and ERs for both HCOOH and CH<sub>3</sub>COOH, along with MCEs for each fire during WE-CAN are reported in Table 7.

**Table 7:** Emission factors and emission ratios of HCOOH and CH<sub>3</sub>COOH during WE-CAN with MCE and physical smoke age for each “unique” fire. Those with “-“ for HCOOH emission factors were when the HRTof-CIMS was not running.

Fire Name	Flight	EF HCOOH (g/kg)	EF CH <sub>3</sub> COOH (g/kg)	ER HCOOH (ppb/ppmCO)	ER CH <sub>3</sub> COOH (ppb/ppmCO)	Physical Smoke Age (min)	MCE
Carr Fire (a)	02	1.96	1.28	8.33	9.47	64.47	0.938
Carr Fire (b)	02	1.72	1.55	8.27	10.2	106.12	0.930
Taylor Creek Fire	03	0.841	1.15	5.34	6.95	25.03	0.937
Sharps Fire (a)	04	0.916	2.47	4.97	13.6	56.74	0.904
Sharps Fire (b)	04	1.02	1.93	5.12	10.9	85.38	0.917
Rabbit Foot Fire (a)	06	0.807	1.60	3.75	6.38	22.58	0.886
Donnell Fire (a)	07	1.10	2.30	7.97	11.2	73.87	0.902
Donnell Fire (b)	07	2.21	2.28	9.30	11.4	73.87	0.902
Bear Trap Fire (a)	09	1.08	2.43	5.48	12.4	30.4	0.907
Bear Trap Fire (b)	09	1.64	3.13	9.32	14.6	74.72	0.898
Dollar Ridge Fire	09	0.525	2.13	4.13	10.2	159.1	0.900
Rabbit Foot Fire (b)	10	1.65	2.52	7.12	11.3	121.69	0.891
Monument Fire	10	2.24	3.16	5.68	11.0	27.34	0.855
Wigwam Fire	10	0.857	2.25	6.33	11.5	36.34	0.889
Goldstone Fire (a)	10	2.14	2.94	4.32	10.0	18.81	0.869
Goldstone Fire (b)	11	1.17	2.76	6.21	12.8	57.77	0.867
Rabbit Foot Fire (c)	11	1.74	3.02	5.52	11.9	128	0.894
Beaver Creek Fire (a)	11	0.882	1.89	3.85	10.0	121.69	0.930
Beaver Creek Fire (b)	11	1.27	2.88	8.88	14.2	53.31	0.883
Mendocino Complex	13	2.39	3.08	13.4	16.7	120.63	0.913
Red Feather Fire (a)	18	-	2.22	2.06	11.7	17.04	0.910
Red Feather Fire (b)	18	-	2.61	3.08	12.1	27.31	0.898
Silver Creek Fire (a)	19	-	2.99	3.10	12.5	23.32	0.882
Silver Creek Fire (b)	19	-	2.65	4.02	13.1	28.88	0.903

Emission factors were also compared to previous literature, including 16 different papers which contained 365 EFs for HCOOH, and 316 for CH<sub>3</sub>COOH (Figure 12). Of these, 139 HCOOH and 176 CH<sub>3</sub>COOH data points were compiled by Smoke Emissions Reference Application (SERA), with the average EF of HCOOH of  $0.28 \pm 0.26$  g/kg while CH<sub>3</sub>COOH is  $2.06 \pm 1.78$  g/kg (Prichard et al. 2020).

Literature sampling varied in location of study, fuel types measured, and whether they were laboratory or field experiments (Table 8). CH<sub>3</sub>COOH EFs from WE-CAN are within the inner quartile range (25<sup>th</sup> – 75<sup>th</sup> percentile) of literature values, reflecting a relatively good constraint on CH<sub>3</sub>COOH emissions.

HCOOH EFs from WE-CAN are all above the median, with all fires being above the 75<sup>th</sup> percentile of literature. As shown in Figure 8, HCOOH ER increased  $5.15 \text{ ppb ppm(CO)}^{-1}$  within the first hour since emission, likely reflecting fast formation from photochemistry. There is not a significant difference in

reported EFs between previous lab and field studies, but it is possible that previous field studies may also be impacted by aged smoke.

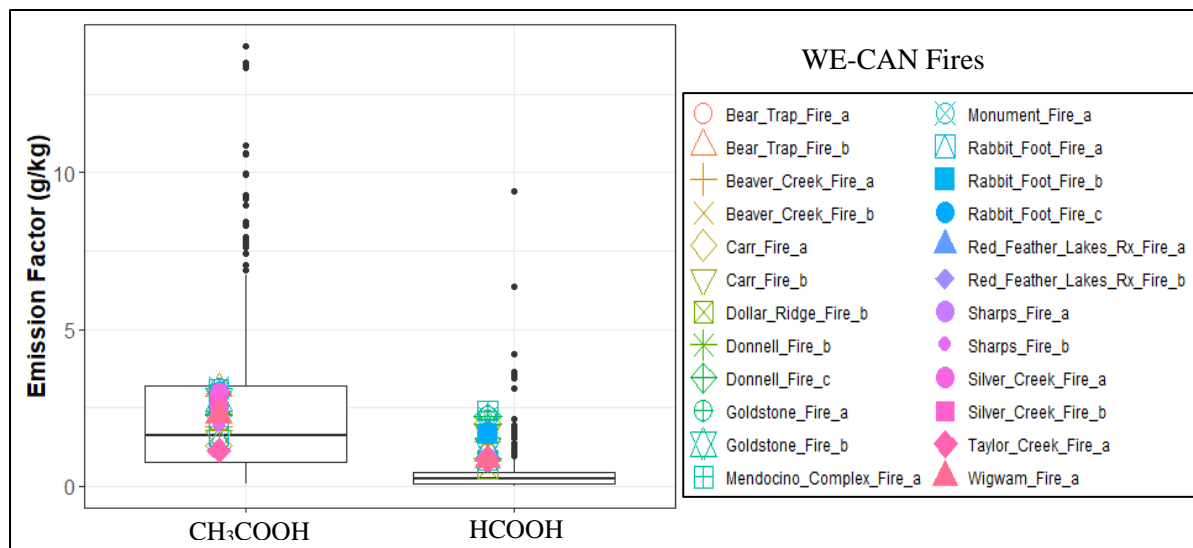


**Figure 12:** Emission factors of HCOOH and CH<sub>3</sub>COOH from both WE-CAN observations and literature. The box and whisker plots consist of all reported HCOOH and CH<sub>3</sub>COOH literature EFs from studies in Table 8 (365 points for HCOOH and 316 for CH<sub>3</sub>COOH). WE-CAN EFs are shown in colored symbols.

I then further assess the compiled EFs from previous studies in the context of WE-CAN and explore if they could differ because of varying fuel or sampling methods (field or laboratory burning). Table 8 shows average reported HCOOH and CH<sub>3</sub>COOH EFs and MCE values for previous literature. All EFs from previous literature are shown in Table C2 in Appendix C. Approximately 23 % of reported literature measurements were obtained via field samples. Two of these papers discuss the same laboratory burning experiment, the Fire Influence on Regional to Global Environments (FIREX, <https://www.esrl.noaa.gov/csl/projects/firex/firelab>), but different instruments (OP-FTIR from (Selimovic et al. 2018) and PTR-ToF-MS from (Koss et al. 2018)) were used that obtained emissions for HCOOH and CH<sub>3</sub>COOH. Fuel locations for these studies listed range from the east coast of the USA to Alaska, and from Africa to Mexico. The range of EFs for HCOOH is 0.00 – 4.17 g kg<sup>-1</sup> (with two larger values of 6.359 and 9.391 g kg<sup>-1</sup>) while CH<sub>3</sub>COOH is 0.08 – 14.01 g kg<sup>-1</sup>. For all previous literature, EFs of

HCOOH are always lower than CH<sub>3</sub>COOH, which is consistent with WE-CAN fires. This implies that this should be the case for all fires, regardless of fuel or study type.

**Table 8:** Average EFs and MCE with standard deviations reported for previous literature, along with if the study came from field or laboratory campaigns. For unreported EFs or MCE, a “-” is present. If only one EF or MCE was reported, no standard deviation is shown.

Author and Year	Average EF CH <sub>3</sub> COOH (g/kg)	Average EF HCOOH (g/kg)	MCE	Laboratory or Field	Dominating Fuels <sup>a</sup>	Instrumentation <sup>b</sup>
Akagi et al., 2013	1.913 ± 0.90	0.078 ± 0.03	0.904 ± 0.05	Field	South Carolina USA fuels	AFTIR
Bertschi et al., 2003	4.870 ± 2.8	1.233 ± 1.1	0.868 ± 0.02	Laboratory	Montana USA and Zambia, Africa fuels	OP-FTIR
Burling et al., 2010	1.572 ± 2.1	0.180 ± 0.22	0.939 ± 0.03	Laboratory	Southeast and Southwest USA fuels	OP-FTIR
Burling et al., 2011	1.67 ± 1.6	0.092 ± 0.08	0.897 ± 0.06	Field	North Carolina and Southwest USA fuels	AFTIR
Christian et al., 2003	8.348 ± 3.9	0.66 ± 0.56	0.879 ± 0.05	Laboratory	Indonesia and Africa fuels	OP-FTIR/PTR-MS
Goode et al., 1999	1.279 ± 0.56	0.570 ± 0.33	0.966 ± 0.01	Laboratory	Grass fires	OP-FTIR
Goode et al., 2000	2.550 ± 0.67	1.132 ± 0.31	0.921 ± 0.01	Field	Alaska USA fuels	AFTIR
Koss et al., 2018	-	0.277 ± 0.22	0.929 ± 0.04	Laboratory	Western USA fuels	PTR-ToF-MS
McKenzie et al., 1995	2.644 ± 2.4	0.534 ± 0.37	-	Laboratory	Montana USA fuels	GC-FID
Müller et al., 2016	0.470	0.130	0.900	Field	Georgia USA fuels	PTR-ToF-MS
Selimovic et al., 2018	1.988 ± 1.6	0.275 ± 0.25	0.926 ± 0.04	Laboratory	Western USA fuels	OP-FTIR
Stockwell et al., 2015	2.427 ± 2.9	0.259 ± 0.34	0.938 ± 0.05	Laboratory	Global fuels	PTR-ToF-MS
Yokelson et al., 1999	3.110	1.170	0.927	Field	North Carolina USA fuels	AFTIR
Yokelson et al., 2003	2.437 ± 0.80	0.729 ± 0.35	0.938 ± 0.02	Field	African savanna fires	AFTIR
Yokelson et al., 2007	3.431 ± 0.41	0.587 ± 0.45	0.910 ± 0.02	Field	Tropical forest, Amazon fuels	AFTIR
Yokelson et al., 2011	3.074 ± 2.6	1.677 ± 2.2	0.925 ± 0.03	Field	Mexican fuels	AFTIR

<sup>a</sup>. “Dominating fuels” is where fuels were sampled and what area of the world they are reflecting.

<sup>b</sup>. Instrumentation acronyms include Airborne Fourier Transfer InfraRed (AFTIR) spectrometer, Open-path Fourier Transfer InfraRed (OP-FTIR) spectrometer, Proton Transfer Reaction Mass spectrometer (PTR-MS), and gas chromatography flame ionization detector (GC-FID).

Emission factors from previous studies were categorized by both the fuel type and field/laboratory to learn if either of these significantly affect EFs reported (Figure 13). 38 % of reported fuel in previous

studies are classified as conifer forest (n = 153 for HCOOH and n = 128 for CH<sub>3</sub>COOH), which is mainly what WE-CAN sampled. Other fuel types found in literature include organic soil, shrubland, hardwood forest, mixedwood forest, and other (garbage, cookstove fuel, and charcoal burning). Organic soil is the second fuel most frequently sampled (n = 70 for HCOOH and n = 69 for CH<sub>3</sub>COOH). For HCOOH, shrubland fuel EFs from the laboratory are more available and larger than field measurements, while both hardwood and mixedwood forest fuel obtained in field measurements are more widely reported and larger than laboratory studies. Conifer forests fuel EFs for HCOOH do not have significant differences between field and laboratory measurements. Organic soil, hardwood forest, and conifer forests have the largest EFs reported. Similar trends as HCOOH occur for CH<sub>3</sub>COOH EFs. Fuel type does not seem to explain much, if any, variability of EFs.

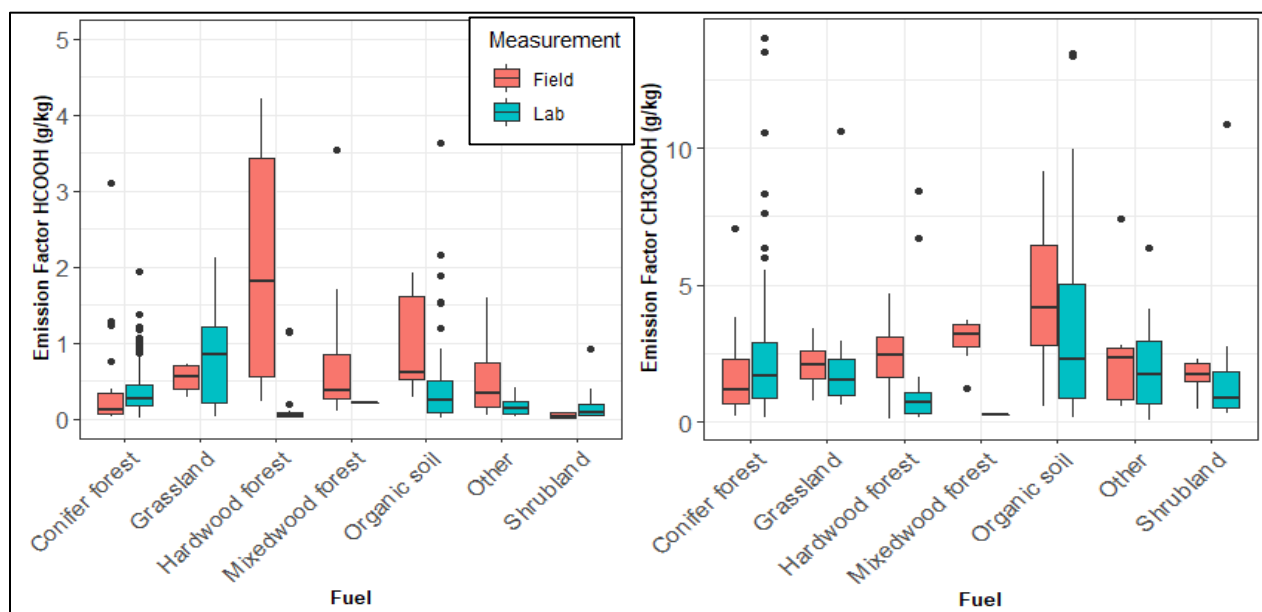


**Figure 13:** HCOOH and CH<sub>3</sub>COOH EFs from previous studies (Table 8 for overarching details or Table C2 for all reported EFs in each publication) categorized both by fuel sampled and if measurements were from the field or laboratory.

Modified combustion efficiency (MCE) was also calculated to explore if combustion phase could explain part of the variability of EFs. MCE is a proxy for the degree of flaming versus smoldering combustion.

MCE uses the plume integrated excess CO and CO<sub>2</sub> mixing ratios following:

$$MCE = \frac{\Delta CO_2}{\Delta CO_2 + \Delta CO} \quad (6)$$

Pure flaming combustion has MCE values around 0.99 from laboratory studies, while smoldering MCE range 0.65 – 0.85 (Akagi et al. 2011). In Figure 14, the MCE during WE-CAN ranged between 0.855 – 0.938, while those in previous studies have a larger range of 0.683 – 0.985. WE-CAN HCOOH EFs have poor correlation with MCE ( $R^2 = 0.03$ ). In contrast,  $CH_3COOH$  EFs correlate better than HCOOH in both previous studies ( $R^2 = 0.25$ ) and WE-CAN ( $R^2 = 0.51$ ).

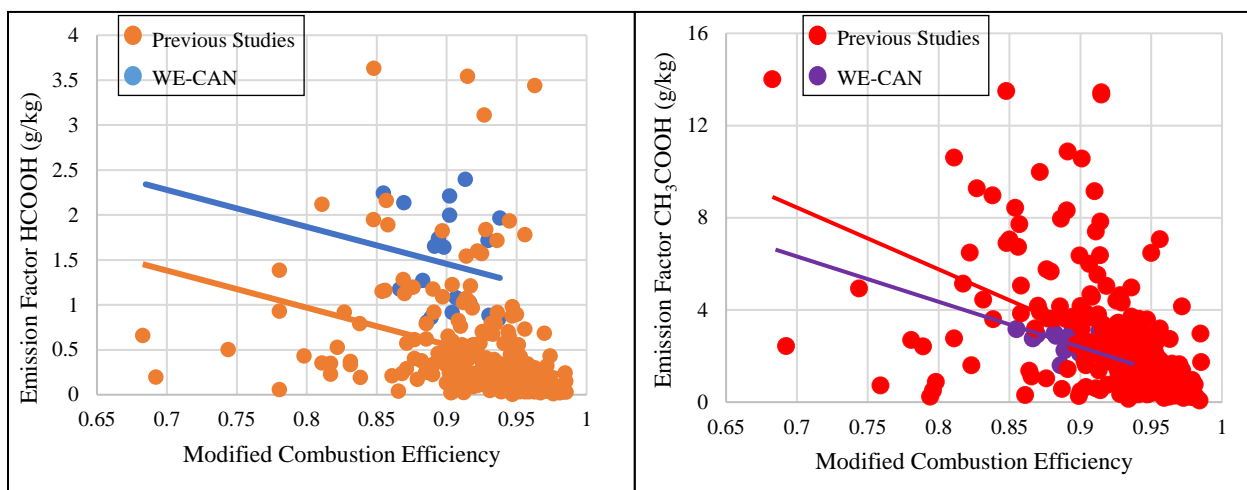


**Figure 14:** EFs of HCOOH (left) and  $CH_3COOH$  (right) from both WE-CAN and literature were compared to modified combustion efficiency (MCE), with linear regressions applied. Yellow and red dots correspond to literature EF and MCE, while blue and purple for WE-CAN results. For HCOOH, the equation for WE-CAN EFs is:  $y = -4.12x + 5.16$  with an  $R^2$  of 0.03. For HCOOH, the equation for previous studies EFs is:  $y = -4.13x + 4.27$  with an  $R^2$  of 0.047. For WE-CAN  $CH_3COOH$ , the EF equation is  $y = -19.7x + 20.1$  with an  $R^2$  of 0.51, while the previous studies EF equation is  $y = -26.8x + 27.2$  with an  $R^2$  of 0.25.

To learn if the correlation between MCE and EF depends on the type of sampling, all previous studies were organized into laboratory versus field samples. In HCOOH, laboratory studies had a general slope of -4.33 and an  $R^2$  of 0.25, while field studies had a slope of -1.10 and an  $R^2$  of 0.00. In contrast,  $CH_3COOH$  field studies had a slope of -5.00 and  $R^2$  of 0.002, while laboratory studies had a slope of -34.56 and  $R^2$  of 0.36. The fact that there is weak to no correlation between EF and MCE for organic acids in both field and laboratory studies suggest that their emissions may not be closely related to combustion phases.

## Chapter Five: Organic acid production

### *Normalized excess mixing ratios*

To examine to what extent the organic acids are chemically produced in the smoke, I calculate and analyzed normalized excess mixing ratios (NEMR) for each plume sampled during WE-CAN. The same as ERs (refer to equation 3), NEMR is the molar ratio between two compounds, calculated from the excess mixing ratios of two species, essentially attempting to remove the influence of dilution effect in plumes and assess the formation occurring moving downwind. For WE-CAN, NEMR was calculated for research flights that had pseudo-Lagrangian pathways in attempt to learn how HCOOH and CH<sub>3</sub>COOH changes as one air mass is followed downwind. Transects within a research flight were removed from analyses if any of the following criteria occurred: (1) significant altitude differences (0.5 km) between plume transects, (2) cloud sampling, or (3) flights not sampling in a pseudo-Lagrangian pathway.

To analyze and simplify the NEMR of HCOOH and CH<sub>3</sub>COOH, the center of the plume is classified as when the CO mixing ratio is within the 75<sup>th</sup> percentile or larger, while the outside of the plume is when the CO is lower than the 25<sup>th</sup> percentile. The background correction was found by interpolating the background prior to entering the plume and after leaving the plume for each pass, and then subtracting from inside of the plume.

Figure 15 depicts NEMR for HCOOH and CH<sub>3</sub>COOH. HCOOH mixing ratios increase by approximately 2.2 ppb/ppmCO/hour of physical aging, implying a consistent formation of HCOOH in wildfire smoke regardless of fires. The only fire that shows a slight decrease of HCOOH over time is RF13, which was the Mendocino complex and may reflect mixed fire sources or unsuccessful pseudo-Lagrangian sampling.

For CH<sub>3</sub>COOH, the NEMR increased within the first hour (or two, depending on research flight) by approximately 2.1 ppb/ppmCO/hour, but then begins to decrease afterwards, as a result of increased importance of chemical loss as smoke ages. Overall, there is an average of -0.8 ppb/ppmCO/hour for CH<sub>3</sub>COOH. The Taylor Creek Fire (RF03), which had very fast formation of O<sub>3</sub>, looks to be dominating this decrease. Excluding RF03 from the NEMR of CH<sub>3</sub>COOH, the average increase becomes

0.2ppb/ppmCO/hour, which still implies the increased importance of chemical loss and the slower formation in comparison to HCOOH.

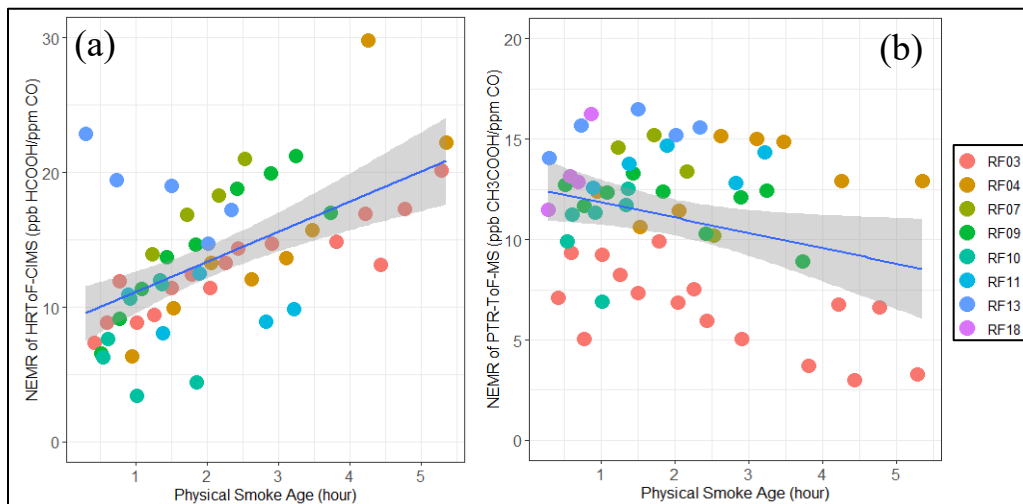


**Figure 15:** NEMRs of (a) HCOOH and (b) CH<sub>3</sub>COOH for research flights with pseudo-Lagrangian transects. The shaded area is the 95% confidence interval for predictions from the linear model. HCOOH NEMR increased on average 2.2 ppb/ppmCO/hour, while CH<sub>3</sub>COOH increased by approximately 2.1 ppb/ppmCO/hour for the first hour, but then decreased afterwards from chemical loss. On average, CH<sub>3</sub>COOH shows -0.8 ppb/ppmCO/hour.

### *Primary vs secondary source of HCOOH and CH<sub>3</sub>COOH*

While we see an increase of organic acid mixing ratios moving downwind of a fire, it is unknown if VOCs emitted from the burning fire are the sole or main contributor of this formation. Other possibilities to explain the increase of HCOOH (and briefly CH<sub>3</sub>COOH) when moving downwind of the fire include anthropogenic sources if passing over a city (which will increase the background of organic acids present in that area) or smoke from a second (or even third) fire mixing with the smoke that the C-130 sampled. To test this theory, HCOOH and CH<sub>3</sub>COOH NEMRs were plotted against the NEMR benzene/NEMR toluene, NEMR of ozone, (peroxyacetyl nitrate) PAN, and isoprene (Figure 16).

Benzene/toluene is used as a photochemical clock, and compared to the NEMR of HCOOH, there is no significant correlation or increase (slope of 0.90, R<sup>2</sup> of 0.01). For the NEMR of CH<sub>3</sub>COOH, we see a decrease as the NEMR benzene/toluene increases (slope of -5.94) but this is mainly influenced by RF03, which had large ozone formation. Excluding RF03, there would not be a significant correlation. Since

both HCOOH and CH<sub>3</sub>COOH are mainly produced photochemically, a lack of correlation between a secondary and primary species is logical.

Ozone and PAN are formed photochemically (secondary production). When compared to the NEMR of HCOOH, both photochemical precursors show an increase (slope of 0.11 ppb HCOOH/ppb O<sub>3</sub>, and 2.78 ppb HCOOH/ppb PAN). However, similarly to above, the NEMR CH<sub>3</sub>COOH decreases with both NEMR O<sub>3</sub> (slope of -0.07 ppb CH<sub>3</sub>COOH/ppb O<sub>3</sub>) and NEMR PAN (slope of -0.44 ppb CH<sub>3</sub>COOH/ppb PAN) and is mainly influenced by RF03. We would expect to see an increase for both organic acids since they are also mainly formed photochemically.

Finally, NEMRs of organic acids are compared to the NEMR of isoprene, which is a known source for both organic acids. With NEMR of isoprene, we see there is a decrease as NEMR of HCOOH increases (slope of -18.04 ppb HCOOH/ppb isoprene). However, there is a positive relationship between NEMR of CH<sub>3</sub>COOH and isoprene but is controlled by RF03 (slope of 5.49 ppb CH<sub>3</sub>COOH/ppb isoprene).

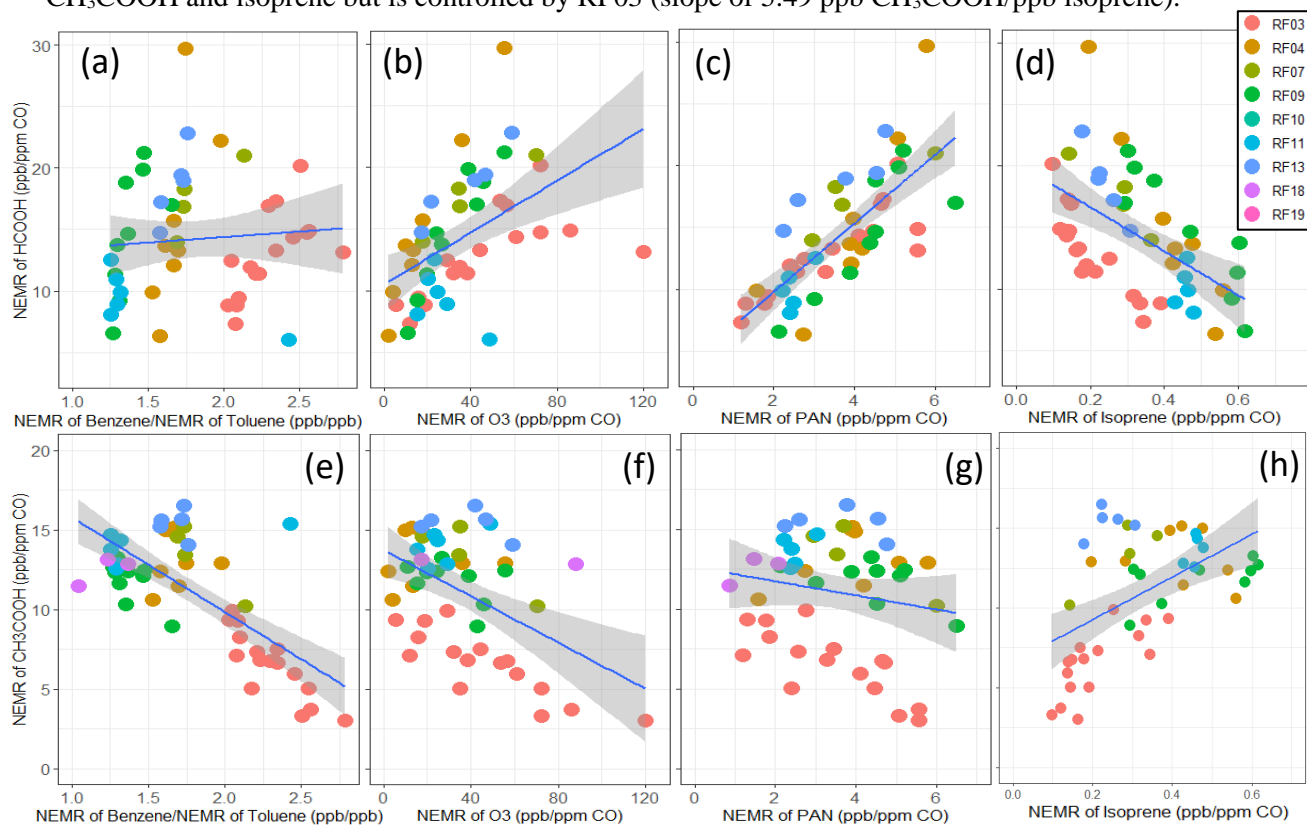


**Figure 16:** NEMR of HCOOH and CH<sub>3</sub>COOH compared to NEMR of different primary and secondary precursors for research flights following a pseudo-Lagrangian pathway. The shaded area is the 95% confidence interval for predictions from the linear model. (a) NEMR HCOOH v. NEMR benzene/NEMR toluene has a slope of 0.90 with

no correlation present ( $y = 0.90x + 12.6$ ;  $R^2 = 0.01$ ). (b) NEMR HCOOH v. NEMR O<sub>3</sub> has a slope of 0.11 and shows a general increase ( $y = 0.11x + 10.5$ ;  $R^2 = 0.25$ ). This is the same with (c) NEMR PAN ( $y = 2.78x + 4.23$ ;  $R^2 = 0.57$ ). (d) NEMR HCOOH v. NEMR isoprene has an inverse relationship ( $y = -18.04 + 20.3$ ;  $R^2 = 0.30$ ). (e) NEMR CH<sub>3</sub>COOH v. NEMR benzene/NEMR toluene has a slope of -5.94, with RF03 driving this relationship ( $y = -5.94x + 21.7$ ;  $R^2 = 0.52$ ). Without it, there would not be much of a correlation. (f) NEMR CH<sub>3</sub>COOH v. NEMR O<sub>3</sub> shows a general decrease ( $y = -0.07x + 13.7$ ;  $R^2 = 0.24$ ). This is the same with (g) NEMR PAN  $y = -0.44x + 12.6$ ;  $R^2 = 0.03$ ). (h) NEMR CH<sub>3</sub>COOH v. NEMR isoprene has a direct relationship ( $y = 5.49x + 8.98$ ;  $R^2 = 0.14$ ). All CH<sub>3</sub>COOH NEMRs are dominated by RF03.

### *Evaporation of organic aerosol as a source of HCOOH and CH<sub>3</sub>COOH*

Besides learning about the formation of HCOOH and CH<sub>3</sub>COOH from VOCs, it is important to also look at the particulate side as possible sources. This analyses only focused on one research flight (RF08) that sampled the Central Valley in California. The Central Valley had many layers of smoke, which the C-130 sampled at low altitude and also through two sets of missed approaches. While particular smoke plumes were not targeted during this flight, smoke was sampled from the Carr Fire, Mendocino Complex, and fires near Yosemite National Park.

Two distinct groups and slopes are found, with more OA formation at low temperatures (high altitudes) (Selimovic et al. In preparation). The hypothesis is that at high temperatures (low altitudes), OA evaporates and may form organic gases, including HCOOH and CH<sub>3</sub>COOH. Acetonitrile and hydrogen cyanide were also compared to CO and did not show bifurcation, implying the OA was coming from the same source (Selimovic et al. In preparation).

HCOOH and CH<sub>3</sub>COOH were compared to CO and OA, with the hypothesis that there may be higher concentrations at low altitudes due to OA evaporation. When comparing HCOOH and CH<sub>3</sub>COOH to CO, we see two small groups for HCOOH, but no bifurcation for CH<sub>3</sub>COOH. However, when comparing HCOOH and CH<sub>3</sub>COOH to OA, we see a bifurcation for both species. During RF08, there is no significant altitude difference on relative humidity. Both acids have more production compared to OA at low altitudes, which may imply that OA evaporation is a source. However, California's Central Valley is a highly polluted region with many large anthropogenic VOC sources from cars, solvents, agriculture, and fracking. More analyses will need to be completed to learn if OA evaporation is a source of HCOOH and

CH<sub>3</sub>COOH. All other research flights were analyzed in a similar pattern (Appendix B), but bifurcation is not obvious against organic acids and CO.

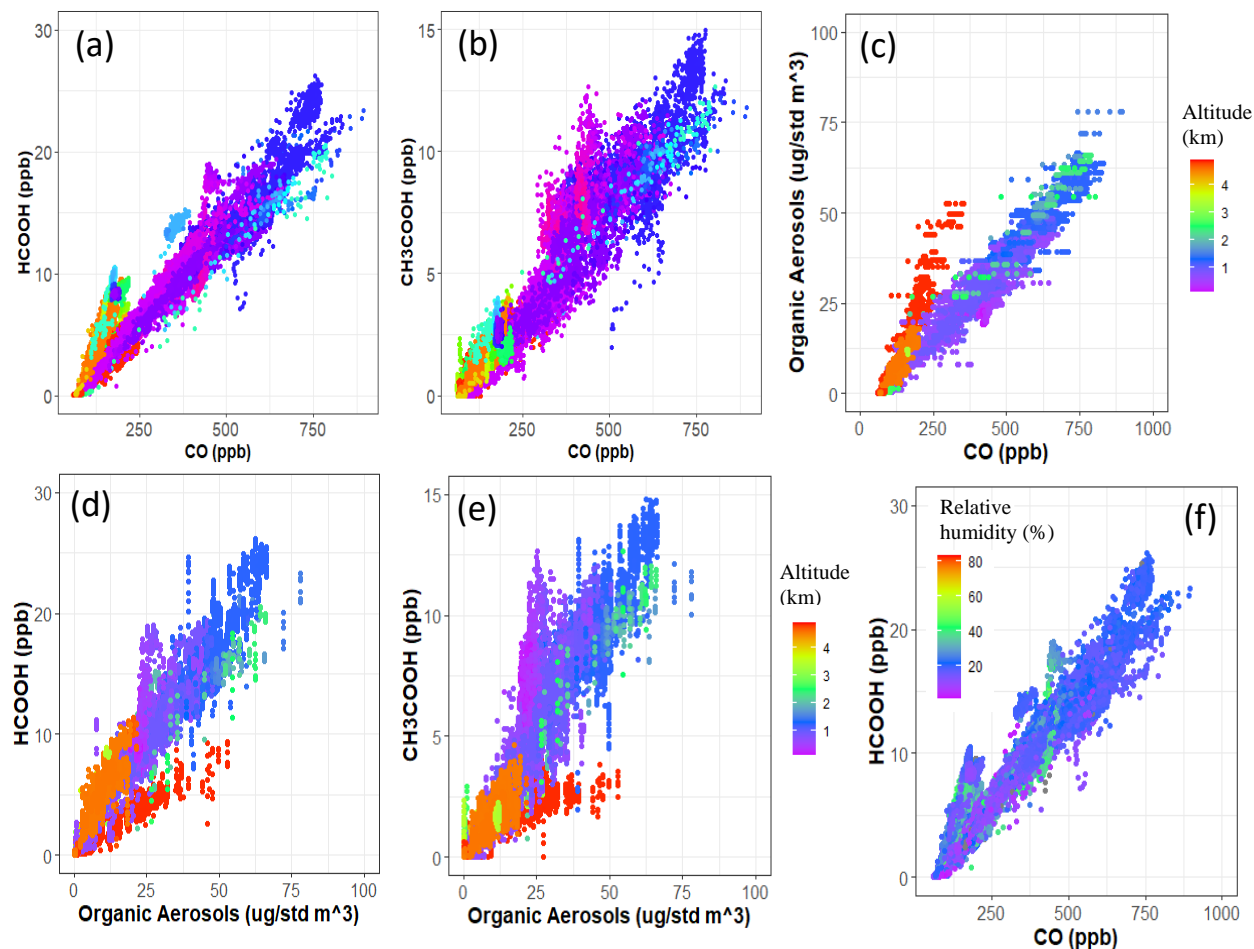


**Figure 17:** HCOOH and CH<sub>3</sub>COOH plotted against CO during RF08 which sampled the Central Valley in California. Plotting HCOOH and CH<sub>3</sub>COOH against organic aerosols, we see that there are two populations, with the highest altitudes having a lower formation of organic acids. Plots (a – e) are colored by altitude, while plot (f) is by relative humidity. In contrast, there is no difference in the two groups based on relative humidity.

### *Heterogeneity in smoke plumes*

When we calculate in-plume and out-of-plume concentrations (specifically used for NEMR), while it provides an overall picture, it fails to describe the diverse chemistries occurring within the smoke plume itself. In the center of the plume, there will be the least amount of sunlight and photooxidation of precursors to HCOOH and CH<sub>3</sub>COOH due to the dense smoke. Moreover, it can also be assumed that between the 25<sup>th</sup> and 50<sup>th</sup> percentile of CO measurements (mostly on the edge of the plume), there is more

photooxidation occurring due to its exposure to sunlight. Between the center of the plume and edge of the plume, there exists a gradient of light, and thus a different rate of light-dependent chemistry could be occurring. It is suggested that there will be heterogeneity with the formation of HCOOH and CH<sub>3</sub>COOH from the center and outer parts of the smoke plumes (Hodshire et al. 2020). To test this hypothesis, I have separated the smoke plume from RF09 into three distinct categories (Figure 18). The center of the plume is when CO >75<sup>th</sup> percentile, where the smoke will be the densest. The second quadrant (where it is between the center of the plume and the edge) is when CO is between the 50<sup>th</sup> and 75<sup>th</sup> percentile, and the edge of the plume is when the CO is between the 25<sup>th</sup> and 50<sup>th</sup> percentile. Each CO percentile was found for every plume pass, and each plume transect was split by the CO criteria, and then averaged to observe differences. With HCOOH, we can see that there is a higher NEMR at the edge of the plume than the center for all plume passes excluding three. On average for the entire research flight, the NEMR of HCOOH is approximately 1.4 times larger at the edge than in the center. This is what was expected since there is more light available for the photooxidation of precursors to organic acids.

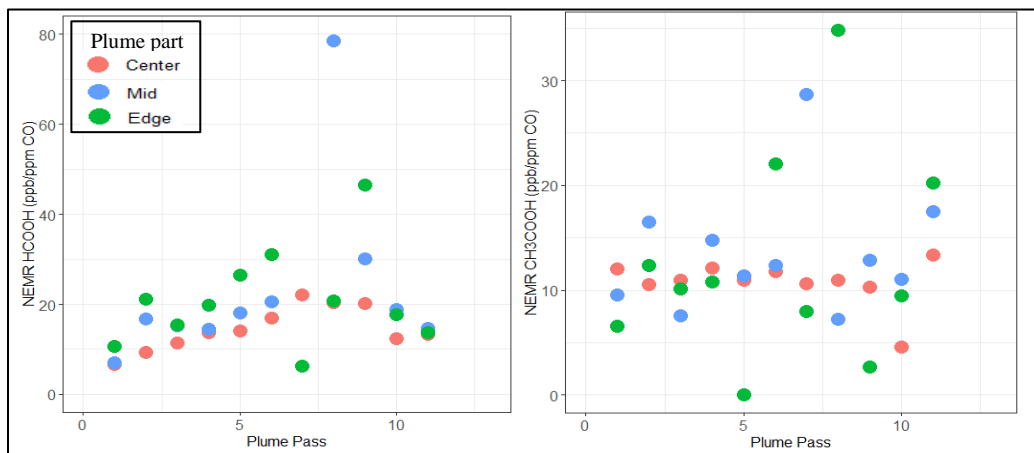


**Figure 18:**  $\Delta$ HCOOH/ $\Delta$ CO and  $\Delta$ CH<sub>3</sub>COOH/ $\Delta$ CO plotted against the plume pass measured during sampling of the Bear Trap Fire (RF09), with Plume Pass 1 being the emission pass, and moving further downwind with each pass. Colored by the part of the plume based on CO measurements, with center (pink) being when CO is >75<sup>th</sup> percentile of the plume pass, mid (blue) is between the 50<sup>th</sup> – 75<sup>th</sup> percentile, and edge (green) is when CO is between the 25<sup>th</sup> – 50<sup>th</sup> percentile.

In contrast, CH<sub>3</sub>COOH is unexpected, and does not have a consistent formation on the edge of the plume that is larger than the center. On average for the entire flight, the edge is only 1.1 times larger than the

$\Delta\text{CH}_3\text{COOH}/\Delta\text{CO}$  found in the center. This could be due to the slower formation of  $\text{CH}_3\text{COOH}$  in the atmosphere. More heterogeneity studies of smoke plumes will need to be completed for more detailed comprehension.

### **Future Directions**

This research can be built upon to help better understand the formation of  $\text{HCOOH}$  and  $\text{CH}_3\text{COOH}$  in smoke plumes. Firstly, by the PTR-ToF-MS correcting for the relative humidity dependence on  $\text{HCOOH}$  sensitivities, both this instrument and the HRTof-CIMS should be within each instrument uncertainty of 30 %, proving accurate real-time measurements.

A second analysis that would be useful to complete would be to compare the enhancement ratio to previous satellite observations to see how the data of primary and secondary sources differ. One could also compare these  $\text{HCOOH}$  and  $\text{CH}_3\text{COOH}$  results to those found in the Fire Influence on Regional to Global Environments and Air Quality (FIREX-AQ) aircraft campaign that occurred in the summer of 2019. Having two aircraft campaigns that measured wildfire smoke in the Western United States will be extremely beneficial to compare and add uncertainty to these measurements. Comparing WE-CAN organic aerosol evaporation at low altitudes to FIREX-AQ may also help us better understand if this is a possible source for  $\text{HCOOH}$  and  $\text{CH}_3\text{COOH}$ . Having two aircraft campaigns that measured wildfire smoke in the Western United States will be extremely beneficial to compare and add uncertainty to these measurements.

Finally, obtaining a better grasp of chemistry occurring in wildfires is essential to improve global models and our understanding of wildfires. Commonly used 0-D to 3-D models are not able to replicate observations. As stated in the introduction, there is likely a missing source or an underestimate of a known source for  $\text{HCOOH}$  and  $\text{CH}_3\text{COOH}$ . The Framework for 0-D Atmospheric Modeling (F0AM) (Wolfe et al. 2016) model should be applied to test our current understanding of the chemical production of organic acids in fire smoke with constraints provided by WE-CAN observations. Proposed sources of organic acids to be added to the model can include the possible organic aerosol evaporation,

phototautomerization of acetaldehyde, or keto-enol tautomerization. It is expected that the additional chemistry added will decrease the gap between the model and observations, and that we will learn what source contributes most to our HCOOH and CH<sub>3</sub>COOH formation in wildfire smoke.

## **Acknowledgements**

I would like to thank my advisor, Dr. Lu Hu, for his mentorship and guidance throughout graduate school. Thanks to Wade Permar for all of his help with R, the PTR-ToF-MS, WE-CAN data processing, and general atmospheric chemistry questions. I want to thank Qian Wang for building our in-house permeation system and acknowledge my other lab mates (Ahsan Mozaffar, Damien Ketcherside, Lixu Jin, Keri Nauman, Amy Christiansen, Sree Chaliyakunnel, and Vanessa Selimovic) for their endless encouragement. Thanks to my committee members, Dr. Robert Yokelson and Dr. Tony Ward, for their support and understanding during this process, especially amidst a pandemic. Thanks to the C-130 flight crew and the entire WE-CAN team (NSF award number 1650275), especially Dr. Emily Fischer for her leadership and coordination for the campaign. Thanks to Dr. Joel Thornton, Dr. Brett Palm, and Qaiyoun Peng for the use of their HRTof-CIMS data, and Dr. Jakob Lindaas for his assistance in organizing the metadata for the WE-CAN team. I would like to thank everyone at the Toolik Field Station (TFS), especially H  l  ne Angot for her mentorship, and Dr. Detlev Helmig for his allowance of UM to be a part of his research in TFS (NSF award number 1707569). Thanks to my great support system of friends, including Emily Taylor, Kourtney Johnson, Jessica Mailhot, Eric John, and Wade Permar. I especially want to thank my Mom for her endless support as my #1 cheerleader throughout all of my life. Finally, the biggest thanks to my life partner Casey Massena (and our cats, Oliver and Adeline) for his endless support, motivation, and love.

## References

- Akagi, S., J. Craven, J. Taylor, G. McMeeking, R. Yokelson, I. Burling, S. Urbanski, C. Wold, J. Seinfeld, H. Coe, M. Alvarado, and D. Weise. 2012. "Evolution of Trace Gases and Particles Emitted by a Chaparral Fire in California." *Atmospheric Chemistry and Physics* 12(3):1397–1421.
- Akagi, S., R. Yokelson, I. Burling, S. Meinardi, I. Simpson, D. Blake, G. McMeeking, A. Sullivan, T. Lee, S. Kreidenweis, S. Urbanski, J. Reardon, D. Griffith, T. Johnson, and D. Weise. 2013. "Measurements of Reactive Trace Gases and Variable O<sub>3</sub> Formation Rates in Some South Carolina Biomass Burning Plumes." *Atmospheric Chemistry and Physics* 13(3):1141–65.
- Akagi, S., R. Yokelson, C. Wiedinmyer, M. Alvarado, J. Reid, T. Karl, J. Crouse, and P. Wennberg. 2011. "Emission Factors for Open and Domestic Biomass Burning for Use in Atmospheric Models." *Atmospheric Chemistry and Physics* 11(9):4039–72.
- Alwe, H., D. Millet, X. Chen, J. Raff, Z. Payne, and K. Fledderman. 2019. "Oxidation of Volatile Organic Compounds as the Major Source of Formic Acid in a Mixed Forest Canopy Supplement." *Geophysical Research Letters* 3(5):1–8.
- Andreae, M., R. Talbot, T. Andreae, and R. Harriss. 1988. "Formic and Acetic Acid over the Central Amazon Region, Brazil 1. Dry Season." *Journal of Geophysical Research* 93(D2):1616–24.
- Atkinson, R., D. Baulch, R. Cox, J. Crowley, R. Hampson, R. Hynes, M. Jenkin, M. Rossi, and J. Troe. 2006. "Evaluated Kinetic and Photochemical Data for Atmospheric Chemistry: Volume II - Gas Phase Reactions of Organic Species." *Atmospheric Chemistry and Physics* 6(11):3625–4055.
- Baasandorj, M., D. Millet, L. Hu, D. Mitroo, and B. Williams. 2015. "Measuring Acetic and Formic Acid by Proton-Transfer-Reaction Mass Spectrometry: Sensitivity, Humidity Dependence, and Quantifying Interferences." *Atmospheric Measurement Techniques* 8(3):1303–21.
- Baltensperger, U., M. Kalberer, J. Dommen, D. Paulsen, M. Alfarra, H. Coe, R. Fisseha, A. Gascho, M. Gysel, S. Nyeki, M. Sax, M. Steinbacher, A. Prévôt, S. Sjögren, E. Weingartner, and R. Zenobi. 2005. "Secondary Organic Aerosols from Anthropogenic and Biogenic Precursors." *Faraday*

*Discussions* 130:265–78.

- Bertschi, I., R. Yokelson, D. Ward, R. Babbitt, R. Susott, J. Goode, and W. Hao. 2003. “Trace Gas and Particle Emissions from Fires in Large Diameter and Belowground Biomass Fuels.” *Journal of Geophysical Research D: Atmospheres* 108(13).
- Bossolasco, A., E. Faragó, C. Schoemaeker, and C. Fittschen. 2014. “Rate Constant of the Reaction between CH<sub>3</sub>O<sub>2</sub> and OH Radicals.” *Chemical Physics Letters* 593:7–13.
- Le Breton, M., M. McGillen, J. Muller, A. Bacak, D. Shallcross, P. Xiao, L. Huey, D. Tanner, H. Coe, and C. Percival. 2012. “Airborne Observations of Formic Acid Using a Chemical Ionization Mass Spectrometer.” *Atmospheric Measurement Techniques* 5(12):3029–39.
- Burling, I., R. Yokelson, S. Akagi, S. Urbanski, C. Wold, D. Griffith, T. Johnson, J. Reardon, and D. Weise. 2011. “Airborne and Ground-Based Measurements of the Trace Gases and Particles Emitted by Prescribed Fires in the United States.” *Atmospheric Chemistry and Physics* 11(23):12197–216.
- Burling, I., R. Yokelson, D. Griffith, T. Johnson, P. Veres, J. Roberts, C. Warneke, S. Urbanski, J. Reardon, W. Hao, and J. De Gouw. 2010. “Laboratory Measurements of Trace Gas Emissions from Biomass Burning of Fuel Types from the Southeastern and Southwestern United States.” *Atmospheric Chemistry and Physics* 10(22):11115–30.
- Cady-Pereira, K., S. Chaliyakunnel, M. Shephard, D. Millet, M. Luo, and K. Wells. 2014. “HCOOH Measurements from Space: TES Retrieval Algorithm and Observed Global Distribution.” *Atmospheric Measurement Techniques* 7(7):2297–2311.
- Chaliyakunnel, S., D. Millet, K. Wells, K. Cady-Pereira, and M. Shephard. 2016. “A Large Underestimate of Formic Acid from Tropical Fires: Constraints from Space-Borne Measurements.” *Environmental Science and Technology* 50(11):5631–40.
- Chattopadhyay, A., P. Chatterjee, and T. Chakraborty. 2015. “Photo-Oxidation of Acetone to Formic Acid in Synthetic Air and Its Atmospheric Implication.” *Journal of Physical Chemistry A* 119(29):8146–55.
- Chebbi, A. and P. Carlier. 1996. “Carboxylic Acids in the Troposphere, Occurrence, Sources, and Sinks:

- A Review.” *Atmospheric Environment* 30(24):4233–49.
- Christian, T., B. Kleiss, R. Yokelson, R. Holzinger, P. Crutzen, W. Hao, B. Saharjo, and D. Ward. 2003. “Comprehensive Laboratory Measurements of Biomass-Burning Emissions: 1. Emissions from Indonesian, African, and Other Fuels.” *Journal of Geophysical Research D: Atmospheres* 108(23).
- Fischer, E. V., D. J. Jacob, R. M. Yantosca, M. P. Sulprizio, D. B. Millet, J. Mao, F. Paulot, H. B. Singh, A. Roiger, L. Ries, R. W. Talbot, K. Dzepina, and S. Pandey Deolal. 2014. “Atmospheric Peroxyacetyl Nitrate (PAN): A Global Budget and Source Attribution.” *Atmospheric Chemistry and Physics* 14(5):2679–98.
- Fortner, E., J. Zheng, R. Zhang, W. Knighton, R. Volkamer, P. Sheehy, L. Molina, and M. André. 2009. “Measurements of Volatile Organic Compounds Using Proton Transfer Reaction-Mass Spectrometry during the MILAGRO 2006 Campaign.” *Atmospheric Chemistry and Physics* 9(2):467–81.
- Gilman, J. B., B. M. Lerner, W. C. Kuster, P. D. Goldan, C. Warneke, P. R. Veres, J. M. Roberts, J. A. De Gouw, I. R. Burling, and R. J. Yokelson. 2015. “Biomass Burning Emissions and Potential Air Quality Impacts of Volatile Organic Compounds and Other Trace Gases from Fuels Common in the US.” *Atmospheric Chemistry and Physics* 15(24):13915–38.
- Glasius, M., C. Boel, N. Bruun, L. Easa, P. Hornung, H. Klausen, K. Klitgaard, C. Lindeskov, C. Moller, H. Nissen, A. Petersen, S. Kleefeld, E. Boaretto, T. Hansen, J. Heinemeier, and C. Lohse. 2001. “Relative Contribution of Biogenic and Anthropogenic Sources to Formic and Acetic Acids in the Atmospheric Boundary Layer C / I • -C Ratio as Atmospheric Carbon While VOC Emitted from Fossil Fuels Are Devoid The Origin of Atmospheric Tbrmic and Acetic Acid.” *Journal of Geophysical Research* 106(2000):7415–26.
- Glasius, M., S. Wessel, C. Christensen, J. Jacobsen, H. Jørgensen, K. Klitgaard, L. Petersen, J. Rasmussen, T. Stroyer Hansen, C. Lohse, E. Boaretto, and J. Heinemeier. 2000. “Sources to Formic Acid Studied by Carbon Isotopic Analysis and Air Mass Characterization.” *Atmospheric Environment* 34(15):2471–79.

- Goode, J., R. Yokelson, R. Susott, and D. Ward. 1999. “Trace Gas Emissions from Laboratory Biomass Fires Measured by Open-Path Fourier Transform Infrared Spectroscopy: Fires in Grass and Surface Fuels.” *Journal of Geophysical Research Atmospheres* 104(D17):21237–45.
- Goode, J., R. Yokelson, D. Ward, R. Susott, R. Babbitt, and M. Davies. 2000. “Measurements of Excess O<sub>3</sub>, CO<sub>2</sub>, CO, CH<sub>4</sub>, C<sub>2</sub>H<sub>4</sub>, C<sub>2</sub>H<sub>2</sub>, HCN, NO, NH<sub>3</sub>, HCOOH, CH<sub>3</sub>COOH, HCHO, and CH<sub>3</sub>OH in 1997 Alaskan Biomass Burning Plumes by Airborne Fourier Transform Infrared Spectroscopy (AFTIR).” *Journal of Geophysical Research* 105(D17):22147–66.
- de Gouw, J. and C. Warneke. 2007. “Measurements of Volatile Organic Compounds in the Earth’s Atmosphere Using Proton-Transfer-Reaction Mass Spectrometry.” *Mass Spectrometry Reviews* 26:223–57.
- Grutter, M., N. Glatthor, G. Stiller, H. Fischer, U. Grabowski, M. Höpfner, S. Kellmann, A. Linden, and T. Von Clarmann. 2010. “Global Distribution and Variability of Formic Acid as Observed by MIPAS-ENVISAT.” *Journal of Geophysical Research Atmospheres* 115(10):1–8.
- Hodshire, A., E. Ramnarine, A. Akherati, M. Alvarado, E. Fischer, S. Jathar, S. Kreidenweis, J. Lindaas, C. Lonsdale, T. Onasch, S. Springston, J. Wang, Y. Wang, L. Kleinman, A. Sedlacek, and J. Pierce. 2020. “Dilution Impacts on Smoke Aging: Evidence in BBOP Data.” *Grl* in prepara(April):1–21.
- Kahle, D. and H. Wickham. 2013. “Ggmap: Spatial Visualization with Ggplot2.” *R Journal* 5(1):144–61.
- Keene, W. and J. Galloway. 1984. “Organic Acidity in Precipitation of North America.” *Atmospheric Environment (1967)* 18(11):2491–97.
- Keene, W. and J. Galloway. 1988. “The Biogeochemical Cycling of Formic and Acetic Acids through the Troposphere: An Overview of Current Understanding.” *Tellus B* 40 B(5):322–34.
- Koss, A., K. Sekimoto, J. Gilman, V. Selimovic, M. Coggon, K. Zarzana, B. Yuan, B. Lerner, S. Brown, J. Jimenez, J. Krechmer, J. Roberts, C. Warneke, R. Yokelson, and J. De Gouw. 2018. “Non-Methane Organic Gas Emissions from Biomass Burning: Identification, Quantification, and Emission Factors from PTR-ToF during the FIREX 2016 Laboratory Experiment.” *Atmospheric Chemistry and Physics* 18(5):3299–3319.

- Koss, A., B. Yuan, C. Warneke, J. Gilman, B. Lerner, P. Veres, J. Peischl, S. Eilerman, R. Wild, S. Brown, C. Thompson, T. Ryerson, T. Hanisco, G. Wolfe, J. St. Clair, M. Thayer, F. Keutsch, S. Murphy, and J. De Gouw. 2017. “Supplement of Observations of VOC Emissions and Photochemical Products over US Oil- and Gas-Producing Regions Using High-Resolution H<sub>3</sub>O<sup>+</sup>.” *European Geosciences Union* 10:2941–68.
- Lee, B., F. Lopez-Hilfiker, C. Mohr, T. Kurtén, D. Worsnop, and J. Thornton. 2014. “An Iodide-Adduct High-Resolution Time-of-Flight Chemical-Ionization Mass Spectrometer: Application to Atmospheric Inorganic and Organic Compounds.” *Environmental Science and Technology* 48(11):6309–17.
- Link, M., T. Nguyen, K. Bates, J. Müller, and D. Farmer. 2020. “Can Isoprene Oxidation Explain High Concentrations of Atmospheric Formic and Acetic Acid over Forests ?” *ACS Earth and Space Chemistry*.
- Liu, X., G. Huey, R. Yokelson, V. Selimovic, I. Simpson, M. Müller, J. Jimenez, P. Campuzano-Jost, A. Beyersdorf, D. Blake, Z. Butterfield, Y. Choi, J. Crouse, D. Day, G. Diskin, M. Dubey, E. Fortner, T. Hanisco, W. Hu, L. King, L. Kleinman, S. Meinardi, T. Mikoviny, T. Onasch, B. Palm, J. Peischl, I. Pollack, T. Ryerson, G. Sachse, A. Sedlacek, J. Shilling, S. Springston, J. St. Clair, D. Tanner, A. Teng, P. Wennberg, A. Wisthaler, and G. Wolfe. 2017. “Airborne Measurements of Western U.S. Wildfire Emissions: Comparison with Prescribed Burning and Air Quality Implications.” *Journal of Geophysical Research* 122(11):6108–29.
- Mckenzie, L., W. Hao, G. Richards, and D. Ward. 1995. “Measurement and Modeling of Air Toxins from Smoldering Combustion of Biomass.” *Environmental Science and Technology* 29(8):2047–54.
- Millet, D. 2012. “Atmospheric Chemistry: Natural Atmospheric Acidity.” *Nature Geoscience* 5(1):8–9.
- Millet, D., M. Baasandorj, D. Farmer, J. Thornton, K. Baumann, P. Brophy, S. Chaliyakunnel, J. De Gouw, M. Graus, L. Hu, A. Koss, B. Lee, F. Lopez-Hilfiker, J. Neuman, F. Paulot, J. Peischl, I. Pollack, T. Ryerson, C. Warneke, B. Williams, and J. Xu. 2015. “A Large and Ubiquitous Source of Atmospheric Formic Acid.” *Atmospheric Chemistry and Physics* 15(11):6283–6304.

- Müller, J., T. Stavrou, and J. Peeters. 2018. “Chemistry and Deposition in the Model of Atmospheric Composition at Global and Regional Scales Using Inversion Techniques for Trace Gas Emissions (MAGRITTEv1.0). Part A. Chemical Mechanism.” (December):1–59.
- Müller, M., B. Anderson, A. Beyersdorf, J. Crawford, G. Diskin, P. Eichler, A. Fried, F. Keutsch, T. Mikoviny, K. Thornhill, J. Walega, A. Weinheimer, M. Yang, R. Yokelson, and A. Wisthaler. 2016. “In Situ Measurements and Modeling of Reactive Trace Gases in a Small Biomass Burning Plume.” *Atmospheric Chemistry and Physics Discussions* 15(21):31501–36.
- Palm, B., X. Liu, J. Jimenez, and J. Thornton. 2019. “Performance of a New Coaxial Ion-Molecule Reaction Region for Low-Pressure Chemical Ionization Mass Spectrometry with Reduced Instrument Wall Interactions.” *Atmospheric Measurement Techniques* 12(11):5829–44.
- Paulot, F., D. Wunch, J. Crouse, G. Toon, D. Millet, P. Decarlo, C. Vigouroux, N. Deutscher, G. Abad Gonzalez, J. Notholt, T. Warneke, J. Hannigan, C. Warneke, J. De Gouw, E. Dunlea, M. De Mazière, D. Griffith, P. Bernath, J. Jimenez, and P. Wennberg. 2011. “Importance of Secondary Sources in the Atmospheric Budgets of Formic and Acetic Acids.” *Atmospheric Chemistry and Physics* 11(5):1989–2013.
- Peng, Q., B. Palm, K. Melander, B. Lee, S. Hall, K. Ullmann, T. Campos, A. Weinheimer, E. Apel, R. Hornbrook, A. Hills, D. Montzka, F. Flocke, L. Hu, W. Permar, C. Wielgasz, J. Lindaas, I. Pollack, E. Fischer, T. Bertram, and J. Thornton. 2020. “HONO Emissions from Western U.S. Wildfires Provide Dominant Radical Source in Fresh Wildfire Smoke.” *Environmental Science & Technology*.
- Prichard, S. J., S. M. O’Neill, P. Eagle, A. G. Andreu, B. Drye, J. Dubowy, S. Urbanski, and T. M. Strand. 2020. “Wildland Fire Emission Factors in North America: Synthesis of Existing Data, Measurement Needs and Management Applications.” *International Journal of Wildland Fire* 29(2):132–47.
- Santín, C., S. Doerr, C. Preston, and G. González-Rodríguez. 2015. “Pyrogenic Organic Matter Production from Wildfires: A Missing Sink in the Global Carbon Cycle.” *Global Change Biology* 21(4):1621–33.

- Sekimoto, K., S. Li, B. Yuan, A. Koss, M. Coggon, C. Warneke, and J. de Gouw. 2017. “Calculation of the Sensitivity of Proton-Transfer-Reaction Mass Spectrometry (PTR-MS) for Organic Trace Gases Using Molecular Properties.” *International Journal of Mass Spectrometry* 421:71–94.
- Selimovic, V., R. Yokelson, C. Warneke, J. Roberts, J. de Gouw, and D. Griffith. 2018. “Aerosol Optical Properties and Trace Gas Emissions from Laboratory-Simulated Western US Wildfires.” *Atmos. Chem. Phys.* 18(4):2929–48.
- Shaw, M., B. Sztáray, L. Whalley, D. Heard, D. Millet, M. Jordan, D. Osborn, and S. Kable. 2018. “Photo-Tautomerization of Acetaldehyde as a Photochemical Source of Formic Acid in the Troposphere.” *Nature Communications* 9(1):1–7.
- Španěl, P., A. M. Diskin, T. Wang, and D. Smith. 2003. “A SIFT Study of the Reactions of H<sub>3</sub>O<sup>+</sup>, NO<sup>+</sup> and O<sub>2</sub><sup>+</sup> with Hydrogen Peroxide and Peroxyacetic Acid.” *International Journal of Mass Spectrometry* 228(2–3):269–83.
- Stavrakou, T., J. Müller, J. Peeters, A. Razavi, L. Clarisse, C. Clerbaux, P. Coheur, D. Hurtmans, M. De Mazière, C. Vigouroux, N. Deutscher, D. Griffith, N. Jones, and C. Paton-Walsh. 2012. “Satellite Evidence for a Large Source of Formic Acid from Boreal and Tropical Forests.” *Nature Geoscience* 5(1):26–30.
- Stockwell, C., P. Veres, J. Williams, and R. Yokelson. 2015. “Characterization of Biomass Burning Emissions from Cooking Fires, Peat, Crop Residue, and Other Fuels with High-Resolution Proton-Transfer-Reaction Time-of-Flight Mass Spectrometry.” *Atmospheric Chemistry and Physics* 15(2):845–65.
- Veres, P., J. Gilman, J. Roberts, W. Kuster, C. Warneke, I. Burling, and J. De Gouw. 2010. “Development and Validation of a Portable Gas Phase Standard Generation and Calibration System for Volatile Organic Compounds.” *Atmospheric Measurement Techniques* 3(3):683–91.
- Wickham, H. 2016. “Ggplot2: Elegant Graphics for Data Analysis.” *Springer-Verlag New York*. Retrieved (<https://ggplot2.tidyverse.org>).
- Wickham, H., M. Averick, J. Bryan, W. Chang, L. McGowan, R. François, G. Golemund, A. Hayes, L.

- Henry, J. Hester, M. Kuhn, T. Pedersen, E. Miller, S. Bache, K. Müller, J. Ooms, D. Robinson, D. Seidel, V. Spinu, K. Takahashi, D. Vaughan, C. Wilke, K. Woo, and H. Yutani. 2019. “Welcome to the Tidyverse.” *Journal of Open Source Software* 4(43):1686.
- Wickham, H., R. François, L. Henry, and K. Müller. 2016. “Dplyr: A Grammar of Data Manipulation.” Retrieved (<https://cran.r-project.org/package=dplyr>).
- Wolfe, G., M. Marvin, S. Roberts, K. Travis, and J. Liao. 2016. “The Framework for 0-D Atmospheric Modeling (F0AM) v3.1.” *Geoscientific Model Development* 9(9):3309–19.
- Wyche, K., P. Monks, A. Ellis, R. Cordell, A. Parker, C. Whyte, A. Metzger, J. Dommen, J. Duplissy, A. Prévôt, U. Baltensperger, A. Rickard, and F. Wulfert. 2008. “Gas Phase Precursors to Anthropogenic Secondary Organic Aerosol: Detailed Observations of 1,3,5-Trimethylbenzene Photooxidation.” *Atmospheric Chemistry and Physics Discussions* 8(3):11685–754.
- Yokelson, R., I. Bertschi, T. Christian, P. Hobbs, D. Ward, and W. Hao. 2003. “Trace Gas Measurements in Nascent, Aged, and Cloud-Processed Smoke from African Savanna Fires by Airborne Fourier Transform Infrared Spectroscopy (AFTIR).” *Journal of Geophysical Research D: Atmospheres* 108(13).
- Yokelson, R., I. Burling, S. Urbanski, E. Atlas, K. Adachi, P. Buseck, C. Wiedinmyer, S. Akagi, D. Toohey, and C. Wold. 2011. “Trace Gas and Particle Emissions from Open Biomass Burning in Mexico.” *Atmospheric Chemistry and Physics* 11(14):6787–6808.
- Yokelson, R., A. Clarke, A. Weinheimer, D. Knapp, D. Montzka, J. Holloway, P. Weibring, F. Flocke, W. Zheng, D. Toohey, P. Wennberg, J. Crouse, C. Wiedinmyer, L. Mauldin, A. Fried, D. Richter, J. Walega, J. Jimenez, K. Adachi, P. Buseck, S. Hall, R. Shetter, P. DeCarlo, T. Karl, S. Urbanski, E. Atlas, T. Campos, Y. Shinozuka, and V. Kapustin. 2009. “Emissions from Biomass Burning in the Yucatan.” *Atmospheric Chemistry and Physics* 9(15):5785–5812.
- Yokelson, R., J. Goode, D. Ward, R. Susott, R. Babbitt, D. Wade, I. Bertschi, D. Griffith, and W. Hao. 1999. “Emissions of Formaldehyde, Acetic Acid, Methanol, and Other Trace Gases from Biomass Fires in North Carolina Measured by Airborne Fourier Transform Infrared Spectroscopy.” *Journal*

*of Geophysical Research Atmospheres* 104(D23):30109–25.

- Yokelson, R., D. Griffith, and D. Ward. 1996. “Open-Path Fourier Transform Infrared Studies of Large-Scale Laboratory Biomass Fires.” *Journal of Geophysical Research: Atmospheres* 101(D15):21067–80.
- Yokelson, R., T. Karl, P. Artaxo, D. Blake, T. Christian, D. Griffith, A. Guenther, and W. Hao. 2007. “The Tropical Forest and Fire Emissions Experiment: Overview and Airborne Fire Emission Factor Measurements.” *Atmospheric Chemistry and Physics* 7(19):5175–96.
- Yuan, B., A. Koss, C. Warneke, M. Coggon, K. Sekimoto, and J. De Gouw. 2017. “Proton-Transfer-Reaction Mass Spectrometry: Applications in Atmospheric Sciences.” *Chemical Reviews* 117(21):13187–229.
- Yuan, B., P. Veres, C. Warneke, J. Roberts, J. Gilman, A. Koss, P. Edwards, M. Graus, W. Kuster, S. Li, R. Wild, S. Brown, W. Dubé, B. Lerner, E. Williams, J. Johnson, P. Quinn, T. Bates, B. Lefer, P. Hayes, J. Jimenez, R. Weber, R. Zamora, B. Ervens, D. Millet, B. Rappenglueck, and J. De Gouw. 2015. “Investigation of Secondary Formation of Formic Acid: Urban Environment vs. Oil and Gas Producing Region.” *Atmospheric Chemistry and Physics* 15(4):1975–93.

## Appendix A: Further WE-CAN details

WE-CAN flight details are discussed below (Table A1), including the date sampled, state, number of emission passes, latitude, longitude, distance from the fire source, and fuel type. The physical age of the smoke during the emission pass(es) were calculated from the distance downwind from the source multiplied by the wind speed obtained from the C-130.

**Table A1:** Details of emission passes sampled during WE-CAN, including fires, location, physical age, and detailed fuel type.

<sup>a</sup> Letters denoted in parentheses are for fires sampled more than 30 minutes apart, and each is treated as a “unique” fire for emission factor calculations.

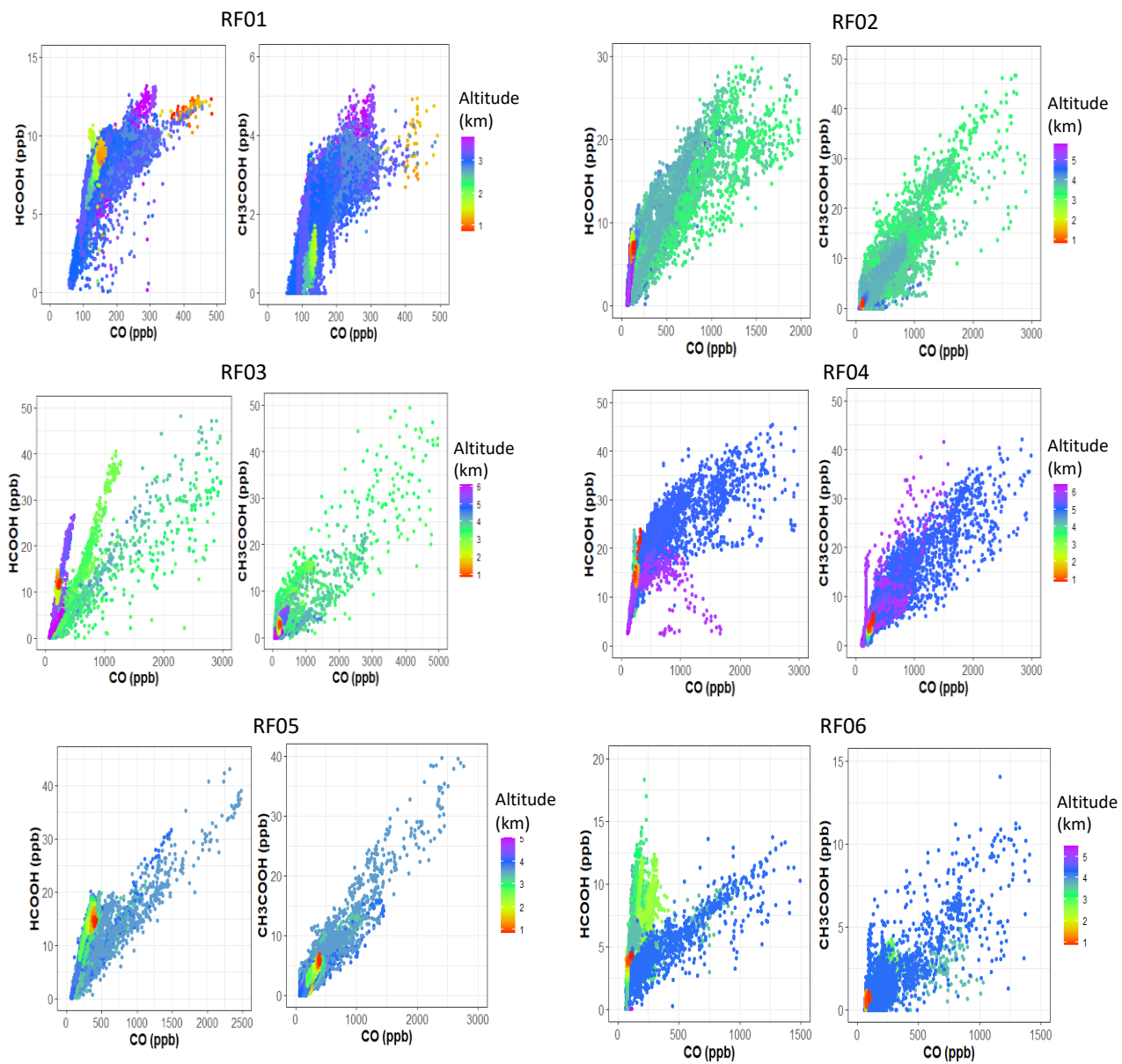
<sup>b</sup> Number of emission passes per fire, denoted by a, b, or c.

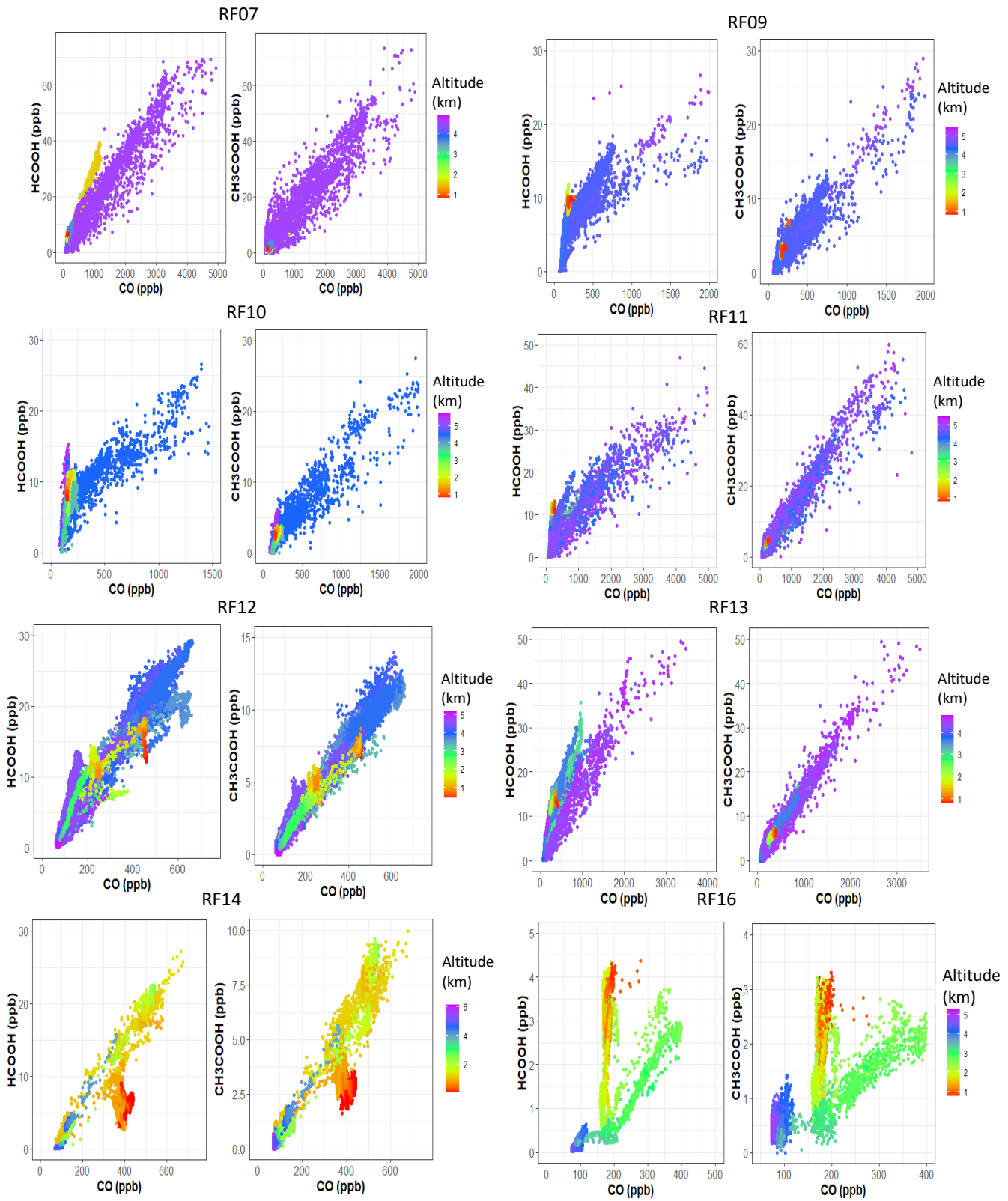
<sup>c</sup> Fuel type obtained from Jakob Lindaas.

Flight	Fire Name <sup>a</sup>	Date (2018)	State	Num. pass <sup>b</sup>	Lat.	Long.	Downwind distance (km)	Physical age (min)	Fuel type <sup>c</sup>
RF02	Carr (a,b)	7/26	CA	1, 1	40.63°	-122.52°	32.8–33.6	64–106	Ponderosa pine, Douglas fir, Jeffrey pine
RF03	Taylor Creek	7/30	OR	2	42.47°	-123.69°	11.5–13.7	22–27	Douglas fir, Madrone, Tanoak forest
RF04	Sharps (a, b)	7/31	ID	2, 1	43.59°	-114.16°	18.4–19.9	50–85	Douglas fir, Pacific ponderosa pine
RF06	Rabbit Foot (a, b, c)	8/03	ID	1	44.86°	-114.27°	11.2–29.8	22–78	Douglas fir, Ponderosa pine
RF10		8/13		1					
RF11		8/15		5					
RF07	Donnell (a, b)	8/06	CA	1, 2	38.36°	-119.88°	35.7–45.5	66–106	Red fir forest
RF09	Bear Trap (a, b)	8/09	UT	1, 1	39.29°	-109.87°	11.5–30.6	30–74	Engelmann spruce, Douglas fir, White fir, Ponderosa pine
RF09	Dollar Ridge	8/09	UT	1	40.14°	-110.88°	29.6	118	Pinyon, Utah Juniper
RF10	Monument	8/13	MT	1	45.00°	-111.82°	15.2	27	Whitebark pine, Subalpine fir
RF10	Wigwam	8/13	MT	1	45.14°	-111.89°	14.4	18	Douglas fir, Ponderosa pine
RF10	Goldstone (a, b)	8/13	MT/ID	1	45.11°	-113.56°	13.8–51.9	19–121	Mature lodgepole pine
RF11		8/15		1					
RF11	Beaver Creek (a, b)	8/15	MT	1, 1	45.94°	-113.51°	27.3–56.2	57–127	Whitebark pine, Subalpine fir
RF13	Mendocino Complex	8/20	CA	1	39.43°	-122.84°	57.1	120	Jeffrey pine, Red fir, White fir, Greenleaf manzanita, Snowbrush
RF18	Red Feather (a, b)	9/10	CO	1, 1	40.85°	-105.58°	3.5–4.8	17–17	Ponderosa pine savanna
RF19	Silver Creek (a, b)	9/13	CO	1, 1	40.23°	-106.60°	24.7–27.3	23–28	Subalpine fir, Lodgepole pine, Whitebark pine, Engelmann spruce

## Appendix B: HCOOH and CH<sub>3</sub>COOH against altitude for research flights.

**Figure B1:** Concentrations of CH<sub>3</sub>COOH and HCOOH against CO colored by altitude (red is low and purple is high altitude). RF10 was CO measured by the Picarro instrument while all other CO measurements here were by the Aerodyne (it was not running during RF10).





## Appendix C: Emissions from previous literature

**Table C1:** Emission ratios (ERs) from previous literature for both CH<sub>3</sub>COOH and HCOOH. Blank spaces indicate unavailable information.

Author	CH <sub>3</sub> COOH ER (ppb ppm(CO) <sup>-1</sup> )	HCOOH ER (ppb ppm(CO) <sup>-1</sup> )
Akagi et al., 2012	14.1 ± 1.2	0.66 ± 0.2
Bertschi et al., 2003	20.7	0.80
Bertschi et al., 2003	15.3	7.50
Bertschi et al., 2003	22.9	8.40
Bertschi et al., 2003	6.0	1.90
Bertschi et al., 2003	19.5	13.40
Bertschi et al., 2003	6.9	2.20
Bertschi et al., 2003	20.3	4.60
Bertschi et al., 2003	24.8	4.40
Bertschi et al., 2003	0.9	0.80
Christian et al., 2003	6.4 ± 2	1.77 ± 0.8
Christian et al., 2003		0.51 ± 0.2
Christian et al., 2003	20.5	2.36
Christian et al., 2003		0.93
Christian et al., 2003	40.4 ± 17.2	3.40 ± 0.7
Christian et al., 2003		2.24 ± 1.1
Christian et al., 2003	27.8 ± 2.5	7.33 ± 1.1
Christian et al., 2003		3.21 ± 0.4
Christian et al., 2003	42.2 ± 21.5	4.51 ± 1.3
Christian et al., 2003		2.04 ± 0.7
Goode et al., 2000	15.8	11.60
Goode et al., 2000	16.5	5.80
Goode et al., 2000	8.7	5.20
Goode et al., 2000	11.5	7.70
Koss et al., 2018	14.7 ± 3.1	2.86 ± 1.4
Koss et al., 2018	13.7 ± 4.9	2.25 ± 1.0
Koss et al., 2018	11.2 ± 5.3	2.41 ± 0.8
Koss et al., 2018	20.1 ± 11.4	2.33 ± 1.0
Koss et al., 2018	9.1 ± 3.1	1.31 ± 0.4
Koss et al., 2018	10.3 ± 0.02	0.74 ± 0.0
Koss et al., 2018	16.5	2.95
Koss et al., 2018	11.6 ± 2.0	1.95 ± 0.1
Koss et al., 2018	12.8 ± 2.2	1.11 ± 0.3
Koss et al., 2018	11.0 ± 2.5	1.64 ± 0.6
Koss et al., 2018	12.4 ± 3.2	1.82 ± 0.4
Koss et al., 2018	7.5 ± 1.5	0.78 ± 0.1
Koss et al., 2018	5.7 ± 0.6	0.71 ± 0.2

Koss et al., 2018	13.3 ± 5.2	1.64 ± 1.0
Koss et al., 2018	70.0	6.80
Koss et al., 2018	53.0	6.27
Koss et al., 2018	7.7	0.97
Koss et al., 2018	35.5	2.91
Koss et al., 2018	22.7 ± 10.9	1.71 ± 0.6
Koss et al., 2018	5.3	0.85
McKenzie et al., 1995	7.4 ± 6.2	1.50 ± 1.5
Müller et al., 2016	2.7 ± 0.3	1.40 ± 0.6
Stockwell et al., 2015	13.6	1.59
Stockwell et al., 2015	14.8	2.36
Stockwell et al., 2015	17.5	2.16
Stockwell et al., 2015	5.6	2.04
Stockwell et al., 2015		1.70
Stockwell et al., 2015		1.80
Stockwell et al., 2015		1.16
Stockwell et al., 2015	5.9	0.75
Stockwell et al., 2015		0.84
Stockwell et al., 2015	6.2	0.99
Stockwell et al., 2015	5.3	1.84
Stockwell et al., 2015	11.7	1.15
Stockwell et al., 2015	25.8	2.39
Stockwell et al., 2015	25.3	4.00
Stockwell et al., 2015	17.0	1.37
Stockwell et al., 2015	12.4	1.66
Stockwell et al., 2015	7.5	0.28
Stockwell et al., 2015	15.9	1.58
Stockwell et al., 2015	80.3	2.00
Stockwell et al., 2015	11.8	0.17
Stockwell et al., 2015	7.4	
Stockwell et al., 2015	14.8	3.55
Stockwell et al., 2015	9.2	2.65
Stockwell et al., 2015	24.5	6.20
Stockwell et al., 2015	13.7	4.06
Stockwell et al., 2015	9.6	1.34
Stockwell et al., 2015	11.9	1.54
Stockwell et al., 2015	6.5	0.95
Stockwell et al., 2015	11.5	1.60
Stockwell et al., 2015	3.4	0.39
Stockwell et al., 2015	12.6	1.28
Stockwell et al., 2015	3.6	0.17

Stockwell et al., 2015	2.2	
Stockwell et al., 2015	7.4	2.18
Stockwell et al., 2015	12.0	3.62
Stockwell et al., 2015	2.0	1.76
Stockwell et al., 2015	18.5	1.56
Stockwell et al., 2015		0.68
Stockwell et al., 2015		0.65
Stockwell et al., 2015	64.4	6.47
Stockwell et al., 2015	51.0	5.74
Stockwell et al., 2015	85.6	9.11
Stockwell et al., 2015	3.9	0.45
Stockwell et al., 2015	16.1	2.16
Stockwell et al., 2015	6.5	1.50
Stockwell et al., 2015	2.9	0.53
Stockwell et al., 2015	2.6	0.34
Stockwell et al., 2015	24.3	1.08
Stockwell et al., 2015	7.8	1.40
Stockwell et al., 2015	7.5	1.05
Stockwell et al., 2015	18.6	1.00
Stockwell et al., 2015	31.8	3.49
Stockwell et al., 2015	14.3	0.92
Stockwell et al., 2015	2.6	0.43
Stockwell et al., 2015	4.6	0.54
Stockwell et al., 2015	6.5	2.14
Stockwell et al., 2015	11.4	1.95
Stockwell et al., 2015	3.1	0.39
Stockwell et al., 2015	6.9	0.82
Stockwell et al., 2015	6.9	1.14
Stockwell et al., 2015	2.1	1.32
Stockwell et al., 2015	7.7	1.03
Stockwell et al., 2015	29.3	2.19
Stockwell et al., 2015	18.9	1.16
Stockwell et al., 2015	3.2	0.34
Stockwell et al., 2015	21.2	4.98
Stockwell et al., 2015	30.9	6.80
Stockwell et al., 2015	26.2	6.54
Stockwell et al., 2015	13.9	4.37
Stockwell et al., 2015	40.8	7.68
Stockwell et al., 2015	24.3	5.05
Stockwell et al., 2015	19.6	5.38
Stockwell et al., 2015	26.1	6.32

Stockwell et al., 2015	28.0	2.18
Stockwell et al., 2015	5.9	0.73
Stockwell et al., 2015	24.5	6.64
Stockwell et al., 2015	8.2	2.67
Stockwell et al., 2015	9.9	3.44
Stockwell et al., 2015	8.7	0.97
Stockwell et al., 2015	6.9	1.13
Stockwell et al., 2015	11.6	1.21
Stockwell et al., 2015	2.8	0.44
Stockwell et al., 2015	8.3	1.16
Stockwell et al., 2015	2.4	0.40
Stockwell et al., 2015	6.7	0.56
Stockwell et al., 2015	2.9	0.50
Stockwell et al., 2015	2.7	0.53
Stockwell et al., 2015	5.4	0.60
Stockwell et al., 2015	3.5	0.18
Stockwell et al., 2015		0.42
Stockwell et al., 2015	7.2	1.52
Stockwell et al., 2015	3.9	0.59
Stockwell et al., 2015	48.9	12.54
Stockwell et al., 2015	31.4	6.50
Stockwell et al., 2015	7.8	0.60
Stockwell et al., 2015		0.38
Stockwell et al., 2015		1.53
Stockwell et al., 2015	9.6	0.94
Stockwell et al., 2015	4.1	0.62
Stockwell et al., 2015	11.0	1.28
Stockwell et al., 2015	6.1	0.95
Stockwell et al., 2015	21.0	2.04
Stockwell et al., 2015	37.3	3.14
Stockwell et al., 2015	34.5	2.19
Stockwell et al., 2015	23.5	4.00
Stockwell et al., 2015	12.4	2.59
Stockwell et al., 2015	22.3	2.75
Stockwell et al., 2015	4.5	0.58
Stockwell et al., 2015	3.9	0.53
Stockwell et al., 2015	3.7	0.36
Stockwell et al., 2015	3.0	1.12
Stockwell et al., 2015	5.9	1.34
Stockwell et al., 2015	5.5	1.31
Stockwell et al., 2015	8.9	1.02

Yokelson et al., 1999	17.3	8.50
Yokelson et al., 2003	19.2	2.10
Yokelson et al., 2003	16.8	6.60
Yokelson et al., 2003	16.9	8.70
Yokelson et al., 2003	16.9	5.40
Yokelson et al., 2003	16.4	4.50
Yokelson et al., 2003	13.2	10.80
Yokelson et al., 2003	14.8	5.10
Yokelson et al., 2003	12.5	8.70
Yokelson et al., 2003	14.6	6.40

**Table C2:** Emission factors (EFs) from previous literature for CH<sub>3</sub>COOH and HCOOH. Blank spaces indicate the information was unavailable in the publication.

Author	CH <sub>3</sub> COOH EF (g/kg)	HCOOH EF (g/kg)	MCE	Measurement Type	Location Found	Fuel	Instrument
Akagi et al., 2013	1.03		0.876	Field	South Carolina	Conifer forest	AFTIR
Akagi et al., 2013	3.84		0.858	Field	South Carolina	Conifer forest	AFTIR
Akagi et al., 2013	2.42		0.789	Field	South Carolina	Mixedwood forest	AFTIR
Akagi et al., 2013	1.24	0.08	0.932	Field	South Carolina	Conifer forest	AFTIR
Akagi et al., 2013	0.75	0.09	0.919	Field	South Carolina	Conifer forest	AFTIR
Akagi et al., 2013	1.25	0.11	0.935	Field	South Carolina	Mixedwood forest	AFTIR
Akagi et al., 2013	1.85	0.03	0.904	Field	South Carolina	Conifer forest	AFTIR
Akagi et al., 2013	2.33		0.938	Field	South Carolina	Conifer forest	AFTIR
Akagi et al., 2013	1.6	0.08	0.933	Field	South Carolina	Conifer forest	AFTIR
Akagi et al., 2013	2.82		0.957	Field	South Carolina	Conifer forest	AFTIR
Bertschi et al., 2003	5.67	0.17	0.879	Lab	Montana	Organic soil	OP-FTIR
Bertschi et al., 2003	5.05	1.89	0.858	Lab	Montana	Organic soil	OP-FTIR
Bertschi et al., 2003	7.72	2.16	0.857	Lab	Montana	Organic soil	OP-FTIR
Bertschi et al., 2003	1.43	0.34	0.891	Lab	Canada	Organic soil	OP-FTIR
Bertschi et al., 2003	6.9	3.63	0.848	Lab	Canada	Organic soil	OP-FTIR
Bertschi et al., 2003	1.6	0.39	0.904	Lab	Montana	Organic soil	OP-FTIR
Bertschi et al., 2003	6.73	1.16	0.856	Lab	Montana	Hardwood forest	OP-FTIR
Bertschi et al., 2003	8.43	1.15	0.854	Lab	Africa	Hardwood forest	OP-FTIR
Bertschi et al., 2003	0.3	0.21	0.861	Lab	Montana	Mixedwood forest	OP-FTIR
Burling et al., 2010	3.688	0.46	0.894	Lab	Georgia	Conifer forest	OP-FTIR
Burling et al., 2010	1.853	0.227	0.934	Lab	North Carolina	Conifer forest	OP-FTIR
Burling et al., 2010	2.743	0.28	0.927	Lab	North Carolina	Conifer forest	OP-FTIR

Burling et al., 2010	1.276	0.119	0.954	Lab	North Carolina	Conifer forest	OP-FTIR
Burling et al., 2010	0.407	0.035	0.965	Lab	Arizona	Hardwood forest	OP-FTIR
Burling et al., 2010	0.366	0.04	0.971	Lab	Arizona	Hardwood forest	OP-FTIR
Burling et al., 2010	9.278	0.917	0.827	Lab	Alaska	Organic soil	OP-FTIR
Burling et al., 2010	0.506	0.051	0.954	Lab	Arizona	Masticated mestique	OP-FTIR
Burling et al., 2010	0.337	0.033	0.959	Lab	North Carolina	Chipped understory hardwood	OP-FTIR
Burling et al., 2010	0.188	0.079	0.959	Lab	Montana	Ponderosa pine	OP-FTIR
Burling et al., 2010	2.17	0.393	0.934	Lab	Montana	Conifer forest	OP-FTIR
Burling et al., 2010	2.119	0.224	0.953	Lab	North Carolina	Shrubland	OP-FTIR
Burling et al., 2010	0.342	0.05	0.948	Lab	California	Shrubland	OP-FTIR
Burling et al., 2010	0.928	0.104	0.939	Lab	California	Shrubland	OP-FTIR
Burling et al., 2010	0.414	0.032	0.952	Lab	California	Shrubland	OP-FTIR
Burling et al., 2010	0.864	0.123	0.946	Lab	California	Shrubland	OP-FTIR
Burling et al., 2010	0.434	0.045	0.944	Lab	California	Shrubland	OP-FTIR
Burling et al., 2010	0.377	0.032	0.939	Lab	California	Shrubland	OP-FTIR
Burling et al., 2011	0.72		0.759	Field	North Carolina	Conifer forest	AFTIR
Burling et al., 2011	0.5		0.796	Field	North Carolina	Conifer forest	AFTIR
Burling et al., 2011	1.6		0.823	Field	North Carolina	Conifer forest	AFTIR
Burling et al., 2011	7.05		0.85	Field	North Carolina	Conifer forest	AFTIR
Burling et al., 2011	1.36		0.864	Field	North Carolina	Conifer forest	AFTIR
Burling et al., 2011	0.52		0.914	Field	North Carolina	Conifer forest	AFTIR
Burling et al., 2011	1.26		0.931	Field	North Carolina	Conifer forest	AFTIR
Burling et al., 2011	0.24		0.794	Field	North Carolina	Conifer forest	AFTIR
Burling et al., 2011	0.67	0.049	0.951	Field	North Carolina	Conifer forest	AFTIR
Burling et al., 2011	0.62	0.047	0.957	Field	North Carolina	Conifer forest	AFTIR
Burling et al., 2011	3.72	0.25	0.885	Field	California	Conifer forest	AFTIR
Burling et al., 2011	2.32	0.177	0.913	Field	California	Conifer forest	AFTIR
Burling et al., 2011	3.29	0.24	0.94	Field	Arizona	Hardwood forest	AFTIR
Burling et al., 2011	0.47	0.002	0.947	Field	California	Shrubland	AFTIR
Burling et al., 2011	2.17	0.082	0.938	Field	California	Shrubland	AFTIR
Burling et al., 2011	1.76	0.02	0.903	Field	California	Shrubland	AFTIR
Burling et al., 2011	1.49	0.039	0.95	Field	California	Shrubland	AFTIR
Burling et al., 2011	2.29	0.082	0.933	Field	California	Shrubland	AFTIR

Burling et al., 2011	0.71	0.061	0.943	Field	North Carolina	Conifer forest	AFTIR
Burling et al., 2011	0.67	0.05	0.951	Field	North Carolina	Conifer forest	AFTIR
Christian et al., 2003	0.73	0.15	0.953	Lab	Africa	Alang Alang	OP-FTIR
Christian et al., 2003		0.04		Lab	Africa	Alang Alang	PTR-MS
Christian et al., 2003	8.97	0.79	0.838	Lab	Africa	Peat	OP-FTIR
Christian et al., 2003		0.3		Lab	Africa	Peat	PTR-MS
Christian et al., 2003	10.56	0.65	0.901	Lab	Africa	Secondary forest litter	OP-FTIR
Christian et al., 2003		0.44		Lab	Africa	Secondary forest litter	PTR-MS
Christian et al., 2003	10.61	2.12	0.811	Lab	Africa	Rice straw	OP-FTIR
Christian et al., 2003		0.8		Lab	Africa	Rice straw	PTR-MS
Christian et al., 2003	10.87	0.92	0.891	Lab	Africa	Semak	OP-FTIR
Christian et al., 2003		0.39		Lab	Africa	Semak	PTR-MS
Goode et al., 1999	1.375		0.972	Lab		Conifer forest	OP-FTIR
Goode et al., 1999	1.262		0.964	Lab		Grassland	OP-FTIR
Goode et al., 1999	2.197	0.895	0.95	Lab		Conifer forest	OP-FTIR
Goode et al., 1999	0.548		0.979	Lab		Conifer forest	OP-FTIR
Goode et al., 1999	0.648	0.245	0.969	Lab		Grassland	OP-FTIR
Goode et al., 1999	1.641		0.96	Lab		Grassland	OP-FTIR
Goode et al., 2000	2.95	1.57	0.925	Lab	Alaska	Grassland	AFTIR
Goode et al., 2000	3.38	1.04	0.916	Lab	Alaska	Conifer forest	AFTIR
Goode et al., 2000	1.61	0.71	0.929	Lab	Alaska	Conifer forest	AFTIR
Goode et al., 2000	2.26	1.21	0.917	Lab	Alaska	Conifer forest	AFTIR
Koss et al., 2018		0.3183	0.9373	Lab		Conifer forest	PTR-ToF-MS
Koss et al., 2018		0.2963	0.931	Lab		Conifer forest	PTR-ToF-MS
Koss et al., 2018		0.1667	0.941	Lab		Conifer forest	PTR-ToF-MS
Koss et al., 2018		0.1872	0.9431	Lab		Conifer forest	PTR-ToF-MS
Koss et al., 2018		0.2376	0.92	Lab		Conifer forest	PTR-ToF-MS
Koss et al., 2018		0.2851	0.9569	Lab		Conifer forest	PTR-ToF-MS
Koss et al., 2018		0.3458	0.926	Lab		Conifer forest	PTR-ToF-MS
Koss et al., 2018		0.6195	0.8856	Lab		Conifer forest	PTR-ToF-MS
Koss et al., 2018		0.3859	0.9279	Lab		Conifer forest	PTR-ToF-MS
Koss et al., 2018		0.231	0.9345	Lab		Conifer forest	PTR-ToF-MS
Koss et al., 2018		0.2123	0.9255	Lab		Conifer forest	PTR-ToF-MS
Koss et al., 2018		0.0868	0.9471	Lab		Conifer forest	PTR-ToF-MS

Koss et al., 2018		0.1229	0.9499	Lab		Conifer forest	PTR-ToF-MS
Koss et al., 2018		0.9307	0.7805	Lab		Conifer forest	PTR-ToF-MS
Koss et al., 2018		0.1042	0.9223	Lab		Conifer forest	PTR-ToF-MS
Koss et al., 2018		0.3046	0.9396	Lab		Conifer forest	PTR-ToF-MS
Koss et al., 2018		0.1854	0.9448	Lab		Conifer forest	PTR-ToF-MS
Koss et al., 2018		0.5987	0.9041	Lab		Conifer forest	PTR-ToF-MS
Koss et al., 2018		0.5726	0.924	Lab		Conifer forest	PTR-ToF-MS
Koss et al., 2018		0.195	0.9377	Lab		Conifer forest	PTR-ToF-MS
Koss et al., 2018		0.074	0.9507	Lab		Conifer forest	PTR-ToF-MS
Koss et al., 2018		0.3012	0.9323	Lab		Conifer forest	PTR-ToF-MS
Koss et al., 2018		0.5485	0.9063	Lab		Conifer forest	PTR-ToF-MS
Koss et al., 2018		0.1032	0.9294	Lab		Conifer forest	PTR-ToF-MS
Koss et al., 2018		0.2591	0.9511	Lab		Conifer forest	PTR-ToF-MS
Koss et al., 2018		0.2515	0.9275	Lab		Conifer forest	PTR-ToF-MS
Koss et al., 2018		0.4411	0.9126	Lab		Conifer forest	PTR-ToF-MS
Koss et al., 2018		0.345	0.9364	Lab		Conifer forest	PTR-ToF-MS
Koss et al., 2018		0.3795	0.9255	Lab		Conifer forest	PTR-ToF-MS
Koss et al., 2018		0.213	0.9421	Lab		Conifer forest	PTR-ToF-MS
Koss et al., 2018		0.2663	0.9284	Lab		Conifer forest	PTR-ToF-MS
Koss et al., 2018		0.2913	0.9401	Lab		Conifer forest	PTR-ToF-MS
Koss et al., 2018		0.7938	0.9319	Lab		Conifer forest	PTR-ToF-MS
Koss et al., 2018		0.2127	0.9394	Lab		Conifer forest	PTR-ToF-MS
Koss et al., 2018		1.089	0.8971	Lab		Grassland	PTR-ToF-MS
Koss et al., 2018		0.2294	0.8171	Lab		Organic soil	PTR-ToF-MS
Koss et al., 2018		0.3339	0.8314	Lab		Organic soil	PTR-ToF-MS
Koss et al., 2018		0.2848	0.8863	Lab		Organic soil	PTR-ToF-MS
Koss et al., 2018		0.6126	0.8771	Lab		Organic soil	PTR-ToF-MS
Koss et al., 2018		0.0692	0.971	Lab		Other	PTR-ToF-MS
Koss et al., 2018		0.3699	0.8993	Lab		Other	PTR-ToF-MS
Koss et al., 2018		0.4252	0.9527	Lab		Other	PTR-ToF-MS
Koss et al., 2018		0.2043	0.9451	Lab		Other	PTR-ToF-MS
Koss et al., 2018		0.0741	0.9508	Lab		Other	PTR-ToF-MS
Koss et al., 2018		0.093	0.948	Lab		Shrubland	PTR-ToF-MS
Koss et al., 2018		0.0686	0.9459	Lab		Shrubland	PTR-ToF-MS

Koss et al., 2018		0.1376	0.9631	Lab		Shrubland	PTR-ToF-MS
Koss et al., 2018		0.052	0.9593	Lab		Shrubland	PTR-ToF-MS
Koss et al., 2018		0.0954	0.963	Lab		Shrubland	PTR-ToF-MS
Koss et al., 2018		0.0811	0.9539	Lab		Shrubland	PTR-ToF-MS
Koss et al., 2018		0.142	0.9622	Lab		Shrubland	PTR-ToF-MS
Koss et al., 2018		0.0795	0.9644	Lab		Shrubland	PTR-ToF-MS
Koss et al., 2018		0.0415	0.9563	Lab		Shrubland	PTR-ToF-MS
Koss et al., 2018		0.0633	0.9539	Lab		Shrubland	PTR-ToF-MS
Koss et al., 2018		0.1841	0.9192	Lab		Shrubland	PTR-ToF-MS
Koss et al., 2018		0.2559	0.9422	Lab		Shrubland	PTR-ToF-MS
Koss et al., 2018		0.116	0.9225	Lab		Shrubland	PTR-ToF-MS
Koss et al., 2018		0.0914	0.9468	Lab		Shrubland	PTR-ToF-MS
McKenzie et al., 1995	4.4	0.97		Lab	Montana	Conifer forest	GC-FID
McKenzie et al., 1995	0.34	0.18		Lab	Montana	Conifer forest	GC-FID
McKenzie et al., 1995	7.6	0.43		Lab	Montana	Conifer forest	GC-FID
McKenzie et al., 1995	5.4	0.48		Lab	Montana	Conifer forest	GC-FID
McKenzie et al., 1995	3.3	0.97		Lab	Montana	Conifer forest	GC-FID
McKenzie et al., 1995	2.4	1		Lab	Montana	Conifer forest	GC-FID
McKenzie et al., 1995	1.3	0.2		Lab	Montana	Conifer forest	GC-FID
McKenzie et al., 1995	0.85	0.038		Lab	Montana	Organic soil	GC-FID
McKenzie et al., 1995	0.66			Lab	Montana	Organic soil	GC-FID
McKenzie et al., 1995	0.19			Lab	Montana	Organic soil	GC-FID
Müller et al., 2016	0.47	0.13	0.9	Field	Georgia	Pine forest understory	PTR-ToF-MS
Selimovic et al., 2018	0.8311	0.2437	0.9373	Lab		Conifer forest	OP-FTIR
Selimovic et al., 2018	0.6692	0.1969	0.931	Lab		Conifer forest	OP-FTIR
Selimovic et al., 2018	1.7072	0.2622	0.9356	Lab		Conifer forest	OP-FTIR
Selimovic et al., 2018	1.4747	0.209	0.9297	Lab		Conifer forest	OP-FTIR
Selimovic et al., 2018	1.2691	0.2129	0.9311	Lab		Conifer forest	OP-FTIR
Selimovic et al., 2018	0.3352	0.1579	0.941	Lab		Conifer forest	OP-FTIR
Selimovic et al., 2018	1.0065	0.1719	0.9431	Lab		Conifer forest	OP-FTIR
Selimovic et al., 2018	1.8529	0.2068	0.92	Lab		Conifer forest	OP-FTIR
Selimovic et al., 2018	2.2881	0.22	0.9259	Lab		Conifer forest	OP-FTIR
Selimovic et al., 2018	1.0578	0.186	0.9435	Lab		Conifer forest	OP-FTIR
Selimovic et al., 2018	1.0191	0.2457	0.9481	Lab		Conifer forest	OP-FTIR

Selimovic et al., 2018	0.5927	0.2623	0.9569	Lab		Conifer forest	OP-FTIR
Selimovic et al., 2018	1.447	0.3386	0.926	Lab		Conifer forest	OP-FTIR
Selimovic et al., 2018	4.1491	0.7894	0.8856	Lab		Conifer forest	OP-FTIR
Selimovic et al., 2018	0.7854	0.0856	0.9544	Lab		Conifer forest	OP-FTIR
Selimovic et al., 2018	8.3122	1.1746	0.8903	Lab		Conifer forest	OP-FTIR
Selimovic et al., 2018	1.7092	0.4078	0.9279	Lab		Conifer forest	OP-FTIR
Selimovic et al., 2018	1.9737	0.212	0.9345	Lab		Conifer forest	OP-FTIR
Selimovic et al., 2018	0.5938	0.1515	0.9355	Lab		Conifer forest	OP-FTIR
Selimovic et al., 2018	1.6113	0.2013	0.9255	Lab		Conifer forest	OP-FTIR
Selimovic et al., 2018	0.6068	0.0892	0.9454	Lab		Conifer forest	OP-FTIR
Selimovic et al., 2018	0.3342	0.0699	0.9471	Lab		Conifer forest	OP-FTIR
Selimovic et al., 2018	0.7524	0.1096	0.9499	Lab		Conifer forest	OP-FTIR
Selimovic et al., 2018		1.3835	0.7805	Lab		Douglas fir	OP-FTIR
Selimovic et al., 2018	0.7625	0.0826	0.9644	Lab		Conifer forest	OP-FTIR
Selimovic et al., 2018	3.9215	0.2876	0.8713	Lab		Conifer forest	OP-FTIR
Selimovic et al., 2018	1.6832	0.1813	0.9396	Lab		Conifer forest	OP-FTIR
Selimovic et al., 2018	1.6803	0.6447	0.9448	Lab		Conifer forest	OP-FTIR
Selimovic et al., 2018	3.8524	0.568	0.9041	Lab		Conifer forest	OP-FTIR
Selimovic et al., 2018	2.4746	0.1644	0.924	Lab		Conifer forest	OP-FTIR
Selimovic et al., 2018	2.3743	0.1985	0.9377	Lab		Conifer forest	OP-FTIR
Selimovic et al., 2018	1.0045	0.0759	0.9513	Lab		Conifer forest	OP-FTIR
Selimovic et al., 2018	0.8804	0.1875	0.9549	Lab		Conifer forest	OP-FTIR
Selimovic et al., 2018	2.6194	0.5501	0.9185	Lab		Conifer forest	OP-FTIR
Selimovic et al., 2018	2.9439	0.2991	0.9323	Lab		Conifer forest	OP-FTIR
Selimovic et al., 2018	5.993	0.3965	0.9063	Lab		Conifer forest	OP-FTIR
Selimovic et al., 2018	1.2418	0.2368	0.9573	Lab		Conifer forest	OP-FTIR
Selimovic et al., 2018	1.77	0.091	0.9294	Lab		Conifer forest	OP-FTIR
Selimovic et al., 2018	1.4519	0.2629	0.9469	Lab		Conifer forest	OP-FTIR
Selimovic et al., 2018	1.0442	0.2219	0.9511	Lab		Conifer forest	OP-FTIR
Selimovic et al., 2018	1.5466	0.2425	0.9275	Lab		Conifer forest	OP-FTIR
Selimovic et al., 2018	3.799	0.4704	0.9126	Lab		Conifer forest	OP-FTIR
Selimovic et al., 2018	1.8323	0.2811	0.9255	Lab		Conifer forest	OP-FTIR
Selimovic et al., 2018	3.6253	0.4037	0.8771	Lab		Conifer forest	OP-FTIR
Selimovic et al., 2018	1.2395	0.2134	0.9284	Lab		Conifer forest	OP-FTIR

Selimovic et al., 2018	2.199	0.0812	0.9422	Lab		Conifer forest	OP-FTIR
Selimovic et al., 2018	1.805	0.2707	0.9319	Lab		Conifer forest	OP-FTIR
Selimovic et al., 2018	1.2095	0.8749	0.9468	Lab		Conifer forest	OP-FTIR
Selimovic et al., 2018	3.592	0.1906	0.8384	Lab		Conifer forest	OP-FTIR
Selimovic et al., 2018	1.2166	0.1533	0.9337	Lab		Conifer forest	OP-FTIR
Selimovic et al., 2018	1.5653	0.9153	0.9364	Lab		Grassland	OP-FTIR
Selimovic et al., 2018	3.1999	0.2353	0.8681	Lab		Organic soil	OP-FTIR
Selimovic et al., 2018	5.1397	0.3478	0.8171	Lab		Organic soil	OP-FTIR
Selimovic et al., 2018	1.9739	0.5398	0.9223	Lab		Organic soil	OP-FTIR
Selimovic et al., 2018	4.4491	0.3685	0.8314	Lab		Organic soil	OP-FTIR
Selimovic et al., 2018	7.9532	0.2765	0.8863	Lab		Organic soil	OP-FTIR
Selimovic et al., 2018	1.7692	0.5556	0.9192	Lab		Organic soil	OP-FTIR
Selimovic et al., 2018	0.838	0.0648	0.971	Lab		Other	OP-FTIR
Selimovic et al., 2018	6.3562	0.3367	0.8993	Lab		Other	OP-FTIR
Selimovic et al., 2018	2.4937	0.2483	0.9527	Lab		Other	OP-FTIR
Selimovic et al., 2018	2.945	0.177	0.9451	Lab		Other	OP-FTIR
Selimovic et al., 2018	1.8809	0.1617	0.9225	Lab		Other	OP-FTIR
Selimovic et al., 2018	0.5994	0.0719	0.948	Lab		Shrubland	OP-FTIR
Selimovic et al., 2018	0.6836	0.0516	0.9459	Lab		Shrubland	OP-FTIR
Selimovic et al., 2018	2.7341	0.2988	0.9631	Lab		Shrubland	OP-FTIR
Selimovic et al., 2018	0.485	0.0444	0.9593	Lab		Shrubland	OP-FTIR
Selimovic et al., 2018	0.3013	0.065	0.963	Lab		Shrubland	OP-FTIR
Selimovic et al., 2018	2.6999	0.055	0.7805	Lab		Shrubland	OP-FTIR
Selimovic et al., 2018	0.7624	0.1099	0.9539	Lab		Shrubland	OP-FTIR
Selimovic et al., 2018	1.0682	0.0648	0.9622	Lab		Shrubland	OP-FTIR
Selimovic et al., 2018	0.6148	0.0329	0.9563	Lab		Shrubland	OP-FTIR
Selimovic et al., 2018	0.769	0.0528	0.9539	Lab		Shrubland	OP-FTIR
Selimovic et al., 2018	1.0276	0.1788	0.9421	Lab		Shrubland	OP-FTIR
Selimovic et al., 2018	0.5451	0.2352	0.9508	Lab		Shrubland	OP-FTIR
Selimovic et al., 2018	1.2895	0.1211	0.9401	Lab		Shrubland	OP-FTIR
Selimovic et al., 2018	0.8215	0.0748	0.9394	Lab		Shrubland	OP-FTIR
Stockwell et al., 2015	0.7223	0.0648	0.9755	Lab	Africa	savanna/sourveld /tall grass or savanna/sweetveld/shortgrass	PTR-ToF-MS
Stockwell et al., 2015	0.8557	0.1049	0.9734	Lab	Africa	savanna/sourveld /tall grass or	PTR-ToF-MS

						savanna/sweetveld/shortgrass	
Stockwell et al., 2015	0.855	0.1049	0.9747	Lab	Africa	savanna/sourveld /tall grass or savanna/sweetveld/shortgrass	PTR-ToF-MS
Stockwell et al., 2015	0.9586	0.0908	0.9789	Lab	Africa	savanna/sourveld /tall grass or savanna/sweetveld/shortgrass	PTR-ToF-MS
Stockwell et al., 2015	0.2561	0.0722	0.9814	Lab	Africa	savanna/sourveld /tall grass or savanna/sweetveld/shortgrass	PTR-ToF-MS
Stockwell et al., 2015		0.053	0.9816	Lab	Africa	savanna/sourveld /tall grass or savanna/sweetveld/shortgrass	PTR-ToF-MS
Stockwell et al., 2015		0.0556	0.984	Lab	Africa	savanna/sourveld /tall grass or savanna/sweetveld/shortgrass	PTR-ToF-MS
Stockwell et al., 2015		0.031	0.9832	Lab	Africa	savanna/sourveld /tall grass or savanna/sweetveld/shortgrass	PTR-ToF-MS
Stockwell et al., 2015	0.2153	0.0212	0.9811	Lab	Africa	savanna/sourveld /tall grass or savanna/sweetveld/shortgrass	PTR-ToF-MS
Stockwell et al., 2015		0.0267	0.9854	Lab	Africa	savanna/sourveld /tall grass or savanna/sweetveld/shortgrass	PTR-ToF-MS
Stockwell et al., 2015	0.1974	0.0244	0.9811	Lab	Africa	savanna/sourveld /tall grass or savanna/sweetveld/shortgrass	PTR-ToF-MS
Stockwell et al., 2015	0.217	0.0581	0.9778	Lab	Africa	savanna/sourveld /tall grass or savanna/sweetveld/shortgrass	PTR-ToF-MS
Stockwell et al., 2015	0.5728	0.0435		Lab	Africa	savanna/sourveld /tall grass or savanna/sweetveld/shortgrass	PTR-ToF-MS
Stockwell et al., 2015	0.5725	0.0434	0.9735	Lab	Africa	savanna/sourveld /tall grass or savanna/sweetveld/shortgrass	PTR-ToF-MS
Stockwell et al., 2015	1.5034	0.1068	0.9705	Lab	Africa	savanna/sourveld /tall grass or savanna/sweetveld/shortgrass	PTR-ToF-MS
Stockwell et al., 2015	1.6383	0.1983	0.9699	Lab	Africa	savanna/sourveld /tall grass or savanna/sweetveld/shortgrass	PTR-ToF-MS
Stockwell et al., 2015	1.1021	0.0684		Lab	Africa	savanna/sourveld /tall grass or savanna/sweetveld/shortgrass	PTR-ToF-MS
Stockwell et al., 2015	1.1011	0.0683	0.9717	Lab	Africa	savanna/sourveld /tall grass or savanna/sweetveld/shortgrass	PTR-ToF-MS
Stockwell et al., 2015	0.7597	0.0778	0.9806	Lab	Africa	savanna/sourveld /tall grass or	PTR-ToF-MS

						savanna/sweetveld/shortgrass	
Stockwell et al., 2015	0.3188	0.0092	0.9763	Lab	Africa	savanna/sourveld/tall grass or savanna/sweetveld/shortgrass	PTR-ToF-MS
Stockwell et al., 2015	0.8246	0.0629		Lab	Africa	savanna/sourveld/tall grass or savanna/sweetveld/shortgrass	PTR-ToF-MS
Stockwell et al., 2015	13.435	0.2563	0.9147	Lab	Colorado	Crop residue	PTR-ToF-MS
Stockwell et al., 2015	13.342	0.2545	0.9147	Lab	Colorado	Crop residue	PTR-ToF-MS
Stockwell et al., 2015	2.0859	0.0231	0.9123	Lab	Colorado	Crop residue	PTR-ToF-MS
Stockwell et al., 2015	2.0775	0.023	0.9123	Lab	Colorado	Crop residue	PTR-ToF-MS
Stockwell et al., 2015	1.0905		0.9279	Lab	Colorado	Crop residue	PTR-ToF-MS
Stockwell et al., 2015	1.4768	0.2713	0.9594	Lab	Alaska	Boreal forest	PTR-ToF-MS
Stockwell et al., 2015	1.4725	0.2706		Lab	Alaska	Boreal forest	PTR-ToF-MS
Stockwell et al., 2015	0.6835	0.1502	0.9702	Lab	Alaska	Boreal forest	PTR-ToF-MS
Stockwell et al., 2015	2.8698	0.5557	0.9514	Lab	Alaska	Boreal forest	PTR-ToF-MS
Stockwell et al., 2015	1.4875	0.3373	0.9559	Lab	Alaska	Boreal forest	PTR-ToF-MS
Stockwell et al., 2015	2.2452	0.2386	0.9027	Lab	California	Chaparral	PTR-ToF-MS
Stockwell et al., 2015	2.5662	0.2548	0.9106	Lab	California	Chaparral	PTR-ToF-MS
Stockwell et al., 2015	1.3694	0.1547	0.913	Lab	California	Chaparral	PTR-ToF-MS
Stockwell et al., 2015	2.0057	0.214	0.9285	Lab	California	Chaparral	PTR-ToF-MS
Stockwell et al., 2015	0.486	0.0427	0.9433	Lab	California	Chaparral	PTR-ToF-MS
Stockwell et al., 2015	0.4857	0.0426		Lab	California	Chaparral	PTR-ToF-MS
Stockwell et al., 2015	1.4201	0.11	0.9544	Lab	California	Chaparral	PTR-ToF-MS
Stockwell et al., 2015	1.1102	0.0407	0.8656	Lab		Cookstove fuel	PTR-ToF-MS
Stockwell et al., 2015	0.5664		0.8869	Lab		Cookstove fuel	PTR-ToF-MS
Stockwell et al., 2015	0.6295	0.1423	0.9632	Lab		Cookstove fuel	PTR-ToF-MS
Stockwell et al., 2015	0.7188	0.1666	0.9741	Lab		Cookstove fuel	PTR-ToF-MS
Stockwell et al., 2015	0.0759	0.05	0.9841	Lab		Cookstove fuel	PTR-ToF-MS
Stockwell et al., 2015	1.9606	0.1266	0.9504	Lab	Ghana	Crop residue and Cookstove fuel	PTR-ToF-MS
Stockwell et al., 2015		0.0371	0.9679	Lab		Cookstove fuel	PTR-ToF-MS
Stockwell et al., 2015		0.0383	0.9658	Lab		Cookstove fuel	PTR-ToF-MS
Stockwell et al., 2015	4.1466	0.3198	0.9717	Lab		Cookstove fuel	PTR-ToF-MS
Stockwell et al., 2015	4.1362	0.319		Lab		Cookstove fuel	PTR-ToF-MS
Stockwell et al., 2015	1.7359	0.1499	0.9852	Lab		Cookstove fuel	PTR-ToF-MS
Stockwell et al., 2015	1.7351	0.1498		Lab		Cookstove fuel	PTR-ToF-MS

Stockwell et al., 2015	2.9712	0.2425	0.9848	Lab		Cookstove fuel	PTR-ToF-MS
Stockwell et al., 2015	2.9696	0.2423		Lab		Cookstove fuel	PTR-ToF-MS
Stockwell et al., 2015	2.5137	0.0856	0.9482	Lab	Colorado	Crop residue	PTR-ToF-MS
Stockwell et al., 2015	0.8416	0.1152	0.9465	Lab	Colorado	Crop residue	PTR-ToF-MS
Stockwell et al., 2015	0.6796	0.0729	0.9555	Lab	Colorado	Crop residue	PTR-ToF-MS
Stockwell et al., 2015	1.768	0.0731	0.9531	Lab	Colorado	Crop residue	PTR-ToF-MS
Stockwell et al., 2015	3.6108	0.3042	0.9414	Lab	Colorado	Crop residue	PTR-ToF-MS
Stockwell et al., 2015	3.5835	0.3019		Lab	Colorado	Crop residue	PTR-ToF-MS
Stockwell et al., 2015	1.2118	0.06	0.9414	Lab	Colorado	Crop residue	PTR-ToF-MS
Stockwell et al., 2015	0.2413	0.0307	0.9629	Lab	Montana	Temperate forest	PTR-ToF-MS
Stockwell et al., 2015	0.2412	0.0306		Lab	Montana	Temperate forest	PTR-ToF-MS
Stockwell et al., 2015	0.4513	0.041	0.9607	Lab	Montana	Temperate forest	PTR-ToF-MS
Stockwell et al., 2015	1.0942	0.2769	0.9303	Lab	California	Chaparral	PTR-ToF-MS
Stockwell et al., 2015	1.8451	0.2414	0.9334	Lab	California	Chaparral	PTR-ToF-MS
Stockwell et al., 2015	1.8403	0.2408		Lab	California	Chaparral	PTR-ToF-MS
Stockwell et al., 2015	0.4695	0.0445	0.9311	Lab	Ghana	Crop residue and Cookstove fuel	PTR-ToF-MS
Stockwell et al., 2015	0.4691	0.0444		Lab	Ghana	Crop residue and Cookstove fuel	PTR-ToF-MS
Stockwell et al., 2015	0.8162	0.0738	0.9454	Lab	Ghana	Crop residue and Cookstove fuel	PTR-ToF-MS
Stockwell et al., 2015	2.7673	0.3527	0.811	Lab	Canada	Boreal peat	PTR-ToF-MS
Stockwell et al., 2015	2.7061	0.3449		Lab	Canada	Boreal peat	PTR-ToF-MS
Stockwell et al., 2015	0.8768	0.4294	0.7981	Lab	Canada	Boreal peat	PTR-ToF-MS
Stockwell et al., 2015	4.9248	0.5029	0.7439	Lab	Indonesia	Indonesian peat	PTR-ToF-MS
Stockwell et al., 2015	4.8113	0.4913		Lab	Indonesia	Indonesian peat	PTR-ToF-MS
Stockwell et al., 2015	9.9773	0.5713	0.8715	Lab	Indonesia	Indonesian peat	PTR-ToF-MS
Stockwell et al., 2015	9.9149	0.5678		Lab	Indonesia	Indonesian peat	PTR-ToF-MS
Stockwell et al., 2015	14.013	0.6598	0.6827	Lab	North Carolina	Temperate peat	PTR-ToF-MS
Stockwell et al., 2015	2.4297	0.197	0.6923	Lab	North Carolina	Temperate peat	PTR-ToF-MS
Stockwell et al., 2015	2.3876	0.1936		Lab	North Carolina	Temperate peat	PTR-ToF-MS
Stockwell et al., 2015	4.5719	0.8257	0.9082	Lab	Montana	Temperate forest	PTR-ToF-MS
Stockwell et al., 2015	6.3668	1.0729	0.9139	Lab	Montana	Temperate forest	PTR-ToF-MS
Stockwell et al., 2015	5.0355	0.9655	0.9184	Lab	Montana	Temperate forest	PTR-ToF-MS
Stockwell et al., 2015	1.8692	0.4497	0.9457	Lab	Montana	Temperate forest	PTR-ToF-MS
Stockwell et al., 2015	13.5	1.9463	0.8478	Lab	Montana	Temperate forest	PTR-ToF-MS
Stockwell et al., 2015	4.4065	0.7024	0.9255	Lab	Montana	Temperate forest	PTR-ToF-MS

Stockwell et al., 2015	3.1975	0.6724	0.933	Lab	Montana	Temperate forest	PTR-ToF-MS
Stockwell et al., 2015	5.526	1.0246	0.9121	Lab	Montana	Temperate forest	PTR-ToF-MS
Stockwell et al., 2015	5.4899	1.0179		Lab	Montana	Temperate forest	PTR-ToF-MS
Stockwell et al., 2015	3.4929	0.2092	0.938	Lab	China	Crop residue	PTR-ToF-MS
Stockwell et al., 2015	3.4786	0.2083		Lab	China	Crop residue	PTR-ToF-MS
Stockwell et al., 2015	0.5171	0.0497	0.9573	Lab	China	Crop residue	PTR-ToF-MS
Stockwell et al., 2015	5.7595	1.1964	0.8761	Lab	Taiwan	Crop residue	PTR-ToF-MS
Stockwell et al., 2015	0.817	0.2024	0.9517	Lab	Taiwan	Crop residue	PTR-ToF-MS
Stockwell et al., 2015	1.1566	0.3088	0.9432	Lab	Taiwan	Crop residue	PTR-ToF-MS
Stockwell et al., 2015	0.8821	0.0751	0.951	Lab	Taiwan	Crop residue	PTR-ToF-MS
Stockwell et al., 2015	0.7555	0.0941	0.9469	Lab	Taiwan	Crop residue	PTR-ToF-MS
Stockwell et al., 2015	0.753	0.0938		Lab	Taiwan	Crop residue	PTR-ToF-MS
Stockwell et al., 2015	7.8294	1.5407	0.9141	Lab	Louisiana	Crop residue	PTR-ToF-MS
Stockwell et al., 2015	7.71	1.5172		Lab	Louisiana	Crop residue	PTR-ToF-MS
Stockwell et al., 2015	4.3232	0.685	0.9293	Lab	Louisiana	Crop residue	PTR-ToF-MS
Stockwell et al., 2015	4.3182	0.6842		Lab	Louisiana	Crop residue	PTR-ToF-MS
Stockwell et al., 2015	0.7843	0.0591	0.9588	Lab	Washington	Crop residue	PTR-ToF-MS
Stockwell et al., 2015	0.3021	0.0351	0.9632	Lab	Washington	Crop residue	PTR-ToF-MS
Stockwell et al., 2015	0.302	0.0351		Lab	Washington	Crop residue	PTR-ToF-MS
Stockwell et al., 2015	0.9571	0.0859	0.9592	Lab	Maryland	Crop residue	PTR-ToF-MS
Stockwell et al., 2015	0.5691	0.0676	0.9567	Lab	Maryland	Crop residue	PTR-ToF-MS
Stockwell et al., 2015	2.6316	0.1955	0.9407	Lab	Colorado	Crop residue	PTR-ToF-MS
Stockwell et al., 2015	4.975	0.3206	0.9361	Lab	Colorado	Crop residue	PTR-ToF-MS
Stockwell et al., 2015	3.1949	0.1554	0.9561	Lab	Colorado	Crop residue	PTR-ToF-MS
Stockwell et al., 2015	1.6161	0.211	0.9678	Lab	Colorado	Crop residue	PTR-ToF-MS
Stockwell et al., 2015	0.8344	0.1338	0.9687	Lab	Colorado	Crop residue	PTR-ToF-MS
Stockwell et al., 2015	1.6719	0.1582	0.9648	Lab	Colorado	Crop residue	PTR-ToF-MS
Stockwell et al., 2015	1.6663	0.1577		Lab	Colorado	Crop residue	PTR-ToF-MS
Stockwell et al., 2015	0.3764	0.0373	0.9638	Lab	South Carolina	Pine forest understory	PTR-ToF-MS
Stockwell et al., 2015	0.3452	0.0355	0.9622	Lab	South Carolina	Pine forest understory	PTR-ToF-MS
Stockwell et al., 2015	0.2821	0.0211	0.9671	Lab	South Carolina	Pine forest understory	PTR-ToF-MS
Stockwell et al., 2015	0.1861	0.0544	0.9729	Lab	South Carolina	Pine forest understory	PTR-ToF-MS
Stockwell et al., 2015	0.3877	0.0677	0.9716	Lab	South Carolina	Pine forest understory	PTR-ToF-MS
Stockwell et al., 2015	0.3876	0.0677		Lab	South Carolina	Pine forest understory	PTR-ToF-MS

Stockwell et al., 2015	0.3956	0.072	0.9692	Lab	South Carolina	Pine forest understory	PTR-ToF-MS
Stockwell et al., 2015	0.5754	0.0506	0.9722	Lab	South Carolina	Pine forest understory	PTR-ToF-MS
Yokelson et al., 1999	3.11	1.17	0.927	Field	North Carolina	Conifer forest	AFTIR
Yokelson et al., 2003	3.44	0.29	0.927	Field	Africa	Grassland	AFTIR
Yokelson et al., 2003	2.32	0.7	0.944	Field	Africa	Grassland	AFTIR
Yokelson et al., 2003	1.84	0.73	0.956	Field	Africa	Grassland	AFTIR
Yokelson et al., 2003	2.82	0.69	0.932	Field	Africa	Other	AFTIR
Yokelson et al., 2003	3.64	0.76	0.91	Field	Africa	Coastal lowland/open forest with grass/brush understory	AFTIR
Yokelson et al., 2003	2.55	1.6	0.922	Field	Africa	Other	AFTIR
Yokelson et al., 2003	2.18	0.57	0.941	Field	Africa	Humid savanna/tropical dry forest/ grass and leaf litter	AFTIR
Yokelson et al., 2003	0.8	0.43	0.974	Field	Africa	Flooded grasslands	AFTIR
Yokelson et al., 2003	2.34	0.79	0.935	Field	Africa	Other	AFTIR
Yokelson et al., 2007	3.134	0.398	0.916	Field	Brazil	Slash under partial canopy	AFTIR
Yokelson et al., 2007	4.172	0.519	0.9	Field	Brazil	Pasture	AFTIR
Yokelson et al., 2007	3.635	0.377	0.882	Field	Brazil	Slash under partial canopy	AFTIR
Yokelson et al., 2007	3.59	0.223	0.89	Field	Brazil	Mixedwood forest	AFTIR
Yokelson et al., 2007	2.643	0.246	0.902	Field	Brazil	Mixedwood forest	AFTIR
Yokelson et al., 2007	3.232	0.508	0.918	Field	Brazil	Mixedwood forest	AFTIR
Yokelson et al., 2007	3.19	0.323	0.901	Field	Brazil	Mixedwood forest	AFTIR
Yokelson et al., 2007	3.579	0.978	0.947	Field	Brazil	Mixedwood forest	AFTIR
Yokelson et al., 2007	3.704	1.715	0.936	Field	Brazil	Mixedwood forest	AFTIR
Yokelson et al., 2011	0.89	0.682	0.97	Field	Mexico	Crop residue fires	AFTIR
Yokelson et al., 2011		1.933	0.945	Field	Mexico	Crop residue fires	AFTIR
Yokelson et al., 2011	4.183	1.125	0.87	Field	Mexico	Crop residue fires	AFTIR
Yokelson et al., 2011	0.6	0.554	0.911	Field	Mexico	Crop residue fires	AFTIR
Yokelson et al., 2011	4.643	1.838	0.928	Field	Mexico	Crop residue fires	AFTIR
Yokelson et al., 2011	6.476	0.294	0.95	Field	Mexico	Crop residue fires	AFTIR
Yokelson et al., 2011	7.07	1.78	0.956	Field	Mexico	Crop residue fires	AFTIR
Yokelson et al., 2011	3.25		0.941	Field	Mexico	Crop residue fires	AFTIR
Yokelson et al., 2011	2.388		0.937	Field	Mexico	Crop residue fires	AFTIR
Yokelson et al., 2011	9.151	0.285	0.91	Field	Mexico	Crop residue fires	AFTIR

Yokelson et al., 2011	6.486	0.526	0.822	Field	Mexico	Crop residue fires	AFTIR
Yokelson et al., 2011	2.534		0.925	Field	Mexico	Tropical dry forest fires	AFTIR
Yokelson et al., 2011	2.412		0.923	Field	Mexico	Tropical dry forest fires	AFTIR
Yokelson et al., 2011	1.431		0.945	Field	Mexico	Tropical dry forest fires	AFTIR
Yokelson et al., 2011	4.678		0.907	Field	Mexico	Tropical dry forest fires	AFTIR
Yokelson et al., 2011	3.416		0.926	Field	Mexico	Tropical dry forest fires	AFTIR
Yokelson et al., 2011	2.497	1.823	0.897	Field	Mexico	Tropical dry forest fires	AFTIR
Yokelson et al., 2011		3.544	0.915	Field	Mexico	Mixed crop	AFTIR
Yokelson et al., 2011		6.359	0.927	Field	Mexico	Mixed crop	AFTIR
Yokelson et al., 2011	0.137		0.934	Field	Mexico	Savanna fires	AFTIR
Yokelson et al., 2011	0.35		0.928	Field	Mexico	Savanna fires	AFTIR
Yokelson et al., 2011		3.44	0.963	Field	Mexico	Savanna fires	AFTIR
Yokelson et al., 2011		4.217	0.94	Field	Mexico	Savanna fires	AFTIR
Yokelson et al., 2011		9.391	0.924	Field	Mexico	Savanna fires	AFTIR
Yokelson et al., 2011		0.28	0.943	Field	Mexico	Rural pine oak forests	AFTIR
Yokelson et al., 2011	0.649	1.226	0.904	Field	Mexico	Rural pine oak forests	AFTIR
Yokelson et al., 2011		1.282	0.869	Field	Mexico	Rural pine oak forests	AFTIR
Yokelson et al., 2011		0.39	0.907	Field	Mexico	Rural pine oak forests	AFTIR
Yokelson et al., 2011	0.265		0.899	Field	Mexico	Rural pine oak forests	AFTIR
Yokelson et al., 2011	3.661	0.176	0.903	Field	Mexico	Rural pine oak forests	AFTIR
Yokelson et al., 2011		0.065	0.942	Field	Mexico	Rural pine oak forests	AFTIR
Yokelson et al., 2011	0.58	0.05	0.964	Field	Mexico	Open burning garbage	AFTIR
Yokelson et al., 2011	7.4	0.14	0.911	Field	Mexico	Open burning garbage	AFTIR
Yokelson et al., 2011	0.92	0.34	0.958	Field	Mexico	Open burning garbage	AFTIR
Yokelson et al., 2011	0.78	0.19	0.968	Field	Mexico	Open burning garbage	AFTIR